Effects of snowmelt infiltration on sulfate redistribution in a reclamation cover

A Thesis Submitted to the College of Graduate and Postdoctoral Studies

In Partial Fulfillment of the Requirements

For the Degree of Master of Science

In the Department of Civil, Geological, and Environmental Engineering

University of Saskatchewan

Saskatoon

By

Shelby Lee DeMars

PERMISSION TO USE

In presenting this thesis/dissertation in partial fulfillment of the requirements for a Postgraduate degree from the University of Saskatchewan, I agree that the Libraries of this University may make it freely available for inspection. I further agree that permission for copying of this thesis/dissertation in any manner, in whole or in part, for scholarly purposes may be granted by the professor or professors who supervised my thesis/dissertation work or, in their absence, by the Head of the Department or the Dean of the College in which my thesis work was done. It is understood that any copying or publication or use of this thesis/dissertation or parts thereof for financial gain shall not be allowed without my written permission. It is also understood that due recognition shall be given to me and to the University of Saskatchewan in any scholarly use which may be made of any material in my thesis/dissertation.

DISCLAIMER

Reference in this thesis to any specific commercial products, process, or service by trade name, trademark, manufacturer, or otherwise, does not constitute or imply its endorsement, recommendation, or favoring by the University of Saskatchewan. The views and opinions of the author expressed herein do not state or reflect those of the University of Saskatchewan, and shall not be used for advertising or product endorsement purposes.

Requests for permission to copy or to make other uses of materials in this thesis/dissertation in whole or part should be addressed to:

Head of the Department of Civil, Geological, and Environmental Engineering

University of Saskatchewan

3B48 Engineering Building, 57 Campus Drive

Saskatoon, Saskatchewan S7N 5A9 Canada

OR

Dean

College of Graduate and Postdoctoral Studies

University of Saskatchewan

116 Thorvaldson Building, 110 Science Place

Saskatoon, Saskatchewan S7N 5C9 Canada

ABSTRACT

Oil sands mining in Alberta involves the removal of large amounts of overburden to access the oil sands. Reclamation of these overburden systems remains a challenge for the industry. Currently, there is a lack of understanding of how overburden cover systems in Alberta oil sands will function with respect to the water balance and long-term build-up and release of solutes. In this research, a conceptual model was developed, informed by interpretations of field observations. A one-dimensional heat, flow, and solute transport model was built to simulate the long-term evolution of sulfate under varying assumptions of snowmelt infiltration and sulfate production. The findings show that snowmelt infiltration is a critical control on the distribution and export of sulfates within the system. Simple infiltration models over-predict runoff and under-predict infiltration. Enhanced snowmelt infiltration scenarios are more consistent with field observations and therefore more representative of the system. The model suggested that larger snowmelt infiltration volumes result in increased soil salinization in the shallow subsurface horizon of the profile, likely due in part to evapoconcentration. Increased infiltration also resulted in increased net percolation, which results in more solute leaching to the deeper groundwater system in the short term. In the long term, it is suspected enhanced net percolation and increased infiltration might lead to a reduction in the salinity of the reclamation cover, reversing the soil salinization.

Table of Contents

LIST OF TABLES

LIST OF FIGURES

1 INTRODUCTION

Oil sands mining operations involve the removal of large amounts of overburden to access the oil sands. Returning these overburden deposits to re-establish ecosystems like those prior to disturbance is a challenge for the oil sands industry in Alberta. Currently, there is a lack of understanding of how these cover systems will function and evolve with respect to long-term salt evolution.

The release of salts from reclamation landscapes into surrounding soils, groundwater, lakes and rivers is a major concern for the oil sands industry in Alberta. High salt concentrations in the subsurface increases the potential hazard associated with changes in hydrology, which subsequently can result in salinization of soils, surface and subsurface water. This thesis will focus on developing an improved understanding on how these cover systems in reclaimed landscapes function with respect to the water balance and the long-term evolution of salts. This will be accomplished by means of a quantitative transport model for a set of extensively instrumented hillslopes within Syncrude's Mildred Lake mine, to simulate the long-term evolution of salts under varying assumptions of snowmelt infiltration. This model will be used to generate modelling scenarios to explore the impacts of snowmelt infiltration into seasonally frozen ground. The proposed research will help to better quantify some of the uncertainties regarding the future performance of reclamation landforms created by the Canadian Oil Sands industry.

The objectives of the proposed thesis are described in Chapter 1 followed by a literature review provided in Chapter 2 that summarizes soil salinity, geochemistry, hillslope processes and research that has been conducted to date at South Bison Hill. The study site and data analyses are described in Chapter 3. Chapter 4 discuss the model development, results and Chapter 5 summarizes the findings of this thesis.

1.1 Problem Overview

The extraction of bitumen and heavy oil from the Athabasca oil sands region is completed by in-situ recovery or surface mining. Surface mining involves the stripping of overburden to access the underlying ore while in-situ methods use steam to assist the extraction of bitumen to the recovery well. Both methods of bitumen recovery have negative environmental impacts. The environmental impacts of surface mining include tailings ponds, overburden dumps and mined out pits. The

natural land disturbance and reclamation requirements are a concern to operators, regulators and the public.

At Syncrude Canada Ltd. (SCL) Mildred Lake Mine, the overburden is predominately Cretaceous clay shale that is both saline and sodic (Wall 2005). The Cretaceous clay shale of the Athabasca region is part of the Clearwater Formation. The Clearwater Formation is a marine interbedded sequence of shale and sandstone deposited in environments ranging from lagoonal to beach and offshore to fluvial deltaic, tidal estuarine and flats (Wall 2005; Stott et al. 1991). These sediments naturally contain high concentrations of soluble ions, especially sodium and sulfate. The elevated salinity creates difficult conditions for vegetation growth. To help alleviate this issue, a soil cover is placed over the shale to allow for vegetation growth. However, past studies have shown that salts from the underlying shale can be transported into the cover soil by various transport processes that could hinder the long-term success of these reclaimed landscapes (Kessler 2007). SCL is expecting to reclaim approximately 70 km^2 or approximately 1/3 of the final disturbed footprint that will comprise of reworked saline-sodic overburden (Kelln et al. 2008). Therefore, there is a need to understand how these cover systems in reclaimed landscapes function with respect to the water balance and the long-term evolution and release of salts into surround soils and water bodies.

1.2 Research Objectives

The release of salts from reclamation landscapes into surrounding soils, groundwater, lakes and rivers has been identified as a major concern for the oil sands industry in Alberta. To preserve the unique boreal plains ecosystems and successfully attain a reclaimed landscape, it is of direct interest to the oil sands industry to understand and mitigate the risks associated with overburden dumps.

The focus of this research is to develop an improved understanding of how these cover systems in reclaimed landscapes function with respect to the water balance and the long-term evolution of salts.

The objectives of this study are as follows:

Objective 1: Develop a conceptual model for the site and conduct a data analysis to assess the water balance and develop insights for various hydrological processes (e.g.., runoff, interflow)

Based on field observation and past research develop a conceptual model for the field site to help inform the data analysis and numerical modelling efforts. Conduct a preliminary data analysis that involves assessing the water balance from the observed site data to develop insights into how interflow, runoff and net percolation are generated.

Objective 2: Develop 1D salt transport model to simulate the long-term evolution of salts

The driving data (e.g., climate data, model parameters) from Objective 1 will be used to develop a 1-dimensional quantitative salt transport model for the extensively instrumented hillslope within Syncrude's Mildred Lake mine, to simulate the long-term evolution of salts. Modelling scenarios will be generated to explore snowmelt infiltration process hypotheses and these different processes of snowmelt infiltration affect the accumulation and transportation of salts within the cover.

1.3 Study Site

This study was conducted at South Bison Hill (SBH) located at Syncrude's Mildred Lake oil sands mine, approximately 40 km north of Fort McMurray, Alberta (Figure 3.1). a

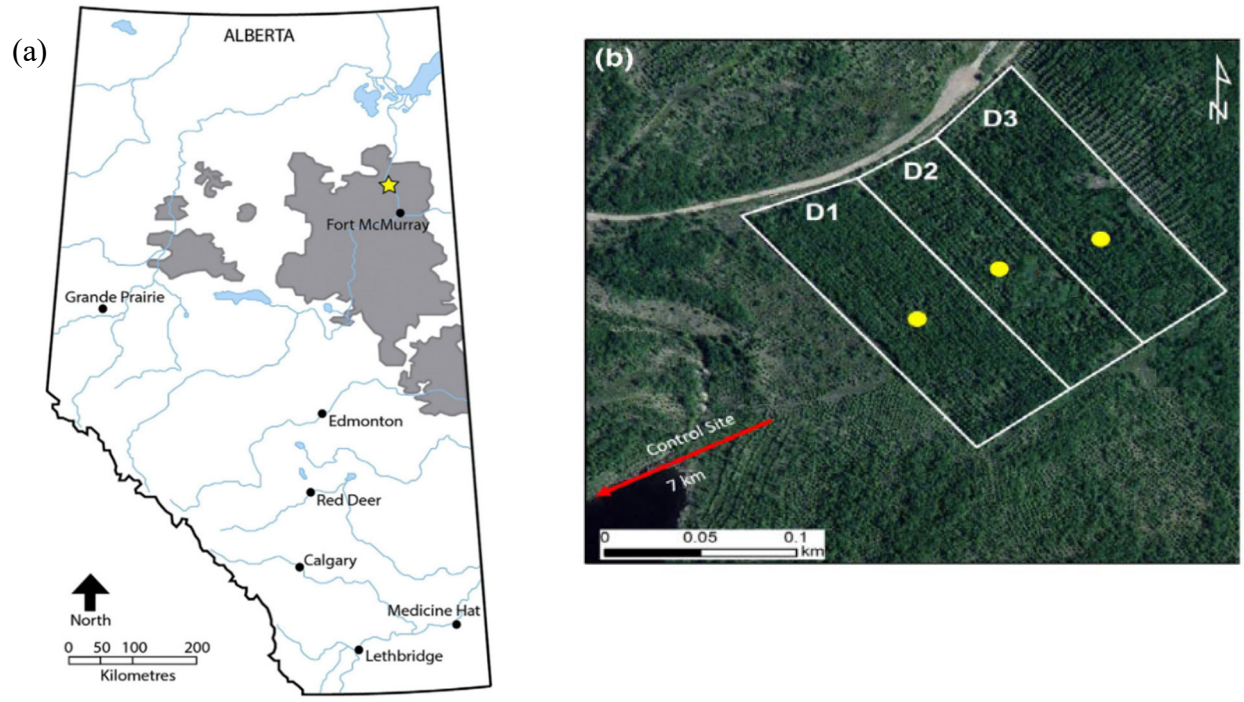

Figure 1.1: (a) Oil Sand Deposits in Alberta (grey areas). Star denotes approximate location of SCL's Mildred Lake Mine (from Dompierre et al. 2016) (b) location of the study cover (SBH). Yellow circles denote instrumented sites.

South Bison Hill was built on an upland saline-sodic shale overburden structure and has an area of 2 km^2 with a plateau rising approximately 60 m above the surrounding landscape. This site was constructed over the course of two decades with the last lift of overburden placed in 1996 and final grading conducted between 1996 and 1999 (Kessler 2007).

In 1999, reclamation cover soil was placed on three research plots along the north facing 5H:1V slope of South Bison Hill. The three research plots, designated as D1, D2 and D3 were each constructed with a differing cover thickness to study the effect of varying thicknesses on reclamation plots. Figure 3.2 illustrates the cover thicknesses for each plot. Following the placement of the cover, the plots were seeded with barley to prevent erosion of the top soil, and in 2000, the plots were planted with aspen and white spruce (Kessler 2007).

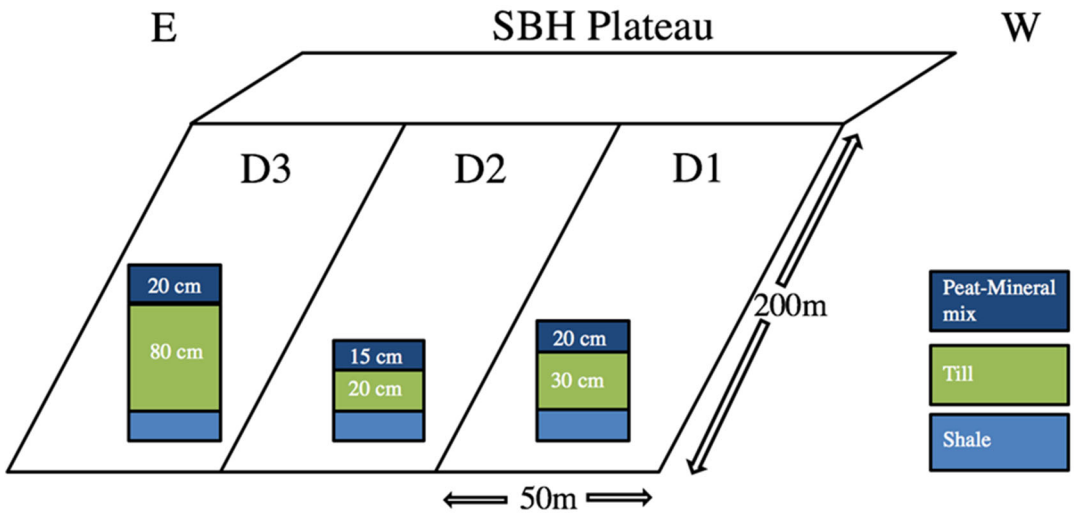

Figure 1.2: Research Plot Cover Prescriptions

1.4 Thesis Structure

Chapter 2 presents a literature review on frozen soil processes, soil salinization, solute transport and previous site research. The study site and data analyses are described in Chapter 3. Chapter 4 presents the numerical modelling results and discussion, and Chapter 5 summarizes the findings of this thesis.

2 LITERATURE REVIEW

2.1 Frozen Soil Processes

Melting of the seasonal snow cover in cold regions is one of the most significant hydrological events of the water year. Partitioning of snow water to soil water and runoff is proportional to the infiltrability of the underlying frozen ground at the time of snowmelt.

Melt water infiltration into frozen soil is a complicated process as it involves coupled heat and mass transfer with phase changes (Gray et al. 2001). This process is affected by many factors such as soil moisture, temperature regimes, the rate of release of water from the snow cover and the energy content of the infiltrating water. In the absence of major structural deformations in the soil profile (i.e. macropores), the most important property of a frozen soil controlling its ability to absorb or transmit water is the soil's water content (Granger et al. 1984). Due to the blockage of water flow by ice-filled pores there is decrease in hydraulic conductivity that effects the tortuosity, flow paths and the distribution and continuity of air-filled pores.

The soil freeze-thaw process affects approximately 50% of soils in the Northern Hemisphere, and influences physical, chemical and biological processes in the vadose zone which in turn affect the water, mass and energy cycles over numerous scales (Zhang et al. 2003). The soil freeze–thaw cycle drives numerous mechanical processes, including frost heave, soil aggregate formation and breakdown, and controls snowmelt infiltration and runoff. These hydrologic processes determine the soil water content conditions, which in turn affect plant mortality and growth, soil microbial activities, and nutrient (e.g., C and N) cycles (Hayashi 2013).

2.1.1 Snowmelt

Areas with a significant seasonal snowpack, snowmelt in addition to rain largely determines the availability of water to vegetation, and the amount and timing of stream flow and groundwater recharge. Snowfall typically contributes more to runoff and groundwater recharge since a smaller proportion of snowmelt in comparison to rainfall is evaporated and transpired (Dingman 2015).

The physical properties of a snowpack (density, depth and water equivalent) are important to understand the hydrology (e.g. water balance) of a system. The snow water equivalent (SWE) is the equivalent depth of water in a snowpack that would result from the complete melting of the snow in place and is defined as:

$$SWE = \frac{\rho_s d_s}{\rho_w} \quad (1)$$

Where, ρ_s is the average snow density (kg m^{-3}), d_s is the snow depth (mm) and ρ_w is the density of water (kg m^{-3}).

Snowmelt rate can be calculated using a physically based approach by way of the net energy balance method. The energy balance for the snowpack element is defined as:

$$Q_{melt} + \frac{\Delta U}{\Delta t} = \Delta Q \quad (2)$$

Where, Q_{melt} (W m^{-2}) is the snowmelt energy flux, ΔQ is the net flux of energy (W m^{-2}) from the atmosphere and ground, and $\Delta U/\Delta t$ is the change in internal energy (temperature) in time period Δt. The components of the energy flux are:

$$\Delta Q = Q_n + Q_e + Q_h + Q_m + Q_g \quad (3)$$

Where, Q_n is the net radiation transfer flux, Q_e and Q_h are the latent heat transfer and sensible heat flux from the atmosphere. Q_m is the advective transfer of heat into the snowpack by meltwater and Q_g is defined as the net flux of sensible heat due to conduction with the ground surface.

The amount of snowmelt is estimated by coupling the energy balance method with the mass balance of the snowpack element using the latent heat of fusion (Gray et al. 1986):

$$M = \frac{Q_{melt}}{\rho_w B \lambda_f} \quad (4)$$

Where, M is the melt (mm day^{-1}), Q_{melt} (W m^{-2}) is the snowmelt energy flux, ρ_w is the density of water (kg m^{-3}), B is the thermal quality of snow (or the fraction of ice in a unit mass of wet snow) and λ_f is the latent heat of fusion of ice (kJ kg^{-1}).

As the snowpack accumulates, net inputs of energy from the atmosphere are generally negative, average snowpack temperature decreases and water equivalent typically increases. The period of increase in the snowpack water equivalent prior to the initiation of snowmelt is the accumulation

period. The melt period of the seasonal snowpack begins when the net input energy becomes continually positive, the melt period can usually be separated into three phases, the warming phase, ripening phase and the output phase (Dingman 2015).

1. Warming phase: The warming phase occurs when the average snowpack temperature increases steadily until the snowpack is isothermal at 0°C.
2. Ripening phase: The ripening phase occurs during which melting occurs but the meltwater is retained in the snowpack. At the end of this phase the snowpack is ripe (i.e. the snowpack is isothermal and cannot retain anymore liquid water).
3. Output phase: The output phase occurs when further inputs of energy cause melting that leaves the snowpack as water output.

Typically, the snowpack does not progress sequentially through this sequence. Melting can occur at the surface of a snowpack prior to the ripening phase when air temperatures rise above 0°C, the meltwater produced percolates into the cold snow at depth and refreezes, releasing latent heat which increases the snow temperature. Comparably, snow-surface temperatures may fall below freezing during the melt period, and the surface layer must warm again before melting can continue (Dingman 2015).

2.1.2 Frozen Soil Fundamental Properties

A depressed (lowered) freezing point exists in the soil freeze-thaw regime. In soil pores, this lowered freezing point is a result of two factors. One being the effect of capillary and adsorptive forces that attract liquid water to the soil pore apertures and particles. The other being, the presence of dissolved salts that results in a shift of the freezing point.

Freezing of soil water occurs across a range of temperatures to several degrees below 0°C and a significant amount of liquid water remains in frozen soil. Based on Gibbs free energy of ice and liquid water, the equilibrium relationship between temperature and pressure is defined by the Clausius-Clapeyron equation (Williams et al. 1989):

$$\frac{dP_w}{dT} = \frac{L_f}{TV_w} \tag{5}$$

Where P_w (Pa) is the pressure of liquid water, T (K) is temperature, L_f (J kg^{-1}) is the latent heat of fusion and V_w (m^3 kg^{-1}) is the specific volume of liquid water. The pressure of ice is assumed constant.

When the temperature drops below the freezing point, a portion of the soil water changes phase and freezes in situ. The portion of this water that remains unfrozen is present in adsorbed films around soil particles, in crevices between particles and in pores of small diameter (Spaans et al. 1996). Soil water can remain unfrozen at temperatures below the freezing point due to matric forces applied by the soil on the water. These forces lower the energy status of the water which subsequently lowers the freezing point of the water. Since soil contains a distribution of pore sizes, there will be a range in depressed freezing points in which the soil will freeze, and over these ranges of temperatures water and ice will coexist in different pores within the soil (Ireson et al. 2013). Therefore, water in larger pores will freeze before water in smaller pores, and the water in small pores will thaw before the water in larger pores. This relationship results in the soil freezing characteristic (SFC) curve. The SFC shows how unfrozen soil moisture in a saturated soil reduces with temperatures below 0°C (Spaans et al. 1996). The SFC curve is also affected by the presence of solutes in soil (Azmatch et al. 2012) which decrease the freezing point of the pore water.

The hydraulic conductivity of frozen soil decreases sharply as ice forms in large pores and liquid water is forced to flow in small pores and thin films, which has strong influence on infiltration process (Watanabe et al. 2008).

2.1.3 Frozen Soil Effects on Hydrological Processes

The most important function of frozen soil from a hydrologic perspective is its effect on overland flow and infiltration. Frozen soil strongly influences the timing and amount of water and spring runoff in cold regions due to the reduced hydraulic conductivity (Section 2.1.1). The infiltration capacity of frozen soil is dependent on soil texture and water content, as well as land use and agricultural practices. Gray et al. (2001) classified snowmelt infiltration in frozen soil into three categories:

(i) Unlimited infiltration: where soils are capable of infiltrating most or all the available water (e.g., coarse-textured soil or soils with cracks and macropores).

(ii) Restricted infiltration: where the infiltration capacity is severely reduced by an impervious surface (e.g., a soil layer nearly saturated with ice or basal ice lens forming at the soil surface).

(iii) Limited infiltration: where the capillary flow is dependent on the water and ice content.

Limited infiltration is governed by soil physical properties in that the infiltration capacity decreases with the pre-melt water content (liquid + ice) of the surface and near-surface soil.

As soil begins to freeze (i.e. when surface temperature drops below 0 ℃), a temperature gradient exists for heat conduction from the freezing front to the soil surface. The soil surface temperature is a function of the surface energy balance (i.e. radiation flux, turbulent flux, sensible and latent heat, heat conduction). When a snowpack is present, the soil temperature is determined by heat conduction through the snow and soil surface. The temporal and spatial variation of a snow cover has significant influence on snowmelt infiltration, since snow acts as an insulator for the soil and prevents further freezing.

2.2 Salinization of Soils

Salts are an integral component of soil and many salts, such as nitrate and potassium, are essential plant nutrients. However, an excessive accumulation of certain salts in soil results in a decline in productivity. At SCL Mildred Lake Mine, the cause of salinity in soil is known to be the presence of sodium and sulfate salts. Salinity in the glaciated plains of North America is a well-studied problem and studies suggest that the weathering of pyrite in the Cretaceous marine shale has caused the production of sulfate salts (Van Stempvoort et al. 1994). The sulfate produced by weathering may be precipitated as gypsum or reduced back to sulfide (Van Stempvoort et al. 1994).

Nachshon et al. (2013) cited that high salt concentration in the subsurface increases the potential hazard associated with changes in hydrology, which can result in the salinization of soils, surface and subsurface water. Alterations in the hydrological system by salt dissolution, migration and crystallization has the potential to result in severe economic and environmental problems (Nachshon et al. 2013). Salt affected soils are classified as either saline, sodic or saline-sodic soils and each possess different properties and require different strategies for remediation (Abrol et al. 1988).

2.3 Salinity and Sodicity Effects on Soil Properties

The saline-sodic Clearwater shale Formation, removed to access the oil-bearing formation at SCL, is known to possess physical and chemical properties adverse to plant growth.

The effects of salinity on the physical properties of soil are mainly biological or chemical. Salinity decreases plant growth by osmotic stress and by specific ion effects. Osmotic stress reduces the plant's capacity to extract soil water, while specific ion effects, such as chloride (Cl-) toxicity, can create an imbalance in ions (e.g. calcium [Ca^{2+}], potassium [K^{+}], sodium [Na^{+}]) required for optimal plant function.

Sodic salts increase the concentration of sodium ions in the soil's exchange complex, which affects both plant productivity and soil properties. Sodicity decreases plant growth by slowing root growth due to high soil strength and limiting gas exchange in the rhizosphere.

Sodic soils display poor physical condition which impacts their hydraulic properties. The hydraulic conductivity of a soil can be affected by the strength and type of cations contained in the soil water (Fetter 1998). Increased salinity when fresh water is present can cause soil swelling and can reduce hydraulic conductivity since clay minerals tend to swell and expand the available pore space. Sodium is particularly important in this process. The electrostatic double layer is thicker when it contains monovalent sodium ions which results in weaker bonds between clay particles. This double layer grows with decreasing concentration of cations in the soil water and will decrease with an increase in the ratio of the concentration of monovalent to divalent cations (Fetter 1998).

2.4 Salt Accumulation and Distribution

During soil salinization, salts can accumulate to high enough levels that will adversely affect vegetation growth. The major effect of salinization on plants is due to the increase in the osmotic potential of the soil which reduces the plants ability to absorb nutrients and water (Bresler et al. 1982; Section 2.3).

Salt accumulation is generally associated with areas of evaporation and transpiration, where water is removed from the soil as vapor from evaporation or by root uptake, leaving salts in the subsurface (Nachshon et al. 2013). A common process of soil salinization occurs when precipitation is greater than evapotranspiration and infiltrated water percolates below the root zone, dissolving salts in the soil profile and carried to the water table. Groundwater flow carries these

dissolved salts to low lying areas. This process ends in these locations when the water evaporates, leaving the salts behind (Wiebe et al. 2007). Another common process observed in dry land salinization is when ponded surface water from rainfall or snowmelt flows laterally to drier zones where the driving force is the soil moisture gradients generated by high evapotranspiration rates (Wiebe et al. 2007).

Different salts have different solubilities and thus accumulate at different positions along a flow path (Nachshon et al. 2013). Slightly soluble salts tend to crystalize and accumulate closer to the source while highly soluble salts (e.g. NaCl, Na_2SO_4) generally undergo longer travel distances in solution before reaching saturation and crystalizing further away (Nachshon et al. 2013).

At South Bison Hill, salt accumulation and distribution into the overlying cover is directly related to soil moisture conditions and the presence of net percolation and/or lateral groundwater flux (Kelln et al. 2008). Salinity profiles have indicated a strong increase in salinity with depth to the greatest concentration in the overburden which is comparable to patterns observed in both mature and natural landscapes (Kessler et al. 2010a). The three research plots exhibited no distinct trends in the salinity or sodicity levels associated with slope position.

2.5 Salt Transport Mechanisms

It is important to understand the advective and diffusive solute transport processes and solutes interactions with soil when dealing with the simultaneous transfer of water and solute in establishing salinity management practices (Bresler et al. 1982).

Merrill et al. (1983) identified molecular diffusion and advection induced by evapotranspiration as the two primary mechanisms causing upward salt migration into soils over a saline-sodic mine spoil. In fine grained soils, diffusion is often the dominant transport process, however, transport by advection can be of greater interest as it has greater potential to move more mass over longer distances. Advective transport is defined as the process in which the movement of dissolved solids is carried by the movement of the bulk liquid phase. The amount of solute transported is a function of its concentration in the groundwater and the quantity of groundwater flowing (Fetter 1998). One-dimensional advective transport is defined as:

$$J_q = qC \tag{6}$$

where J_q is the mass flux due to advective contaminant transport ($M/L^2/T$), q is the specific discharge (L^3/L^2T) and C is the concentration of contaminant in pore water (M/L^3).

Solute transport by molecular diffusion depends on the concentration gradient of a specified ion. When solutes are not distributed uniformly throughout a solution, concentration gradients exist, therefore, solutes tend to diffuses from zones of higher concentration to lower (Hillel 2003). Fick's first law describes one-dimensional diffusion, where a diffusion coefficient relates mass flux to the concentration gradient given by:

$$J_d = -\theta_e D_h \frac{\partial C}{\partial x} \tag{7}$$

where J_d is the diffusive flux ($M/L^2/T$), θ_e is the effective volumetric water content, and x is the distance (L), and C is the concentration (M/L^3). D_h (L^2/T) is the coefficient of hydrodynamic dispersion comprising of a molecular diffusion component and a mechanical dispersion component as follows:

$$D_h = D_o\tau + \alpha v \tag{8}$$

where D_o is the free solution molecular diffusion coefficient for a particular solute at a particular temperature (L^2/T), τ is the tortuosity factor, α is dispersivity (L) and v is the advective velocity (L/T). The product of D_o and τ is referred to as the effective diffusion coefficient for the porous media, D_e. Mechanical dispersion is conceptualized as an apparent mixing that occurs as a result of sampling across a range of different fluid pathways which are experiencing differing advection rates.

In the soil's liquid phase, the effective diffusion coefficient is usually less than the diffusion coefficient in bulk water because the liquid phase occupies only a fraction of the soil volume. Secondly, the soil's pore passages are tortuous so the actual path of diffusion is considerably greater than the apparent straight-line distance. Tortuosity is a factor that accounts for the complex

geometry of a porous media.

Fick's first law describes how a solute will move due to a concentration gradient; however, it does not show how a concentration is subject to change over time. So, Fick's second law can be used to determine the time dependent concentration changes,

$$D_h \frac{\delta^2 C}{\delta x^2} = \frac{\delta C}{\delta t} \tag{9}$$

where δC/δt is the change in concentration with time ($M/L^3/T$). The advection-dispersion equation is defined as:

$$-v \frac{\delta C}{\delta x} + D_h \frac{\delta^2 C}{\delta x^2} - \frac{\delta q}{\delta t} = \frac{\delta C}{\delta t} \tag{10}$$

where C is concentration (M/L3), t is time (s), v is pore water flow velocity (m/s), x is distance (m), Dh is the hydrodynamic dispersion coefficient (Equation 10). The term $-v\ \delta C/\delta x$ represents advective transport, $D_h(\delta^2\ C)/(\delta x^2\ )$ represents dispersive transport, and $\delta q/\delta t$ is the change in concentration in the solid phase due to reactions (q in the same units as C).

In systems with low hydraulic conductivity, molecular diffusion tends to be the dominant transport process (Shackelford et al. 1991). Merrill et al. (1983) corroborated this idea by citing that diffusion can only occur if the hydraulic conductivity of the mine spoil is very low otherwise, precipitation causing downward infiltration would reduce the upward diffusion of salts. The study by Merrill et al. (1983) was conducted at a semi-arid research site in North Dakota.

At the South Bison Hill site, large salt concentration gradients are created between the cover material and shale overburden that have low and high concentrations respectively, immediately after cover placement (Kessler 2007). This gradient drives the upward migration of salts into the soil cover. As the initial high concentration gradients created by cover placement is reduced, advective transport becomes a more dominant transport process (Huang, Hilderman, et al. 2015). Evapotranspiration-induced advection is the dominant mechanism of upward salt migration when the rate of evapotranspiration exceeds the rate of net percolation (Huang, Hilderman, et al. 2015).

In semi-arid regions, these conditions are often related to the presence of shallow water tables that can provide a source of water required to maintain a net upward movement of water.

The net percolation of water from the base of the cover into the shale can result in salts being flushed downward and act as a process that counteracts the effects of upward diffusion and advective transport into the cover. A second process that has been identified as a counteracting process in the South Bison Hill cover system is interflow (Kelln et al. 2008). Interflow is the gravity driven flow of water along the base of the cover created as a result of seasonally perched water tables caused by snowmelt infiltration or prolonged seasonal rainfall. Interflow of groundwater can carry with it salts that have accumulated along the cover-shale interface to lower slope locations, which acts as an important mechanism for salt flushing which protects the soil cover from ongoing salt ingress from the underlying shale (Kelln et al. 2007, 2008, 2009).

2.6 Hillslope Processes

Hillslope processes are an important aspect in understanding landscape evolution as well as the practical implication and hazards of upland land use and controls on the supply of water and sediments to surrounding soils, groundwater, lakes and rivers. Flow follows routes which attenuate and delay the flow to different extents, therefore, it is important to define what relevant mechanisms are present. Runoff is the portion of precipitation or snowmelt that flows over and through soils, eventually connecting to surface water systems. Overland flow, interflow and groundwater flow contribute to these hillslope processes.

Net precipitation is partitioned at the surface between subsurface flow and overland flow. Overland flow occurs when rainfall or snowmelt rates exceed the current infiltration capacity of the soil (Kirkby 1988). Subsurface flow is the movement of runoff predominantly below the ground surface. Return flow occurs when subsurface flow is constrained to flow out of the soil, overland, in areas of concavity and/or flow convergence, or where soil thickness and permeability are decreasing downslope (Kirkby 1988). Interflow is here defined as lateral movement of water along a layer of soil or rock material that restricts downward movement. At SBH, interflow is initiated during the spring snowmelt when the cover thaws and water migrates from the preferential flow paths into the soil matrix, causing a perched water table to form on the cover-shale interface. The cessation of interflow coincides with a recession of the perched water table and an increase in

matric suction within the cover in response to elevated evapotranspiration demands (Kelln et al. 2008).

The flow pathways of water and solute through soils can be highly irregular due to heterogeneity in the soil, which subsequently leads to difficulty in predicting the movement of these masses at larger field scales. This often results in more rapid movement and transport of masses than what would typically be expected from the soil matrix properties (Allaire et al. 2009). This accelerated transport is often associated with flow through burrows, fractures or flow related with soil layering and hydrophobicity. These processes together are referred to as preferential flow. In other words, preferential flow is defined as the flow mechanisms where transport of water and solute is primarily associated with a smaller fraction of the total pore network and can result in a delay or acceleration in the movement of this mass depending on the flow pathway (Allaire et al. 2009). Preferential flow in soil can occur by one or more of three possible mechanisms, these being macropore flow, unstable flow or finger flow, and funnel flow (Figure 2.1).

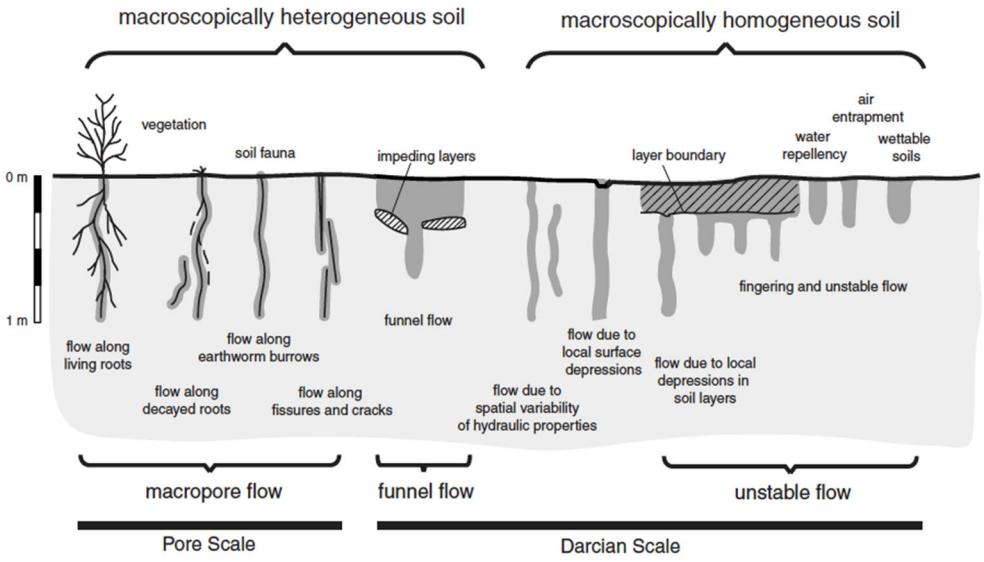

Figure 2.1: Preferential water movement in the vadose zone due to a) macropores b) finger flow and c) funnel flow (Fetter, 1998)

Perched groundwater is subsurface water that forms a saturated zone within porous media at an elevation higher than the local or regional water table. Perched water tables may result from various field conditions but generally occurs when a soil or rock layer of significantly lower vertical hydraulic conductivity occurs along contrastingly higher conductive strata.

Interflow monitoring has been conducted at South Bison Hill and has indicated that interflow is flushing salts from the cover system (Kelln et al. 2007; Hilderman 2011). Kessler (2007) speculated that this interflow would likely shift salts from the cover soil at upper slope locations to lower slope locations. Kelln et al. (2008) stated that salt transport in the cover is proportional to soil moisture conditions and the presence of net percolation and lateral, downslope interflow. Preferential flow has been observed at South Bison Hill, Kelln et al. (2007) showed that snowmelt infiltration was occurring through macropores when the ground is frozen and as the ground thaws, interflow is initiated and water migrates from the macropores into the soil matrix leading to a perched water table to develop at the cover-shale interface.

2.7 Previous Site Research

A number of studies have been conducted at South Bison Hill to answer questions related to site specific hydrology, cover soil characteristics, chemistry and soil-water dynamics. Some of the studies related to salinity are described below.

Wall (2005) studied the geochemistry of the overburden material in SBH and the evolution of geochemistry due to geochemical reactions. Wall concluded that sulphide mineral oxidation and carbonate mineral dissolution are the primary geochemical reactions occurring within the SBH overburden pile. These dominant reactions result in increased porewater salinity, especially SO_4^{2-} and Na^+. The oxidation zone was characterized as extending 5 m into the soil profile with SO_4^{2-} production rate between the range of 1×10^{-8} to 1×10^{-3} g/m^2/day. These flux rates are strongly dependent on water content and can change with changes in water content.

Appels et al. (2017) conducted a geochemical survey and modelling investigation of the weathering processes at SBH. The results obtained corroborated with Wall (2005) stating that sulphide mineral oxidation and carbonate mineral dissolution are the primary geochemical reactions occurring in the subsurface. Solid chemistry of soil samples from the unoxidized portion of the dump exhibited total and reduced concentrations similar to those in natural shale deposits. Gas concentration profiles for different locations, cover thicknesses and slope positions were similar. SO_4^{2-} production rates were calculated and ranged between 0.29-7.7 g SO_4^{2-} m^{2}d^{-1} six years after dump construction. The VWC of the cover layers is driest in the thinner cover while the thicker covers sustain a saturated zone below the cover/shale interface. Appels states the

elevated saturation at this zone can limit SO_4^{2-} production and the downward propagation of the oxidation front over time.

Kessler (2007) developed and compared the salinity profiles of four reclamation treatments with three layered covers of varying thickness (35, 50 and 100 cm) and one non-layered cover (100 cm). These profiles were compared to soil quality guidelines to evaluate the soil suitability for reclamation. Characterization of the soil systems confirmed the presence of salts and that the majority of these salts were sodium and sulfate released through pyrite oxidation of the saline-sodic overburden. During the initial 4-year period of placement, the dominant transport mechanism driving the salt upwards was diffusion. Kessler concluded that the extent of salt migration into the cover was similar for the different cover thicknesses but the overall quality of the thinner covers for vegetation growth was compromised by the increased salinity levels. Kessler et al. (2010) compared these profiles from different slope positions and found that salt redistribution was not related to slope position (i.e., upper slope, mid-slope, and bottom of slope).

Kelln et al. (2007) examined the contribution of preferential flow to the hydrological response of a reclamation cover using hydrometric and geochemical data. Kelln showed that snowmelt infiltration was occurring through macropores when the ground is frozen. As the ground thaws, interflow is initiated and water migrates from the macropores into the soil matrix leading to a perched water table to develop at the cover-shale interface. The downslope interflow water exhibits a seasonal evolution from fresh snowmelt to pre-event water dominated by higher concentration water from the soil matrix.

Kelln et al. (2008) conducted a field study to map the spatial distribution of soil water content and salt transport on the D3 test plot. The soil moisture data suggested that lower slope locations were wetter than upper slope locations due to down slope movement of surface run-off. Salt transport in the cover is proportional to soil moisture conditions and the presence of net percolation and lateral, downslope interflow. Increased soil moisture in lower slope positions result in an increased salt mass flux into the cover through diffusion while interflow activated by vertical preferential flow acts as a flushing mechanism to dilute the pore water salt concentrations near the interface, while drier conditions in upper slope positions limit transport by diffusion. Numerical modeling from this study also suggested that infiltration of snowmelt occurs through macropores. Kelln et al. (2009) applied the findings from the first two papers to produce a numerical flow and transport

model. Numerical modeling of the subsurface flow indicated that the macroporosity of the cover soil was approximately 3-4%. Kelln concludes that discharge concentrations increase as the depth of the perched water table decreases with time and water drains through these macropores that are associated with a matrix of high solute concentrations lower in the cover profile.

Hilderman (2011) developed profiles of the stable isotopes of water (^{2}H & ^{18}O) in the soil profiles and implemented a 1D numerical model to estimate the net percolation at various topographic locations. Soil samples were also collected at the same locations and compared to those collected by Kessler in 2002 and 2004. This comparison suggested that for the thinner cover (D1 and D2) the salt concentrations in the upper Clearwater overburden had decreased slightly, while the concentrations in the cover soil showed little change. For the thicker cover (D3), the concentration of salts did not change significantly in the upper Clearwater overburden but increased in the cover soil. For locations assessed on the plateau, the salt concentrations in both the cover and upper Clearwater overburden seemed to decrease slightly with time. The highest rates of net percolation were estimated to be occurring on the plateau and a mid-slope bench location. Hilderman concludes that net percolation is opposing upward diffusion of salts from the shale into the cover, and that comparison of salinity profiles collected several years apart indicate that, in some locations, the downward advection of salts by net percolation is likely causing a decrease in salinity in the cover and upper shale.

Huang et al. (2015) extended the work completed by Hilderman (2011) and developed a dual-porosity of water flow and solute transport to simulate stable isotope and salt transport. The estimated average net percolation rates varied from 2.08×10^{-6} m/d at plateau locations to 2.2×10^{-5} m/d at slope locations. A production term related to the reoccurring pyrite oxidations within the shale had to be included in the modeling to accurately represent the transport of SO_4^{2-}. These rates of production varied with varying net percolation rates and topographic position.

Current research to date conducted at South Bison Hill has primarily focused on quantifying the current mechanisms and processes associated with salt transport within the covers. It is expected that there will be a demand to understand how these cover systems and salt releases will develop over time and if it is possible to design landforms that help to mitigate the problems associated with salt, which the proposed research aims to achieve.

3 DATA AND METHODS

This section addresses the first objective, which was to conduct a preliminary data analysis that involves assessing the water balance from the observed site data to develop system hypotheses about interflow, runoff generation and net percolation.

3.1 Conceptual Model

A conceptual model was developed to summarize the processes involved in moisture and salt transport for the SBH cover system (Figure 3.1). Water ingress into the hillslope is assumed to occur by infiltration. This process is governed by the infiltration capacity of the soil which is affected by the ice content in the soil which is controlled by the pre-freeze up water content (Granger et al. 1984). Infiltration is comprised of either rainwater or snowmelt. Water that enters the subsurface contributes to storage, and is partitioned between lateral interflow, vertical net percolation and evapotranspiration. Net percolation accounts for the water passing through the cover into the shale.

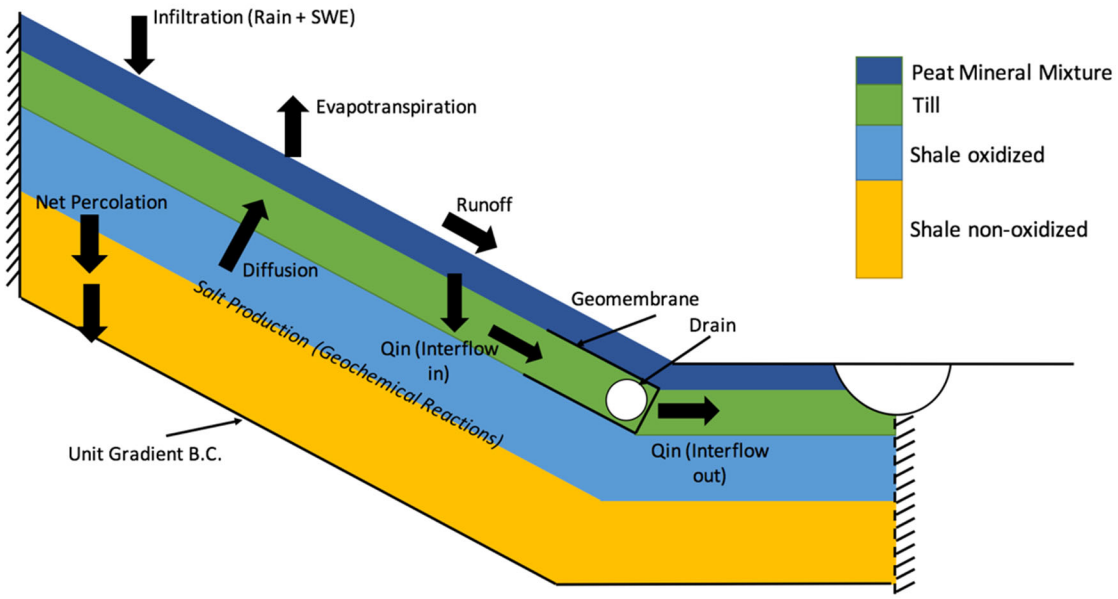

Figure 3.1: Conceptual Model of Hillslope at SBH

Based on the conceptual model (Figure 3.1) system hypotheses were developed in attempt to explain the relationship between interflow, runoff generation and net percolation. Observed site data was used to gain a better understanding of what controls interflow and how the time of melt and magnitude of the snowpack will affect these processes.

3.2 Available Data

SBH is a heavily instrumented site that has been the focus of multiple research projects over the past decade and as such, a comprehensive volume of data exists. A component of the current research project was to sort through existing data and determine the relevance and application as it pertains to the proposed research. The covers at SBH have instrumentation stations to monitor soil temperature, soil water and matric suction throughout the cover profile and upper portion of the underlying shale. A meteorological tower was placed at the center of SBH that provides measurements of air temperature, wind speed, relative humidity, and net radiation (Boese 2003). The covers are also instrumented to monitor volumetric water content by eight Time Domain Reflectometry (TDR) sensors, temperature is measured by eight CS-229 sensors and matric suction by thermal conductivity sensors at varying depths. A geomembrane was constructed to cut off and collect water moving downslope within the reclamation covers to measure interflow. Boese (2003) and Kessler (2010) provide detailed descriptions of field instrumentation and measurements at SBH.

The soil water characteristics curves (SWCC) are derived from the grain size distributions of the peat-mineral mixture, till, and underlying shale. Soil samples were measured using the method prescribed by ASTM D422-63. The SWCC for the cover soils and shale were measured using low pressure (100 kPa) acrylic Tempe cells and glass desiccators. The physical properties of three materials are shown in Table 3-1 (Boese 2003; G. Meiers et al. 2006; McMillan et al. 2007).

Table 3-1: Soil Properties of the peat-mineral mixture, till and shale at South Bison Hill

Soil Property	Peat-mineral mixture	Till	Shale
Sand (%)	59.5	16.5	12.5
Silt (%)	29.3	39.0	47.5
Clay (%)	11.3	44.5	40.0
Porosity	0.59	0.55	0.57
Average bulk density (g/cm^3)	0.92 ± 0.31	1.28 ± 0.21	1.47 ± 0.20
Specific gravity	2.62	2.61	2.73
Organic matter content	9.3%	4.7%	-
USCS classification	Sandy loam	Silty loam	Silty clay

3.3 Water Balance Components

The primary components of the water balance for the cover involve the following: infiltration (precipitation and snowmelt, INF), runoff (R), net percolation (into the shale below the cover, NP), interflow (lateral subsurface flow along the till/shale interface) and actual Evapotranspiration (AET), all in units of mm. The annual rainfall, potential evapotranspiration (PET) and SWE for SBH are shown in Figure 3.2.

These components can be related to changes in soil storage (ΔS) as follows:

$$\Delta S = INF - NP - I - AET \tag{11}$$

where INF is infiltration (precipitation minus runoff), NP is net percolation, I is interflow and AET is actual evapotranspiration (Equation 11). The instrumentation at SBH monitors precipitation,

runoff, interflow and changes in soil storage. Rates of net percolation through the shale have been estimated from field measurements of hydraulic conductivity.

The climate in this region is sub-humid continental, defined by warm summers and cold winters. Over the period of 2000-2015, the average rainfall was approximately 288 mm, the average snow water equivalent (SWE) was 69 mm, and the average potential evapotranspiration was 560 mm (Syncrude SharePoint [accessed 2017]).

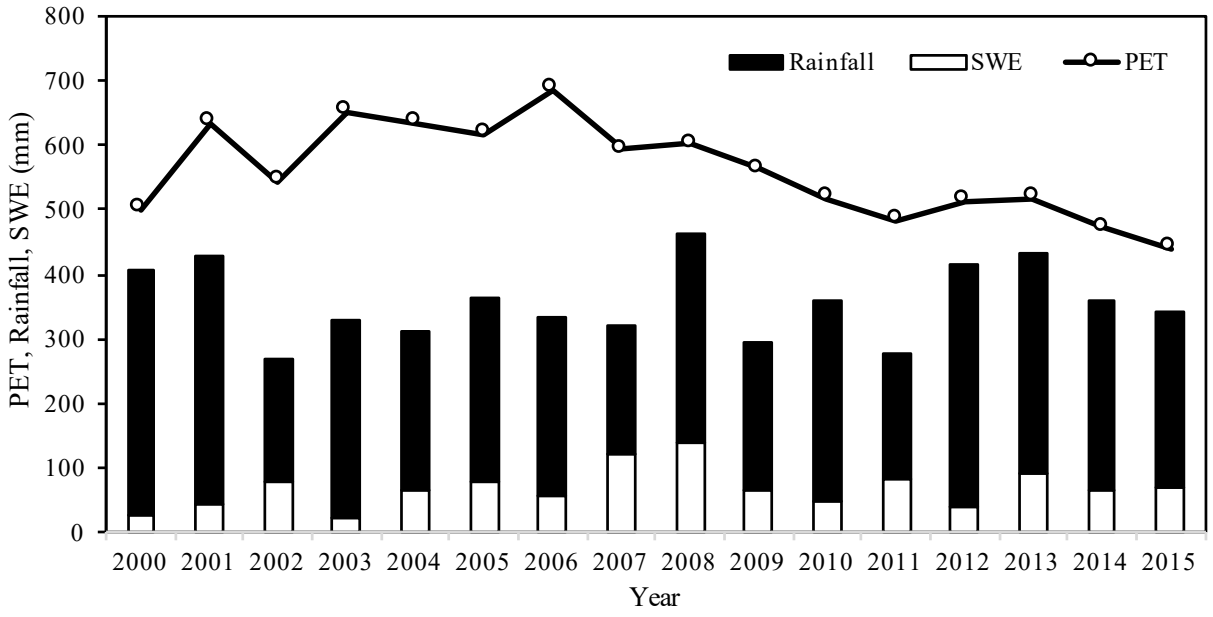

Figure 3.2: Annual rainfall, Potential Evapotranspiration and SWE over time (Syncrude SharePoint [accessed 2017]).

3.4 Winter Processes

Drawing upon observed site data from the 30 dump weather stations, the Cold Regions Hydrological Model platform (CRHM) was used to estimate snowmelt and the snow-water equivalent (SWE) for the period between 2001-2015. CRHM is a modular model that uses tools to develop, support and apply dynamic model routines (Pomeroy et al. 2007). It includes modules describing radiative, turbulent and conductive energy exchanges to snow in open and forest environments.

Snow surveys were conducted on site from 2001-2015 on an arbitrary day during the winter. Using the measured data from the 30-dump weather station, SWE was modelled in CRHM using a module that calculates SWE from snow fall which is based on the precipitation data during the winter and the daily net radiation. For years when the winter precipitation data was not available, the measured SWE was injected gradually over the winter period. Overall, results show that CRHM can reliably characterize the SWE in any given year when compared to the measured SWE (Appendix A; Figure A-1). To validate the snow depth data from CRHM, the measured snow depth data from Environment Canada from the Fort McMurray airport was used as comparison (Appendix A; Figure A-1). Generally, the simulated data was less than the measured depths. It should be noted that the measured snow fall data was observed at the Fort McMurray airport is some distance away from the SBH site, spatially varying snow fall can account for any difference between simulated and measured snow depths.

Snowmelt rate along with SWE controls the duration and intensity of snowmelt and the delivery of water from snow into the soil when it is frozen and during spring melt. CRHM uses the energy equation as the physical framework for snowmelt calculations. It involves the application of the energy equation to a "control volume" of snow as developed by Gray et al. (1988). An example of the cumulative SWE and snowmelt calculated by CRHM for the years 2002 and 2015 is presented in Figure A-2 (Appendix A).

Snowmelt occurs under very different conditions of frozen soil as the depth of freezing in any given year is highly variable (Figure 3.3). For example, in 2003 a small snowpack was recorded resulting in a deep-freezing front extending into the shale, soil thaw was prolonged and occurred well after snowmelt. In 2008, one of the largest snowpacks was recorded with a freezing front only extending 80 cm into the cover soil, snowmelt and thawing of the soil appeared to happen simultaneously. 2005 and 2013 illustrate typical snowpacks and freeze-thaw behavior.

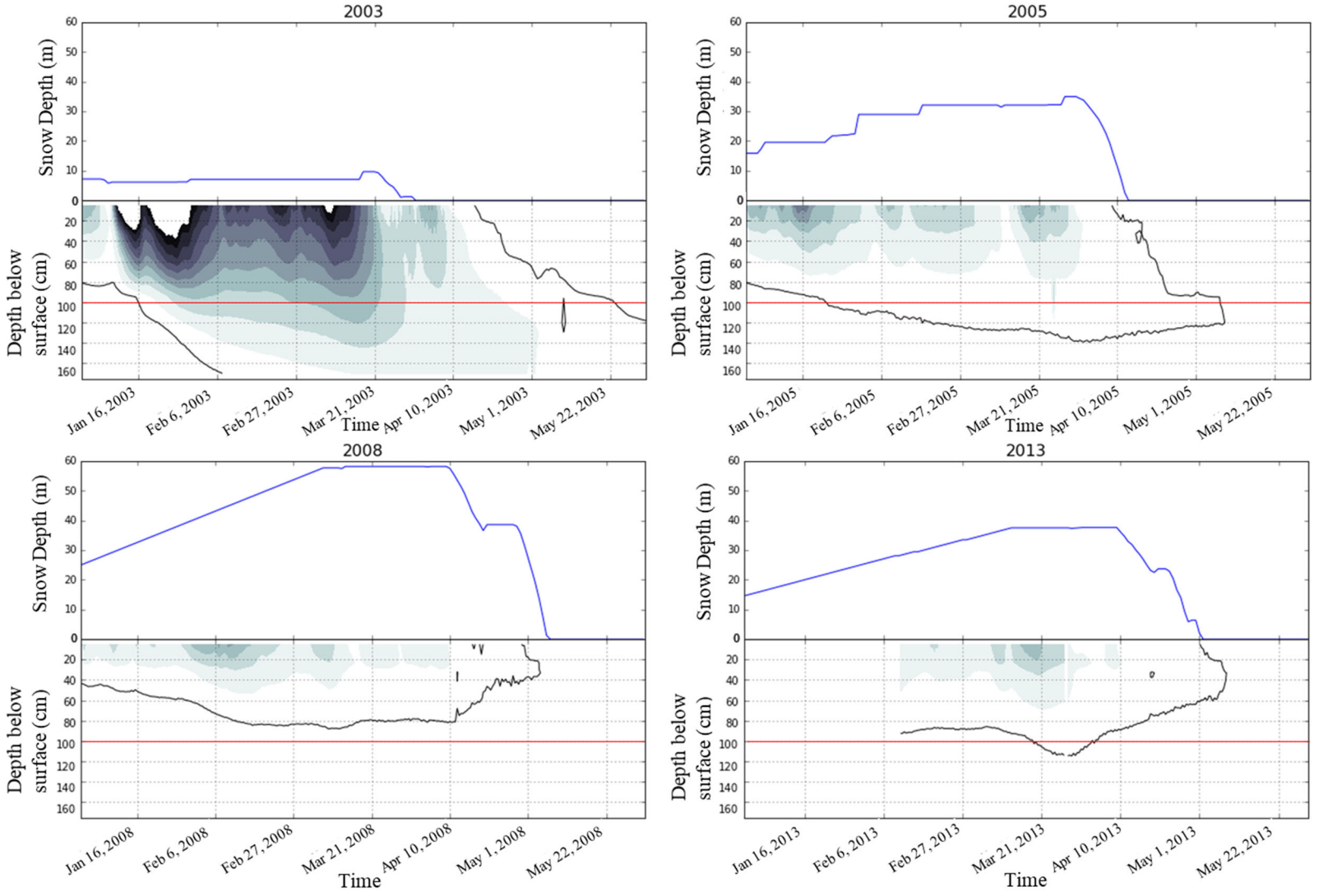

Figure 3.3: Snow Depth vs. Soil Temperature for the years 2003, 2005, 2008 and 2013 (the red line shows the till/shale interface)

3.5 Snowmelt Infiltration

The spring season is a particularly important time at SBH. As temperatures increase, snowmelt and ground thaw contribute to net percolation and the generation of interflow. Net percolation and interflow are the only known mechanisms that can flush soluble salts from the soil cover. It is anticipated that interflow will only provide a potential mechanism for salt flushing and that net percolation may act as the dominant flushing mechanism.

A rough water balance can be observed using pre-melt SWE, change in storage (of the peat and till layers), interflow and average flow from the weir Figure 3.4. These water balance components do not add up well, in 2003 and 2005 the average flow from the weirs exceed the average SWE on the hillslope. In 2007 and 2008, the average SWE on the hillslopes is significant with very little stream flow and storage observed.

The pre-freeze up (fall) and thaw (spring) soil moisture profiles for D3 are presented in Figure A-3 (Appendix A). The data suggests that at the D3 cover, most of the infiltration occurs in the cover soil (upper 100 cm). At the D2 cover, infiltration appears to extend into the shale to depths greater than 35 cm (Appendix A; Figure A-4).

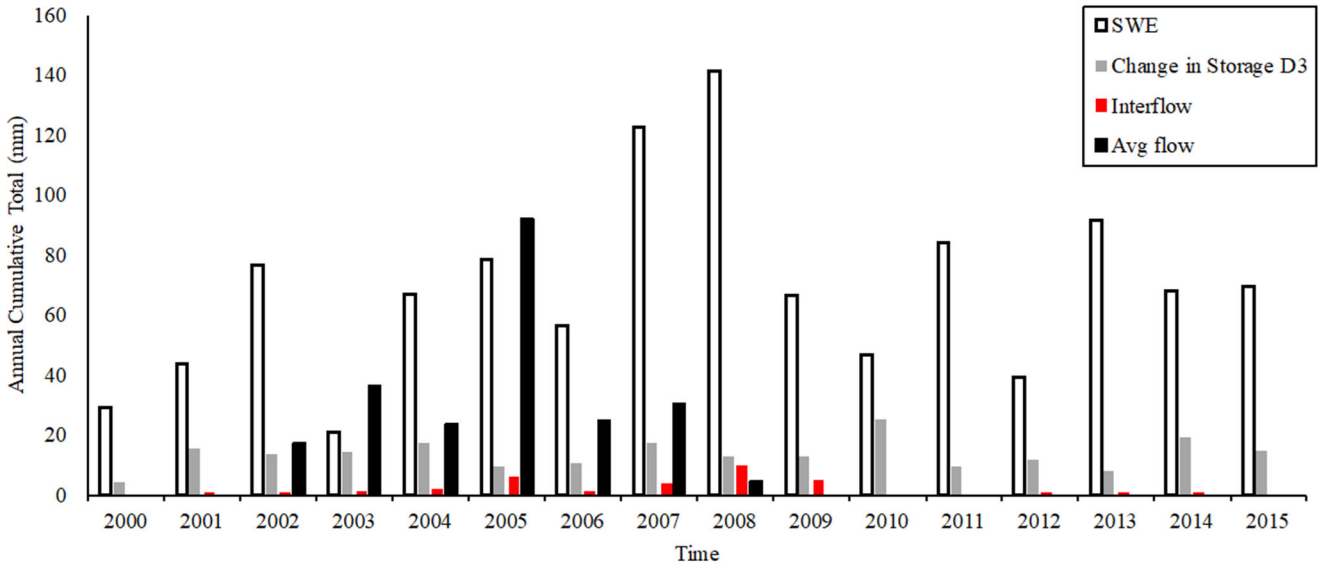

Figure 3.4: Annual cumulative water balance during the spring

Each year snowmelt occurs while the ground is frozen, and the infiltration capacity of the soil matrix is reduced due to pore ice blockage. The snowmelt calculated from CRHM, the start and end date of melt and the start date of interflow generation was plotted against soil temperature for the years 2003, 2005, 2008 and 2013 in Figure 3.5. The data suggests that the initiation of interflow along the till-shale interface is directly correlated to the onset of ground thaw and occurs after snowmelt has begun. Figure 3.6 shows the response in the soil water content as the snowpack depletes. Generally, as the snowpack is melting, there is a response in the water content in the till and upper shale, this could be indicative of melt occurring during frozen soil conditions (suggesting snowmelt may be passing through the macropores) and/or soil thaw increasing the liquid water content.

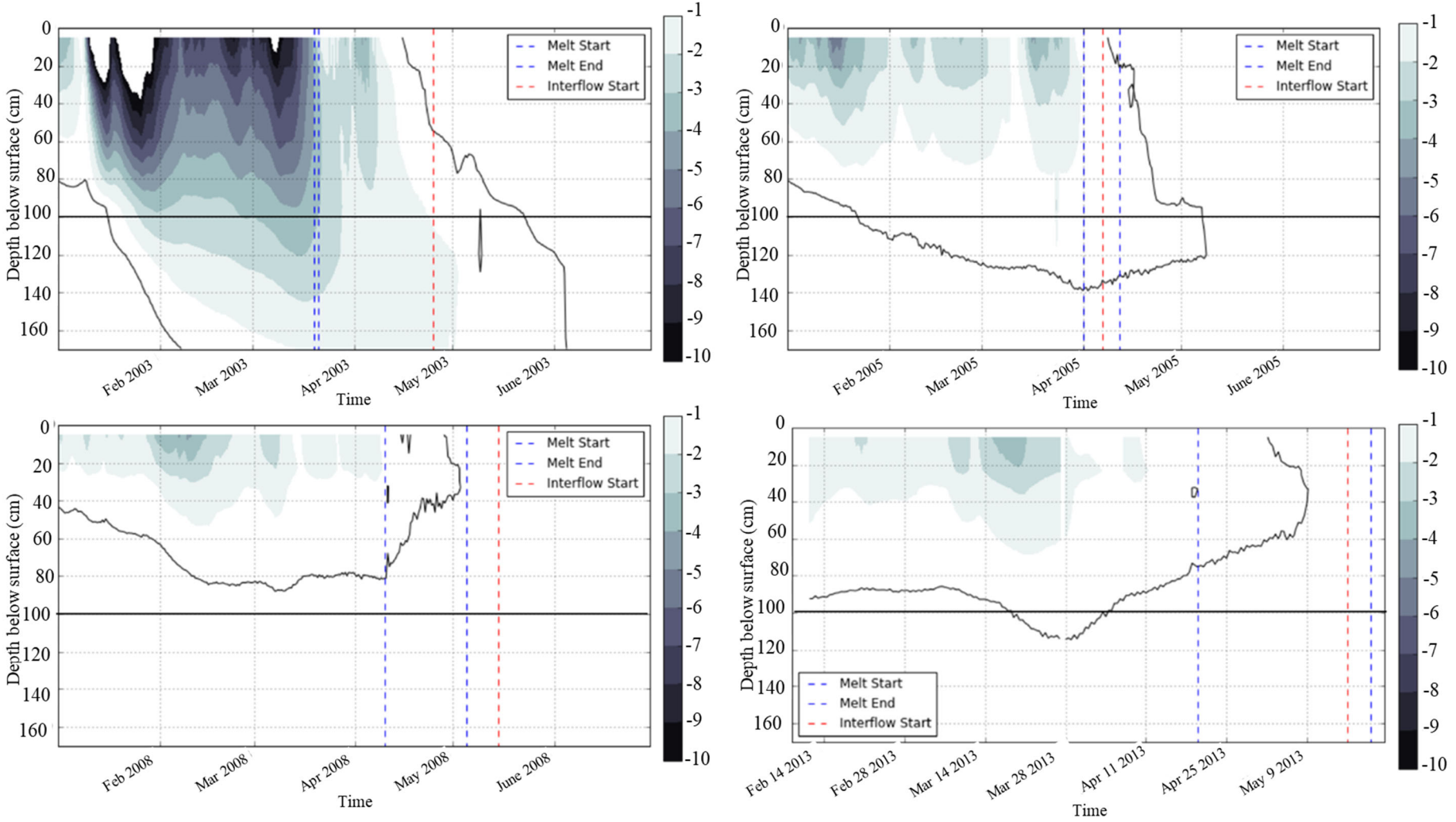

Figure 3.5: Depth Image of Soil Temperature with snowmelt start, snowmelt end and interflow generation date for the years of 2003, 2005, 2008 and 2013 (black line denotes the till-shale interface)

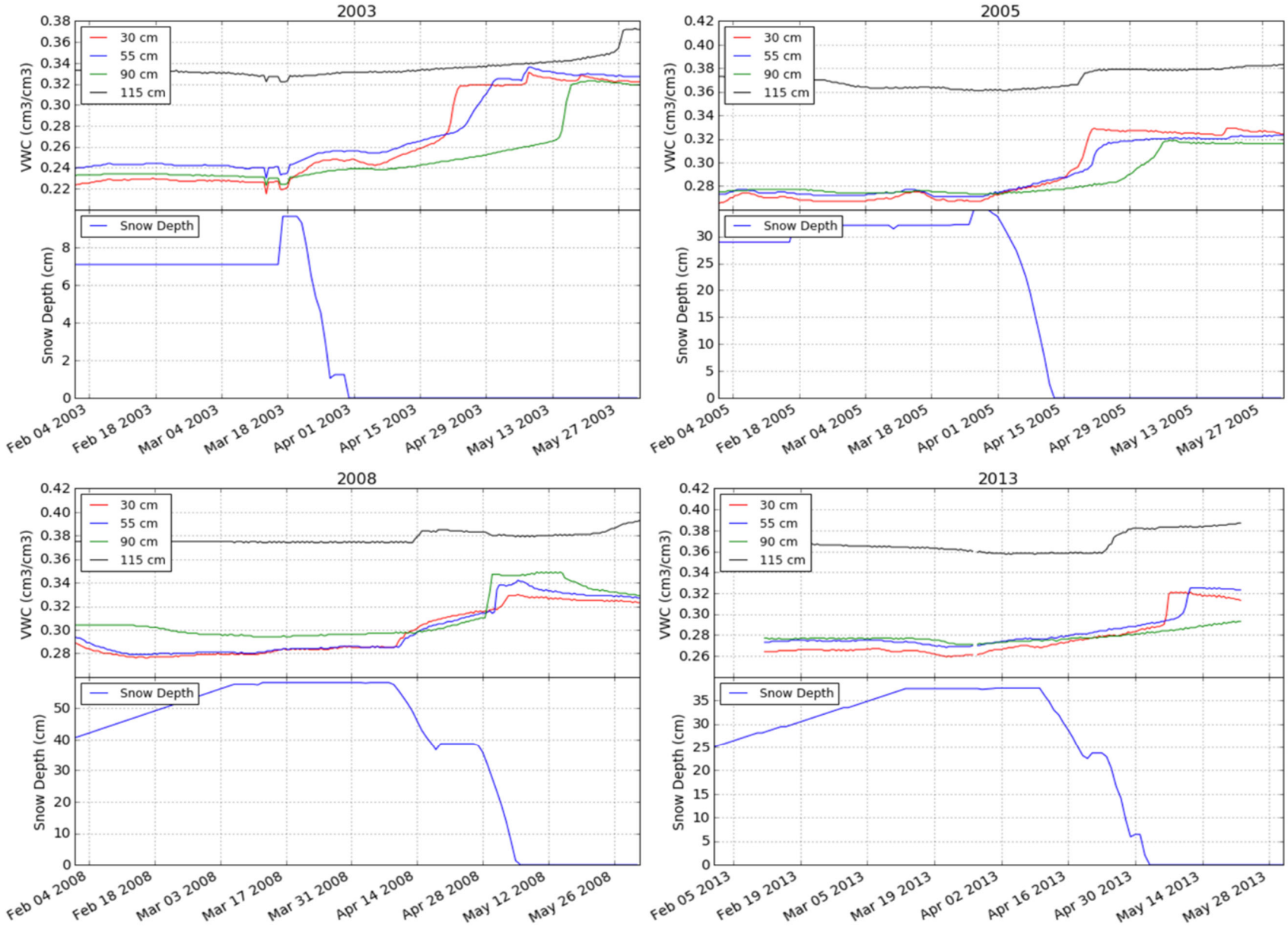

Figure 3.6: VWC for varying depths and Snow depth for the years 2003, 2005, 2008 and 2013

3.6 Soil Water Content & Soil Temperature

Measured soil water contents for the D2 and D3 cover are present in Figure 3.7 and Figure 3.8, respectively. The D1 cover was not included as there was a reinstallation of instrumentation in 2007 and it was not successful in providing continuity with past monitoring trends (O'Kane Consultants 2012). The data denoted by the white circles represent the water contents observed during the winter. A significant dip in the water contents during the winter is observed when the soil moisture probe is not expected to detect the presence of ice. This behavior is observed in both covers. The soil water contents in the upper peat mineral mixture exhibits strong rapid responses to rainfall for both covers. The water contents in the lower till show no significant response to climatic conditions, however, a dip in water content during the winter is observed similarly to the peat mineral mixture. The shale water contents in the thinnest cover, D2, show changes in water content with response to climatic conditions whereas, the shale in D3 appears to be less responsive.

Depth time image of soil temperature is plotted over time for D1, D2 and D3 cover in Figure 3.9, Figure 3.10 and Figure 3.11, respectively. The freezing fronts observed at the D1 and D2 cover appear to remain constant, as the freezing front generally extends down to the depth of monitoring. The soil temperature data from the D3 cover suggest that from the years 2001-2004, the frost penetrated as deep as 1.6 m below the ground surface. From 2005-2011, the frost only penetrated as deep as 1.4 m. In recent years, frost is observed at deep as 1.6 m.

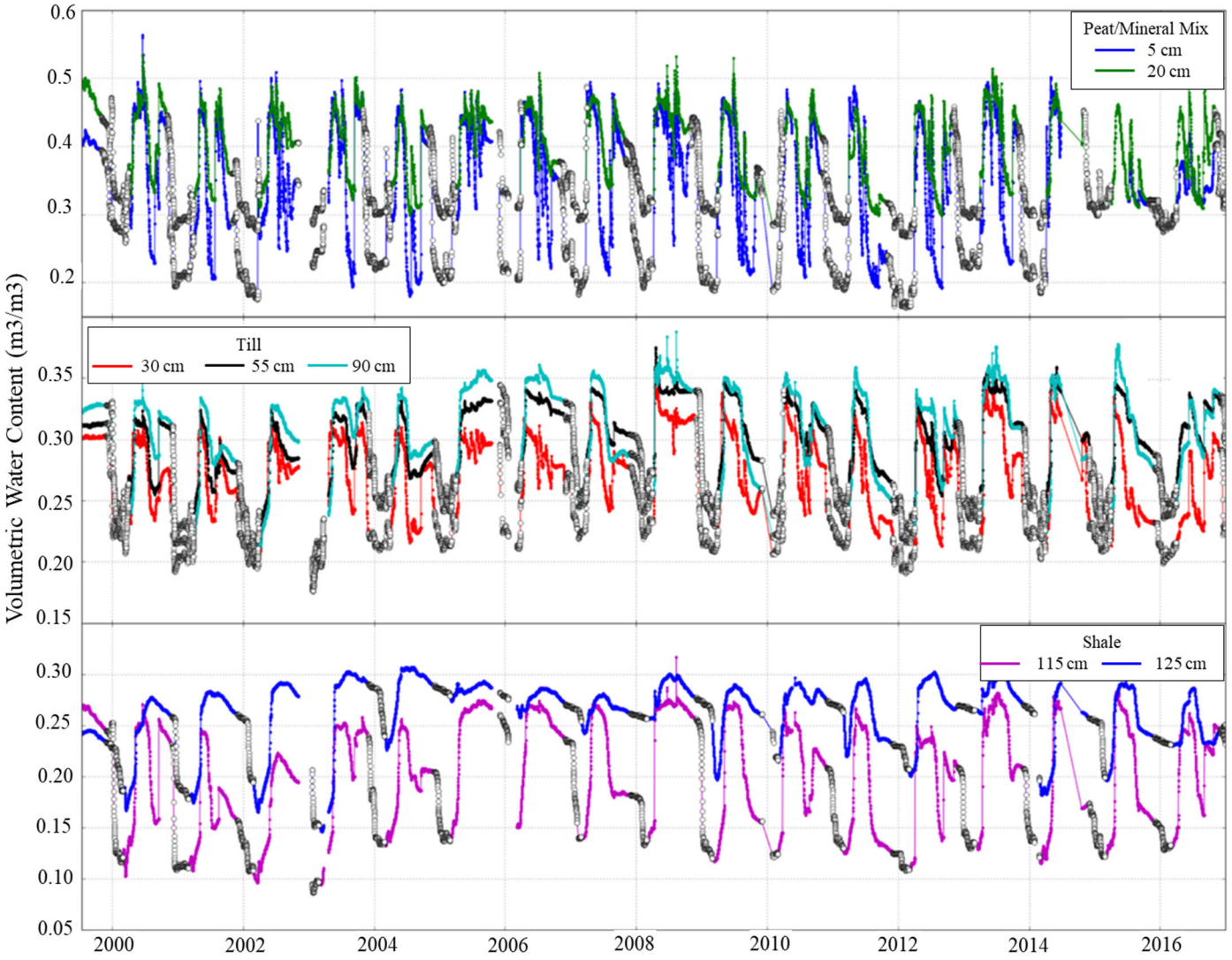

Figure 3.7: Measured water contents at different depths for D2 (white circles denote winter data)

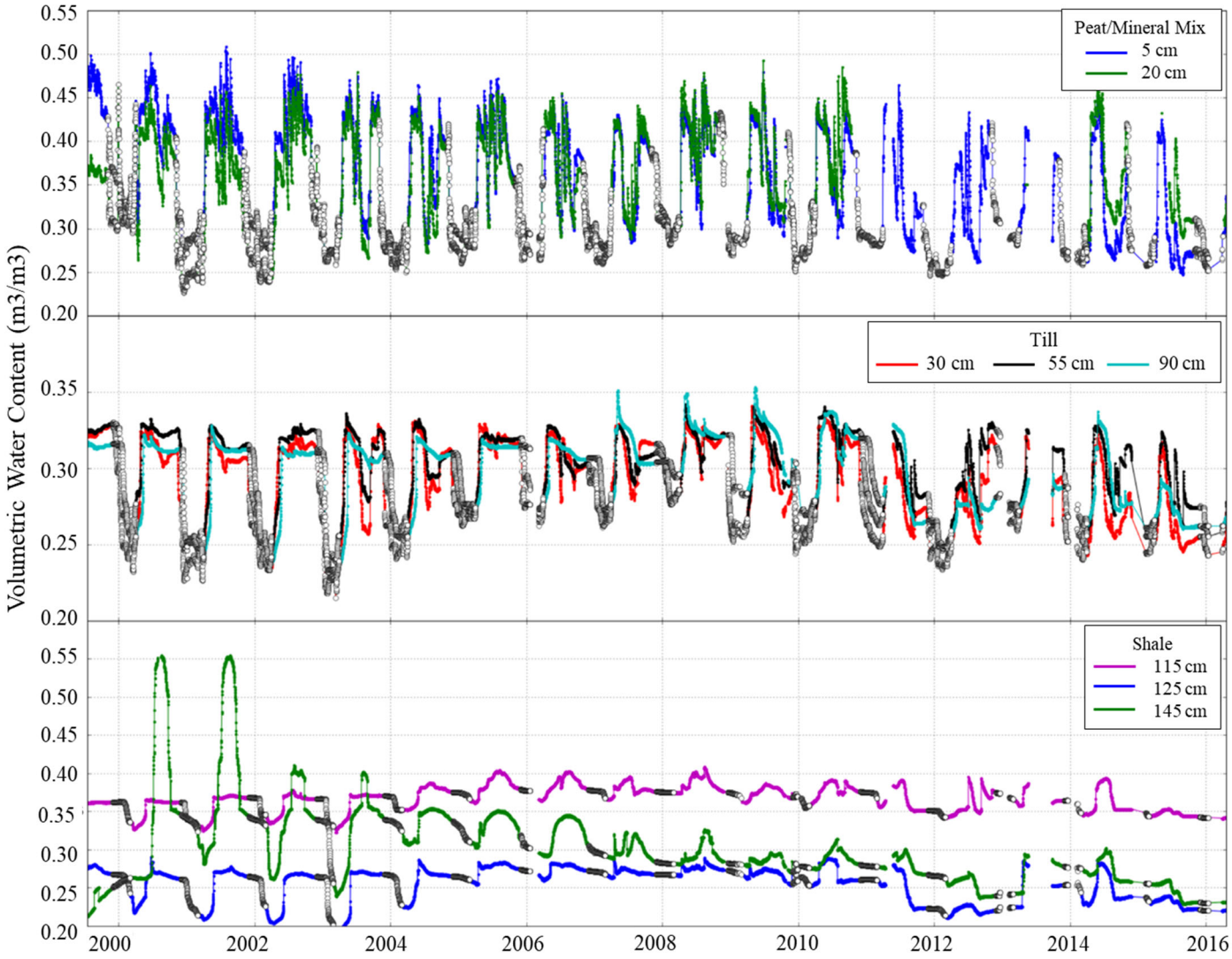

Figure 3.8: Measured water contents at different depths for D3 (white circles denote winter data)

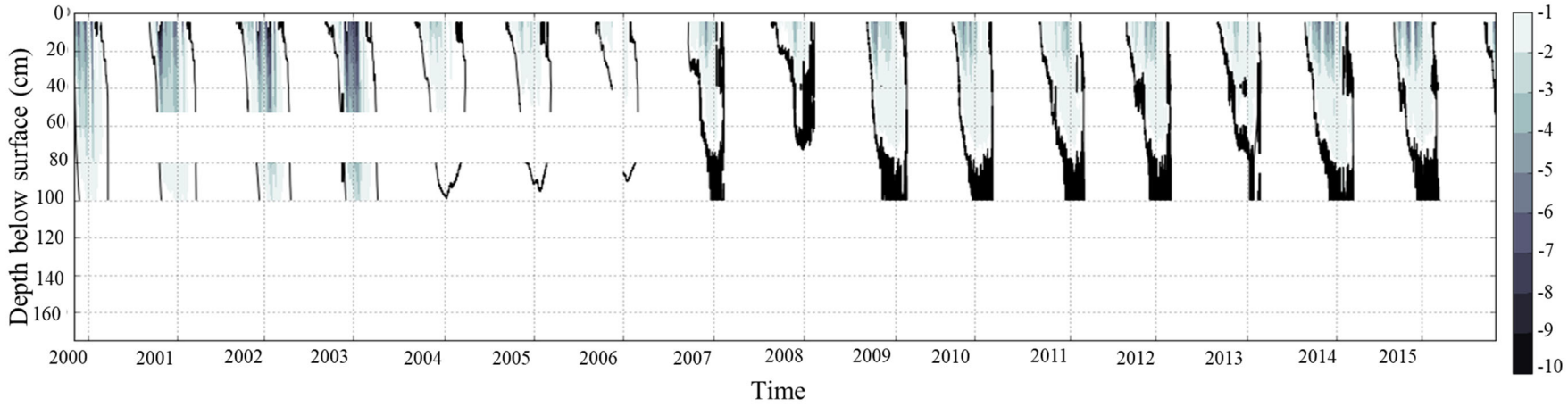

Figure 3.9: Depth-Time image of soil temperature on cover D1

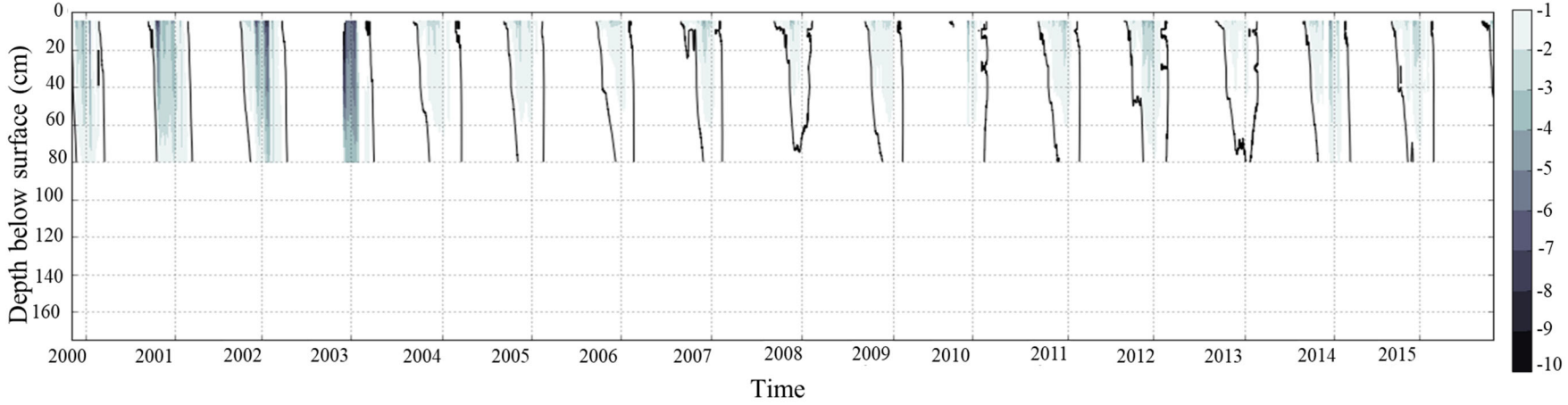

Figure 3.10: Depth-Time image of soil temperature on cover D2

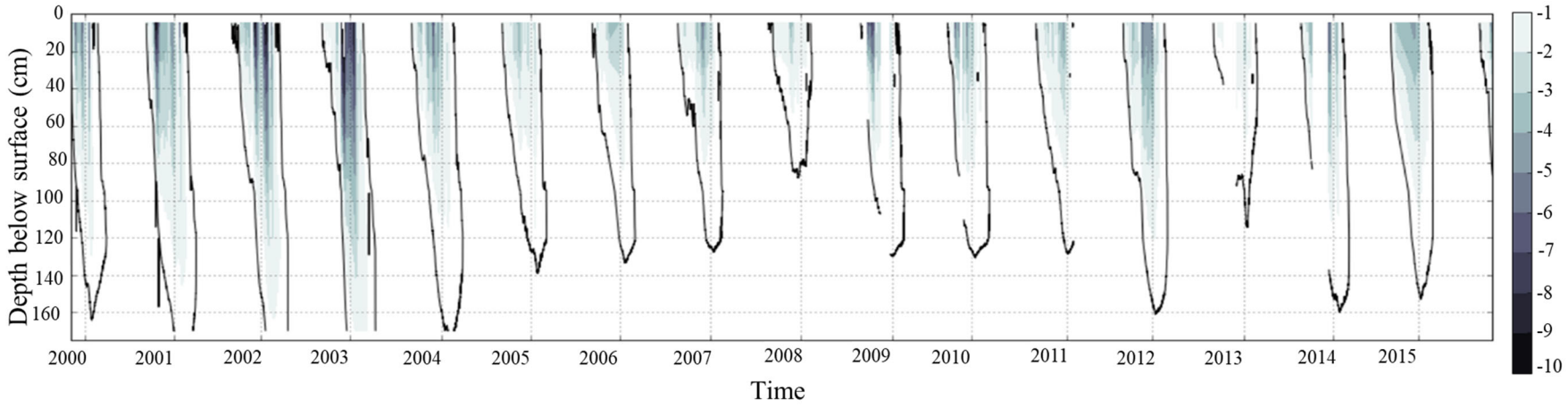

Figure 3.11: Depth-Time image of soil temperature on cover D3

3.7 Interflow

A portion of this data analysis involved developing process hypotheses regarding the controls of interflow. Interflow is defined as gravity driven flow of water that becomes perched along the interface of the cover soil and underlying shale overburden, it is caused by the development of a transient water table that develops on the lower hydraulic conductivity shale (Kelln et al. 2007). This lateral flow of groundwater can carry with it salts that have accumulated above the cover-shale interface.

Initial hypotheses were developed in attempt to explain the mechanisms that controlled interflow. The processes considered were pre-winter soil storage in the cover soil and antecedent moisture conditions at the till-shale interface.

Kelln et al. (2007) used hydrometric and stable isotope of water data to examine the contribution of macropore flow to the hydrological response of the D1, D2 and D3 covers during spring thaw. The data demonstrated that snowmelt water initially infiltrated into the macropores of the frozen cover where it then freezes. This water was then generated as interflow as the cover thawed and the water from the macropores began to mix with the water in the soil matrix forming a perched water table to develop at the cover-shale interface. Generally, higher volumes of interflow were observed in the earlier years and volumes have decreased in more recent years. Based on Kelln's findings, an excess in pre-winter water storage in the cover soil was thought to coincide with higher interflow rates as there would be more available water in the soil matrix with the addition of snowmelt that would promote perched conditions at the interface during snowmelt infiltration.

Rainfall simulation experiments by Redding et al. (2008) on two adjacent plots of contrasting antecedent soil moisture storage on an aspen forested hillslope on the Boreal Plain demonstrated that greater amounts of interflow occurred from the plot with higher antecedent moisture content. Following Redding's work, it is assumed that antecedent moisture conditions at the till-shale interface are thought to control the amount of interflow generated. Higher antecedent moisture conditions at the interface should promote perched water table conditions as higher water contents in the shale would enable ponding since the infiltrability into the shale would be lowered.

3.8 Results and Discussion

Initial hypotheses were developed in attempt to explain the mechanisms that controlled interflow. Interflow data was analyzed and compared to pre-winter soil storage in the cover soil and antecedent moisture conditions at the till-shale interface; as these processes are understood to be the dominant controls infiltrations as presented in Zhao and Gray, 1997. To date, interflow volumes at SBH has varied significantly from year to year since material placement (Figure 3.12). From 2001-2005, the interflow volumes rank as D3 experiencing the largest amount of interflow followed by D2 and D1. From 2006-2009, the volumes correspondingly ranked with cover depth, from D3, D1 to D2. From 2012 to present the covers produce roughly the same amount of interflow. Generally, the higher volumes of interflow (> 1mm/year) that were observed prior to 2010, have not been observed from 2012 onwards.

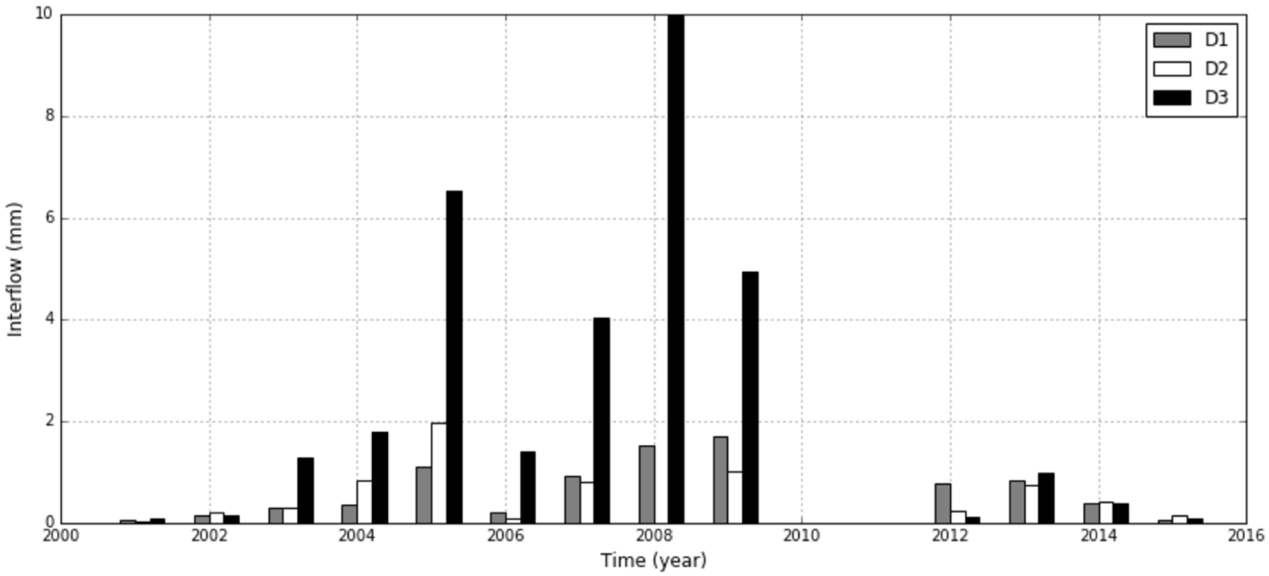

Figure 3.12: Interflow volume over time

Figure 3.13 plots interflow and melt period potential infiltration (SWE plus spring rain). A total SWE of approximately 200 mm exhibits two very difference responses in interflow, the second largest interflow volume was observed at 7 mm however, this same amount of SWE also produced less than 1 mm of interflow, this raises the question of what the additional controlling factor on interflow is.

To determine whether pre-winter storage may be a controlling factor on interflow, Figure 3.14 illustrates the relationship between interflow, melt period potential infiltration (SWE plus spring rain) and pre-winter storage. No unique relationship is observed between interflow and pre-winter storage. However, there appears to be a correlation between the amount of SWE and interflow recorded as the highest amount of interflow observed corresponded to the second highest SWE.

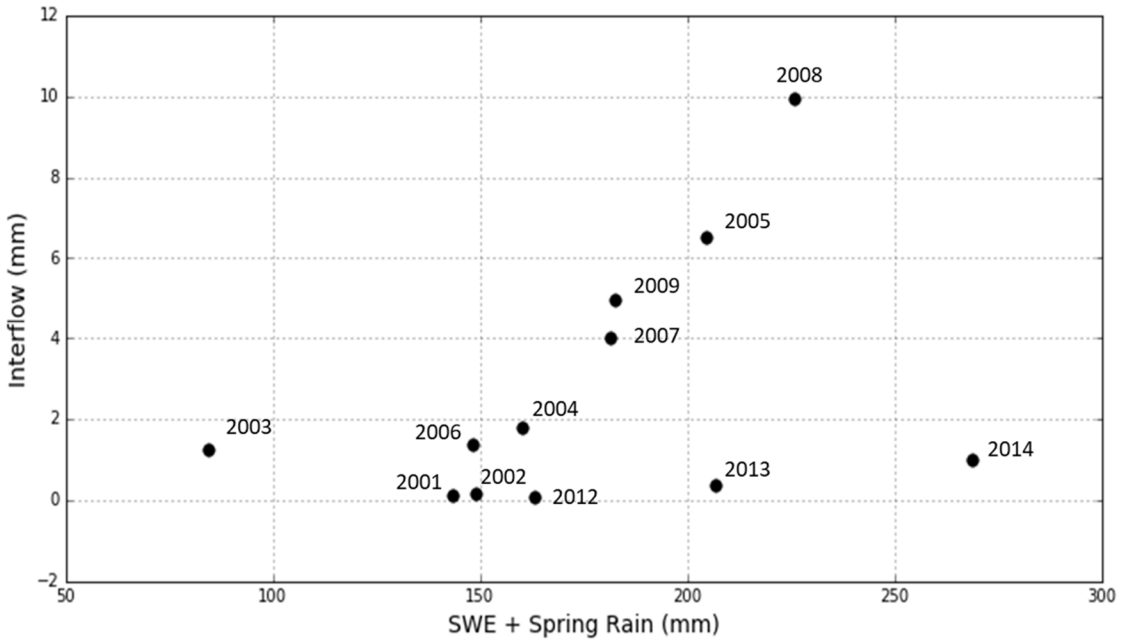

Figure 3.13: Interflow vs. Total SWE

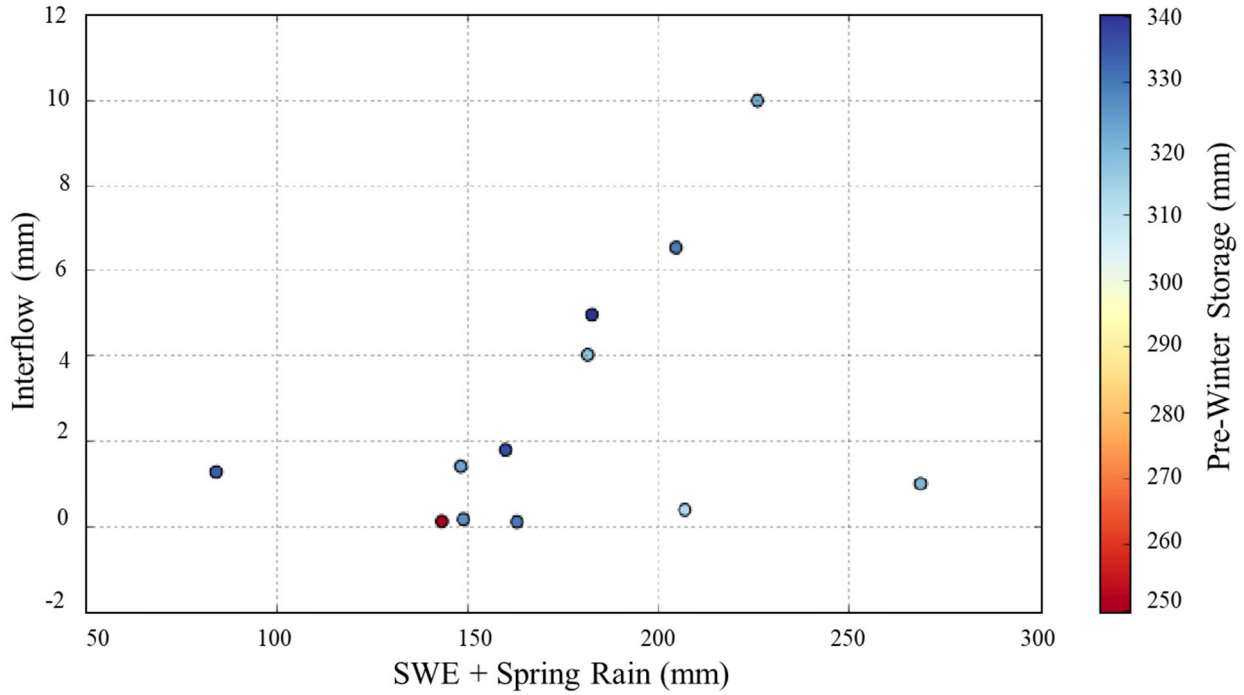

Figure 3.14: Interflow vs. Total SWE as a function of Pre-Winter Storage

It was anticipated that higher antecedent water contents will generate more interflow since soil saturation (or storage) is limited and if there is no capacity to absorb more water, interflow will occur. (Redding et al. 2008; L. T. Zhao et al. 1999). To test if antecedent water conditions at the till-shale interface control interflow, the pre-freeze up till and shale water contents, interflow and total SWE were examined. Figure 3.15 plots interflow against melt period potential infiltration (SWE plus spring rain) as a function of pre-freeze up till and shale water content. Figure 3.16 plots interflow as a function of pre-winter till and shale water content.

The overlying till water content is positively correlated with interflow, corroborating the assumption made by Redding's work (Figure 3.16). However, the underlying shale water content is negatively correlating (drier soils have resulted in more interflow) (Figure 3.16). This behaviour can likely be explained by the behaviour of shale soil under wet vs. dry water contents, where, the hydraulic conductivity of the shale is typically reduced at lower water contents, and since the hydraulic conductivity in the till is higher this results in reduced net percolation capacity in the shale and increased lateral flow capacity (interflow).

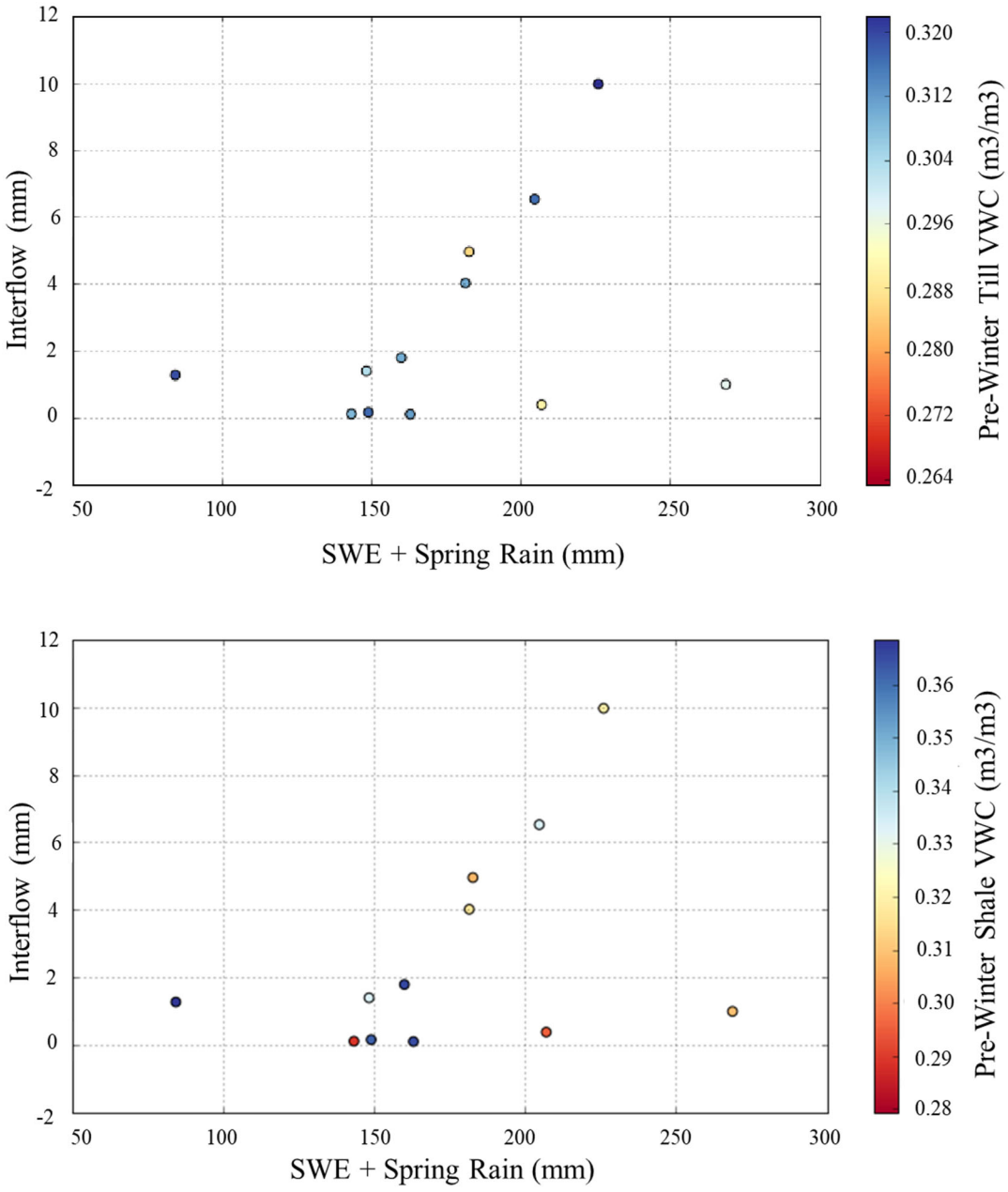

Figure 3.15: Interflow vs Total SWE as a function of pre-winter till water content (top) and pre-winter shale water content (bottom).

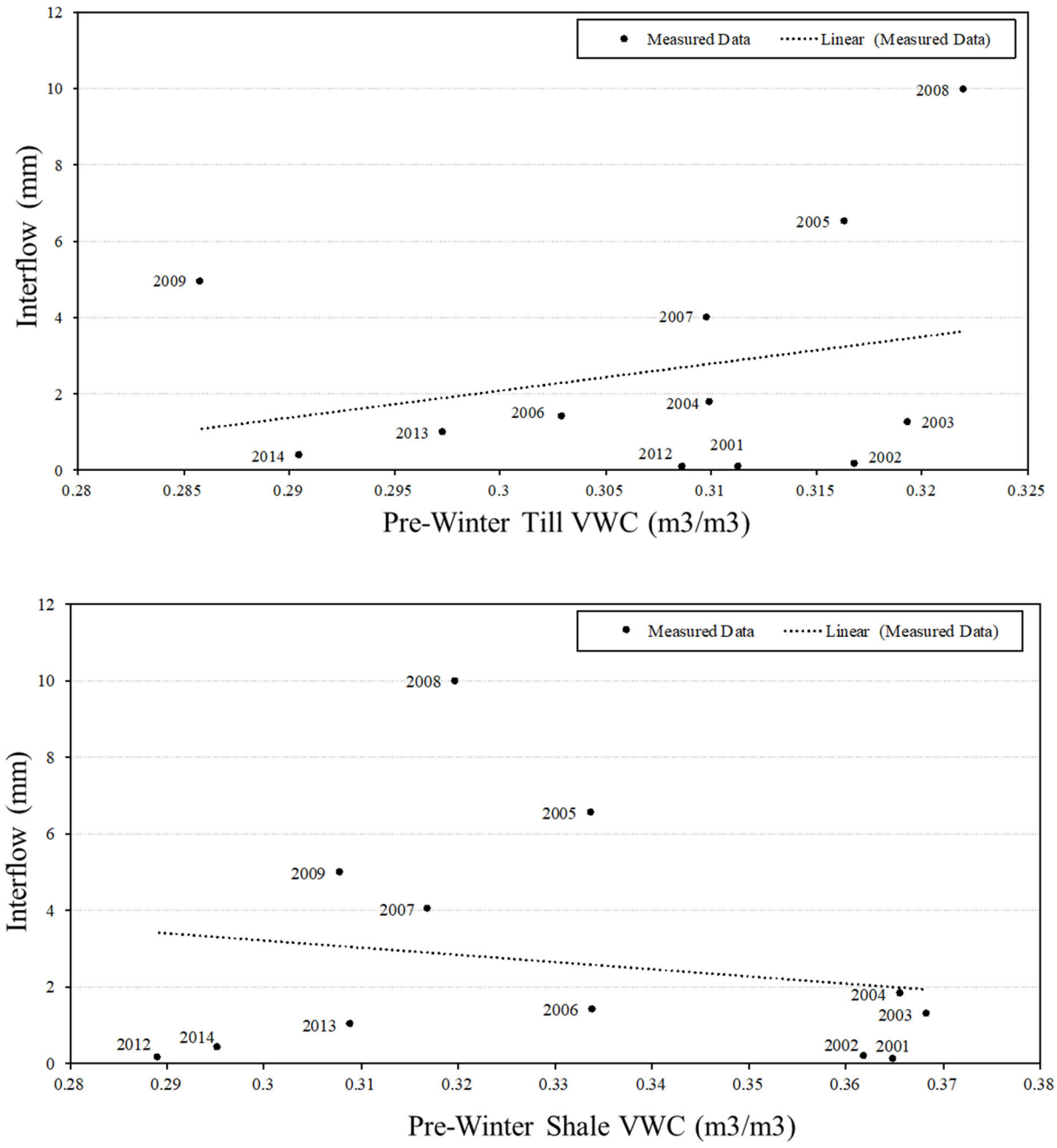

Figure 3.16: Interflow as a function of Pre-Winter Till Water Content (top) and Pre-Winter Shale Water Content (bottom).

Figure 3.17 plots interflow for D1, D2 and D3 as a function of peak SWE and spring rain. Early recorded interflow data from 2001-2008 all plot on different lines for each cover (denoted with black markers). However, measurements made from 2009-2015 all plot on a similar low-slope line which represents lower interflow volumes (denoted with red markers). Presenting the same data in Figure 3.18 for the D3 cover, it can be observed that in the years 2005 and 2013, similar snowpacks were measured but very different responses in interflow were observed, 6.5 mm and 0.99 mm, respectively.

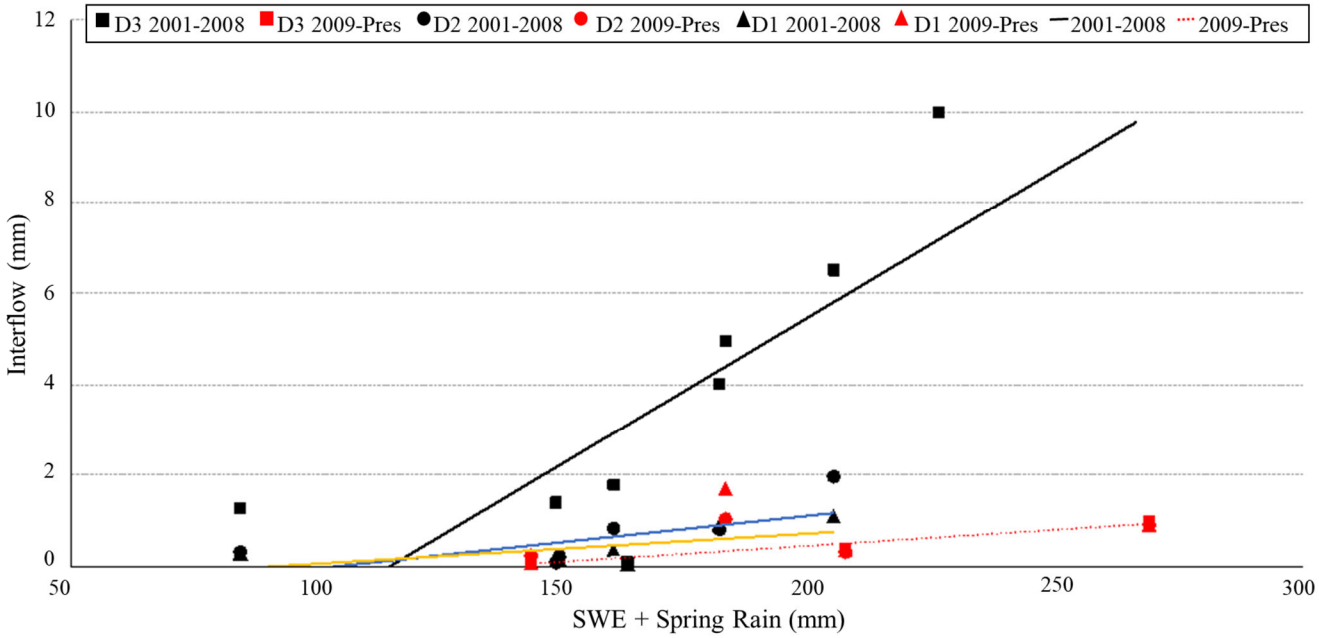

Figure 3.17: Yearly interflow volumes for D1, D2, D3 as a function of the peak SWE and spring rain.

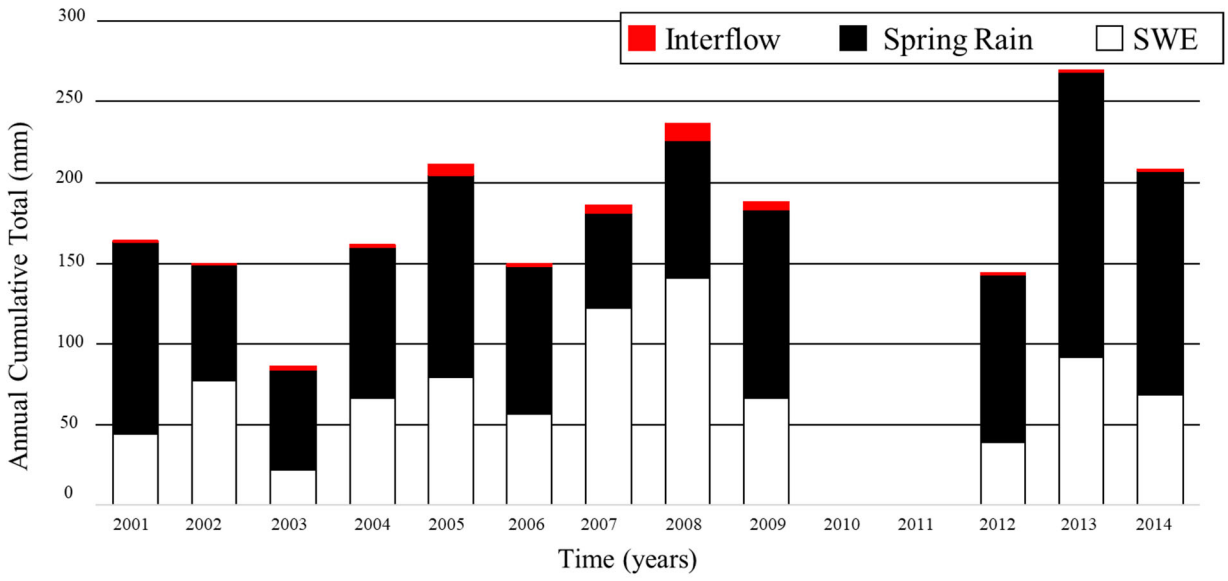

Figure 3.18: Contribution of SWE, Spring Rain & Interflow over time

Leaf area index (LAI) represents the amount of leaf material in ecosystems and is an important metric for assessing vegetation growth. LAI data is available for the plateau on SBH. The saplings on the covers were planted 2-3 years prior to the plateau so it is necessary to assess if the vegetation matured at a similar rate between the plateau and hillslope covers to determine if the plateau LAI can be applied to the hillslope. Vegetation growth on the plateau and hillslopes can be interpreted from the wind speeds data collected from the anemometers. The anemometers on the hillslope and plateau were not installed above the vegetation, so as wind speeds decreased vegetation correspondingly increased. Figure 3.19 plots the average daily wind speeds observed on the plateau and D2 cover, these data suggests that the vegetation on the covers most likely took off at the same time as they did at the plateau. Between 2008 and 2009, the wind speeds decreased significantly at both stations from prior years which corresponds to an increase in LAI measured at the plateau (Figure 3.20). This could explain the different interflow responses in 2005 and 2013 since the LAI was lower in 2005, it is expected that there would have been less evapotranspirative demand from the vegetation and therefore more water would be available to generate as interflow. It can be observed that interflow has decreased relative to increasing LAI which suggests that interflow could be impacted by site vegetation maturity.

Redding et al. (2008) used rainfall simulation experiments to examine lateral flow thresholds for an aspen-forested hillslope. They concluded that lateral flow generation from uplands is a function of precipitation intensity, available soil moisture storage capacity and soil permeability. This study concluded that significant lateral flow (>1mm) did not occur for precipitation events with return periods of less than 20 years. Interflow at SBH is decreasing as the vegetation is maturing, and based on the findings by Redding, it is possible that interflow may be an infrequent process on an aspen-forested hillslope that is a function of precipitation intensity, soil storage capacity and permeability.

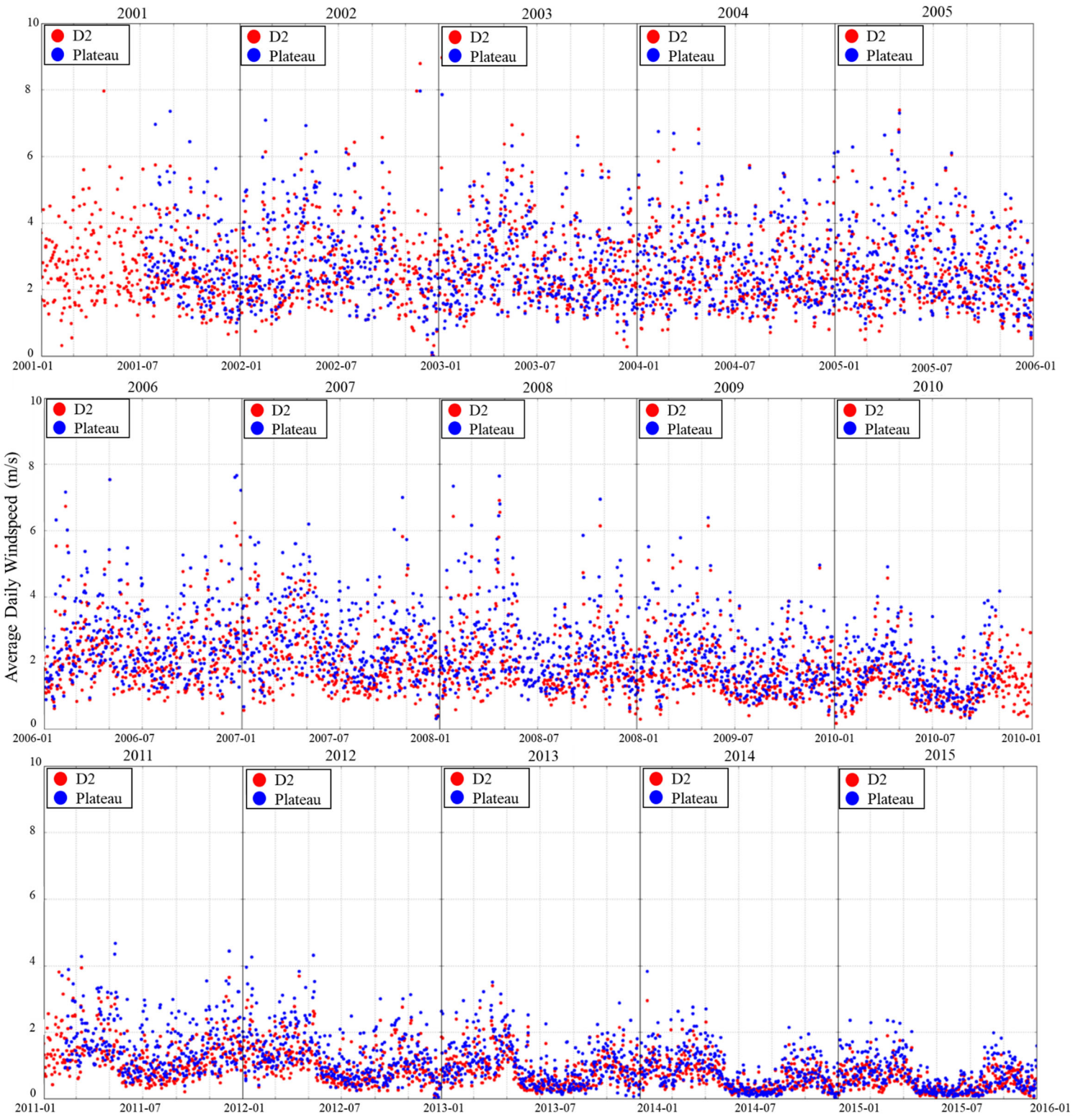

Figure 3.19: Average daily wind speeds for the D2 cover and plateau stations

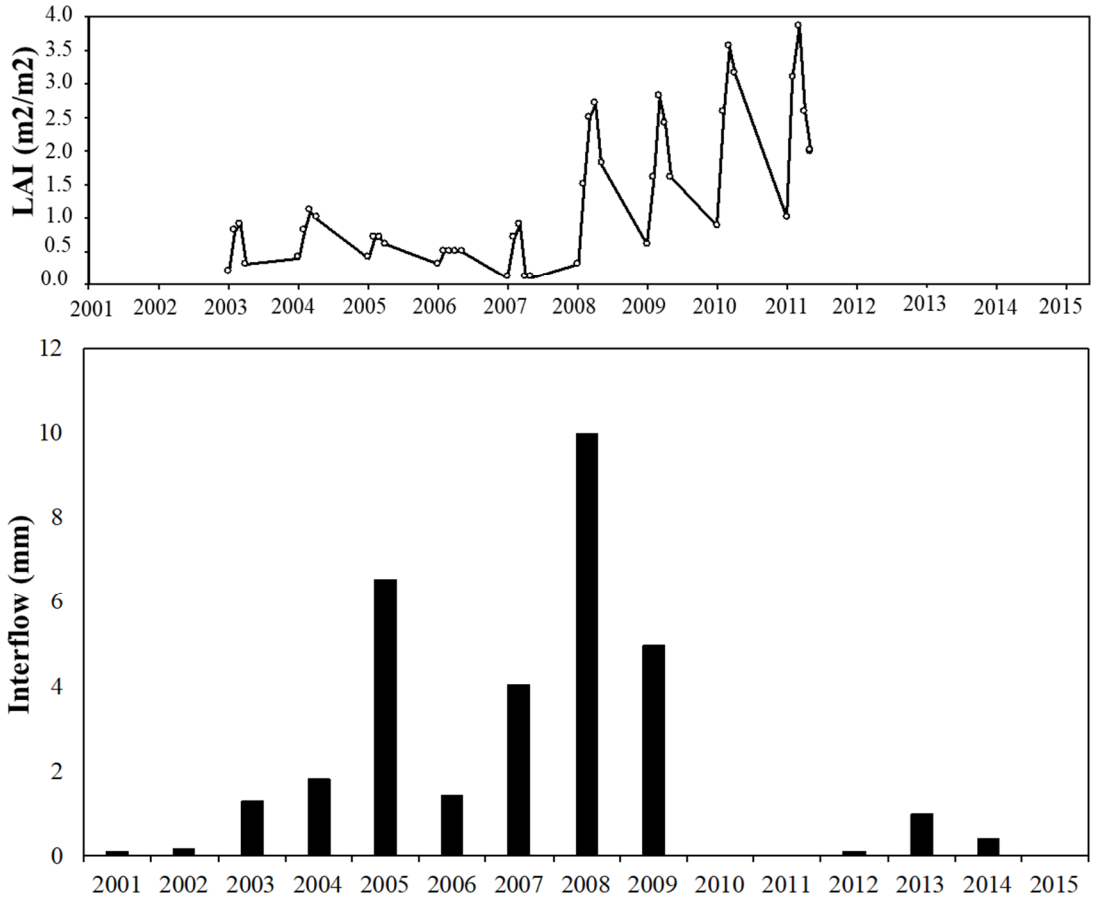

Figure 3.20: Leaf area index (LAI) & Interflow for D3 over time

3.9 Conclusion

Data analysis was conducted for the data available at SBH. Through this analyses and past research, hypotheses were developed regarding the mechanisms that controlled interflow.

Interflow flow data was compared against melt period potential infiltration (SWE plus spring rain) and surface water content in the fall (understood to be the dominant controls on infiltration; Zhao et al. 1999), and no unique relationship was observed. This suggests that the controls on infiltration are more complex than the simple model presented by Zhao and Gray (1999). However, different patterns of interflow generation are apparent with time. Prior to 2010, interflow followed a simple relationship with melt period potential infiltration (i.e., the highest amount of interflow observed corresponded to the second highest melt period potential infiltration), independent of water content

After 2010, interflow significantly decreased due to enhanced vegetation cover and evapotranspiration (increase in LAI).

Interflow was likely an important flux in earlier years and may have resulted in early flushing of salt from the profile however, in later years due to the change in profile (LAI), interflow and associated flushing is heavily reduced. For the purpose of this research and on the basis of the data analysis described herein, interflow is interpreted to act as a marginal flux when there is a well-established vegetation cover and subsurface flow and transport processes at this site can be represented by a 1D model as described in Section 4.1

4 NUMERICAL MODEL DEVELOPMENT AND RESULTS

A two-dimensional conceptual model for the understanding of the flow and transport processes was described in Section 3. This conceptual model was revised to represent the system as one-dimensional for the model simulations based on the data analysis described in Section 3 that showed that interflow is negligibly small when there is an established vegetation cover which justifies the assumption that subsurface flow and transport processes at the site can be represented by a one-dimensional model (further discussed in Section 4.1). From there, a one-dimensional coupled heat, water and solute transport model was constructed for the SBH site using the Geoslope® finite element software package SEEP/W (for water flow) coupled with CTRAN/W (for solute transport). The primary objective of the numerical modelling in this study was to gain a better understanding of how snowmelt infiltration, under varying assumptions, effects the accumulation and transport of sulfate within the cover. There were three uncertainties in attempting to understand this problem: uncertainty in the models and data used to quantify snowmelt infiltration, uncertainty of the future climate at SBH, and uncertainty in how much salt will be produced by oxidation of pyrite in shale and for how long. Several model scenarios were developed to address these range of uncertainties and are described in detail herein. This section details the revised conceptual flow model that was used to build the one-dimensional model, model configuration, modelled scenarios and results.

4.1 Revised Conceptual Flow Model

A conceptual model for the understanding of the flow and transport processes was described in Section 3. The conceptual model presented in Section 3 (Figure 3.1) is a two-dimensional hillslope model where perched conditions resulting in interflow are generated at the shale-till interface following snowmelt.

The feasibility of simulating the partitioning of snowmelt/rainfall into runoff versus infiltration and the partitioning of percolation into deep percolation versus interflow on the shale-till interface using two-dimensional numerical models was investigated. The two-dimensional model was unable to simulate interflow in a realistic manner, which requires partitioning of the percolation flux at the base of the till layer between deeper net percolation and interflow. However, the data

analysis described in Section 3, showed that interflow is negligibly small when there is an established vegetation cover. This justifies the assumption that subsurface flow and transport processes at the site can be represented by a one-dimensional model as shown in Figure 4-1.

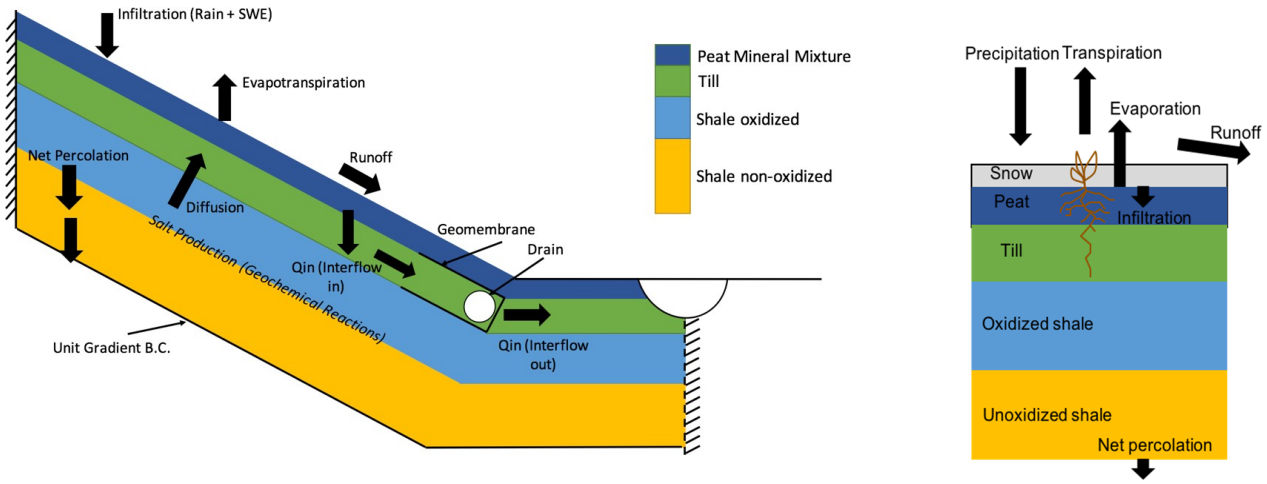

Figure 4-1. Original (left) and revised (right) conceptual model of dominant flow and transport processes at SBH.

4.2 Model Overview and Configuration

The following sections provide an overview of the basis for model configuration and geometry, material types and associated properties, boundary conditions and modelled scenarios.

4.2.1 Modelled Section

A one-dimensional solute transport model was constructed for the SBH site using the Geoslope® finite element software package SEEP/W (for water flow) coupled with CTRAN/W (for solute transport). This study only focused on the D3 cover which represents an optimal cover thickness at SBH (Huang et al. 2015). The development and assessment of the numerical modelling was based on the field monitoring data from 2001 to 2015. The model also includes: layered and time evolving hydraulic properties (hydraulic conductivity) of the hillslope construction material (Section 4.2.2), vegetation properties which vary seasonally and inter-annually, both of which are well characterized with field observations (Section 4.2.3); a lateral free drainage boundary condition to represent interflow (if applicable) at the till/shale interface; winter processes of

snowmelt and infiltration into frozen soils (Section 4.2.4); geochemical processes that generate sulfate salts, that have been characterized by Wall (2005) and Hilderman (2011) (Section 4.2.5).

The model domain was a 7.02 m deep profile, including 0.02 m of mulch cover, 0.2 m peat-mineral mixture, 0.8 m of glacial clay till, 0.5 m of oxidized shale, and 5.5 m of non-oxidized shale. The spatial discretization size was 0.4 cm for the mulch cover, 1.0 cm for the peat-mineral mixture, glacial clay till, and oxidized shale, and 6.5 cm for the deep non-oxidized shale. The temporal step was set to 1/50 day. The monitoring nodes within the model were located at the following soil depth locations, 5, 20, 30, 55, 90, 115, 125, 145 and 170 cm (Figure 4-2).

For the solute transport model, sulfate was modelled as the solute of interest as it is the dominant anion released from the shale but is rarely adsorbed by clay particles except under low pH conditions and is generally considered conservative within pore water (Huang, Hilderman, et al. 2015).

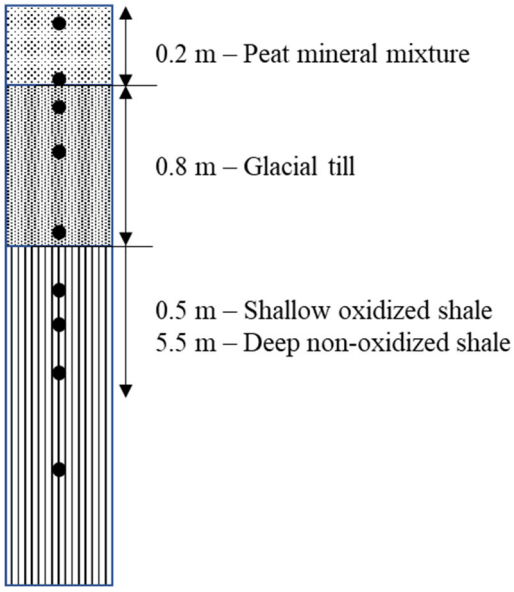

Figure 4-2. Schematic of D3 cover. Black circles represent monitoring nodes.

4.2.2 Material Parameters

As noted in Section 3.2, previous research at the SBH site has helped to interpret various parameters needed to characterize the salt and water dynamics in the cover and underlying shale. These parameters include but are not limited to: hydraulic conductivity (G. Meiers et al. 2006),

effective diffusion coefficient (G. Meiers et al. 2006), pyrite oxidation rate in the shale (Nichol et al. 2006), sulfate production rate (Appels et al. 2017; Huang et al. 2015), and interflow mass transport rates (Kelln et al. 2009).

A bi-modal SWCC (i.e., wetting curve) was used to describe the volumetric water content functions for the peat-mineral mixture, glacial clay till, and oxidized shale. A single porosity SWCC was used for the deep non-oxidized shale. The SWCC for each material is shown in Figure 4-3.

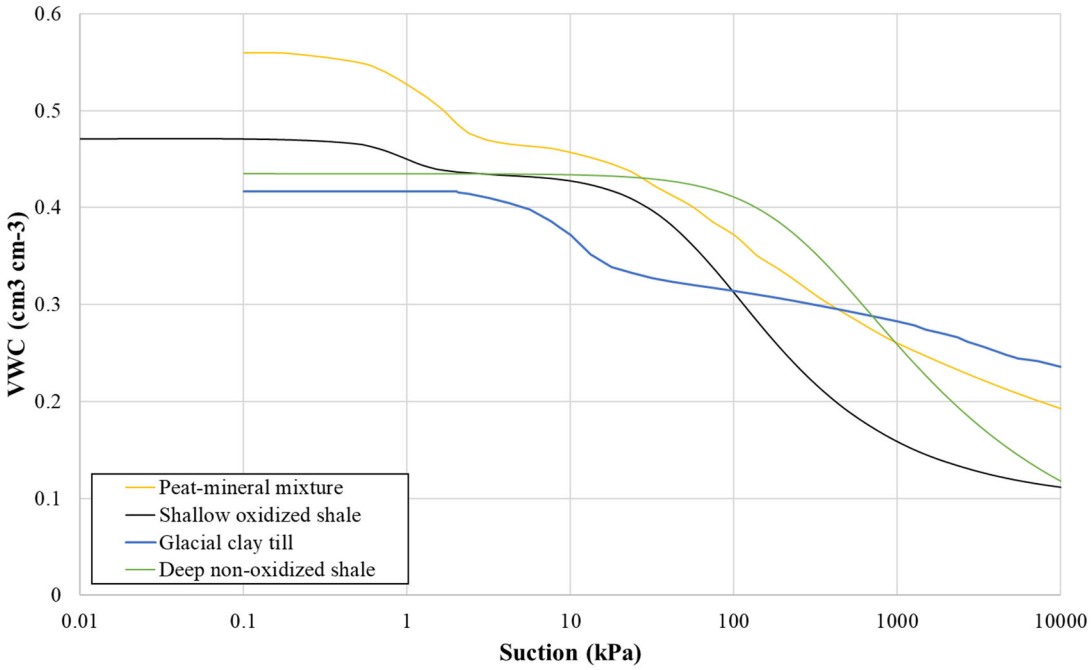

Figure 4-3. Soil water characteristic curve for each material.

The unsaturated hydraulic conductivity functions (K(h)) for each material was estimated using the measured saturated hydraulic conductivity (K_s) values (G. Meiers et al. 2006) and van Genuchten-Mualem equations (van Genuchten 1980). Table 4-1 provides the measured and fitted parameters of the van Genuchten-Mualem equations for each material. The K(h) relationship for each material, based on the constant K_s assumed for each material, is shown in Figure 4-4.

The K_s values of cover materials increased by one to two orders of magnitude over the first five monitoring seasons (2001-2005), while the K_s of the shallow oxidized shale increased

approximately one order of magnitude over the same time. The WRC were assumed to remain constant during the study period as no significant change was observed. The temporal variations of K_s in the first five seasons (2001–2005) were incorporated into the simulations to calculate hydraulic conductivity using the van Genuchten-Mualem equations (van Genuchten 1980), while the value of Ks was treated as a constant after 2005 (i.e., through to the end of model simulation, 2064).

The modelled assumed the same K_s function for the shale from 2005 to end of simulations. This is a simplified assumption as the physical characteristics of the shale are expected to evolve over time (e.g., Plasticity of shale varies with water content; Ks can decrease or increase depending on swelling and fracturing).

Table 4-1. Measured and fitted soil hydraulic and thermal properties for the modelled materials.

Soil Parameters	Model Year	Peat-mineral mixture		Glacial clay till		Oxidized shale		Non-oxidized shale	Source
Suction range (cm)	2001-2064	<= 23	> 23	<= 113	> 113	<= 112	> 112		Fitted
Saturated soil water content (Θ_s) (cm^3cm^{-3})	2001-2064	0.560	0.502	0.417	0.382	0.446	0.446	0.435	Measured[1]
Residual soil water content (Θ_r) (cm^3cm^{-3})	2001-2064	0.393	0.053	0.301	0.063	0.093	0.093	0.019	Fitted
Inverse of the air-entry value (α) (cm^{-1})	2001-2064	0.074	0.007	0.012	0.015	0.002	0.002	0.004	Fitted
Empirical shape-defining parameter of the pore-size distribution (N)	2001-2064	1.991	1.184	2.319	1.078	1.546	1.546	1.403	Fitted
Saturated hydraulic conductivity (K_s) (ms^{-1})	2001	4.00E-05		2.00E-06		1.00E-08		1.80E-09	Measured[2]
	2002	4.70E-05		2.80E-06		3.00E-08		1.80E-09	
	2003	4.80E-05		3.50E-06		3.00E-08		1.80E-09	
	2004	5.00E-05		4.00E-06		3.00E-08		1.80E-09	
	2005-2064	6.00E-05		4.30E-06		3.00E-08		1.80E-09	
Soil thermal conductivity ($kJ\ d^{-1}\ m^{-1}\ K^{-1}$)	2001-2064	95.0		113.2		141.7			

Soil Parameters	Model Year	Peat-mineral mixture	Glacial clay till	Oxidized shale	Non-oxidized shale	Source
Soil specific heat capacity ($kJ\ d^{-1}\ m^{-1}\ K^{-1}$)	2001-2064	600.0	950.0	1047.0		Measured or calibrated[3]

Notes:

1. From Boese (2003) and Shurniak (2003).
2. From Meiers et al. (2011).
3. Thermal conductivity for the peat-mineral mixture, glacial clay till, and shale were from the measured values presented in Zhao et al. (2018), Alrtimi et al. (2014) and Pasquale et al. (2011), respectively. The specific heat capacity for the peat-mineral mixture and glacial clay till were from the calibrated values presented in Shurniak (2003); the specific heat capacity for the shale is from the measured values presented in Brandt (2008).

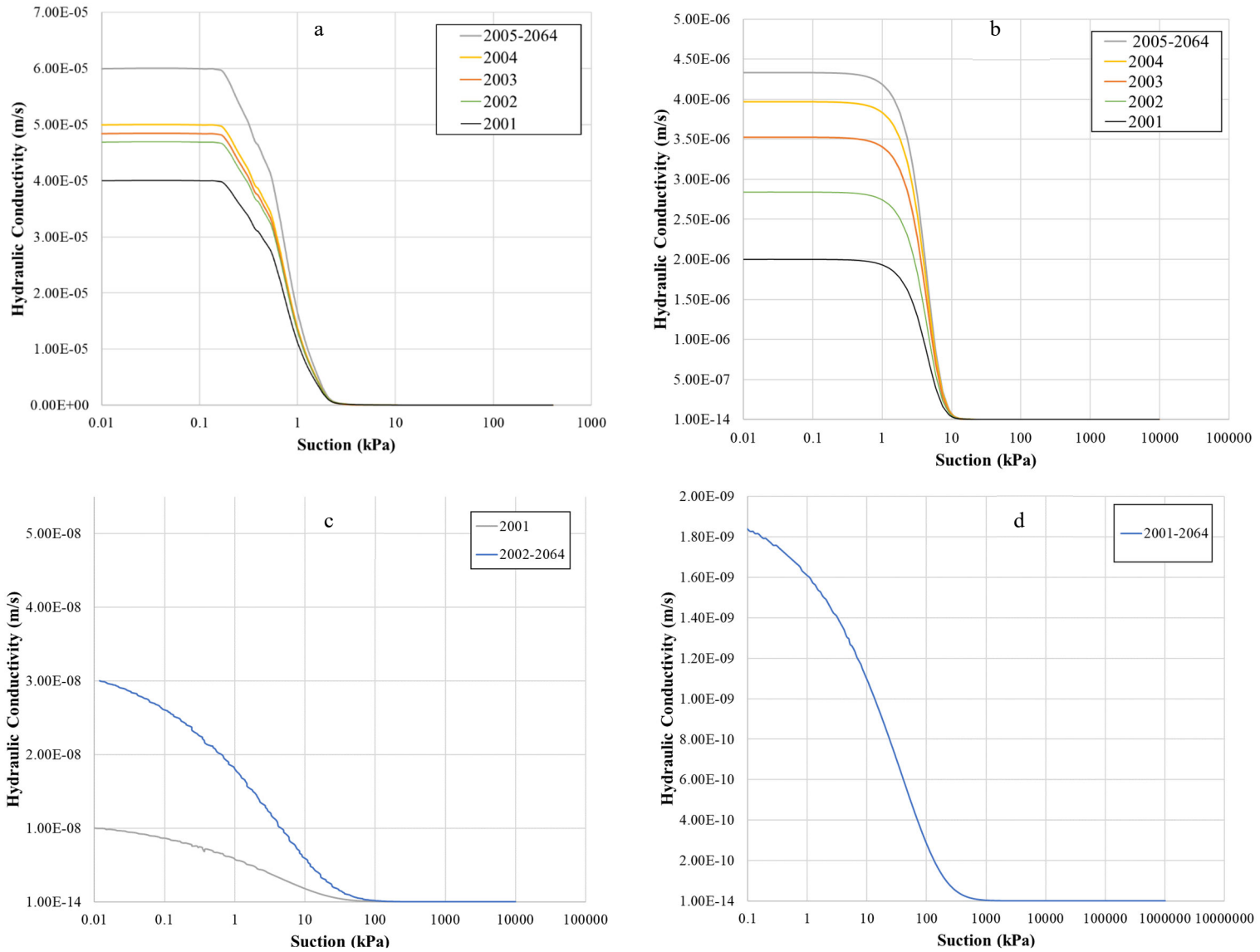

Figure 4-4. Hydraulic conductivity functions for the model years (2001-2064) for each material; a) peat-mineral mixture, b) glacial clay till, c) shallow oxidized shale, and d) deep non-oxidized shale.

As described in Section 2.1.2, it is necessary to specify how the soil hydraulic properties change in frozen conditions, as liquid water in the pore space is replaced by ice. Patterson et al. (1985) measured SFC curves for silty clay at various solute concentration and found the freezing point shifted from -1.0 °C for a 10 g/L sample to -2.7 °C for a 35 g/L sample. The peat-mineral mixture and glacial clay till cover layers were observed to have low aqueous solute salt concentrations (i.e., 0.1 to 1.5 g/L). The oxidized shale pore-water salt concentration ranged from 6.5 to 9.5 g/L and the unoxidized shale had higher salt concentrations ranging from 6.5 to 15.0 g/L (Appels et al. 2017; Hilderman 2011; Huang et al. 2015; Kessler et al. 2010).

The SFC curve for each material was empirically estimated using the results of Patterson et al. (1985) to create a freezing point temperature, for pore-water only, of -0.05, -0.052, -0.62, and -1.0 °C for the peat-mineral mixture, glacial clay till, shallow oxidized shale, and deep non-oxidized shale, respectively (Figure 4-5). Below the freezing point, the SFC was estimated using the Clapeyron equation based on the similarity between the WRC and SFC (Equation 12):

$$\psi = -L_f \rho_w \ln\left(\frac{T}{273.15}\right) \tag{12}$$

Where, ψ is the matric potential (kPa) and T is temperature (K) (Azmatch et al. 2012; Ren et al. 2017).

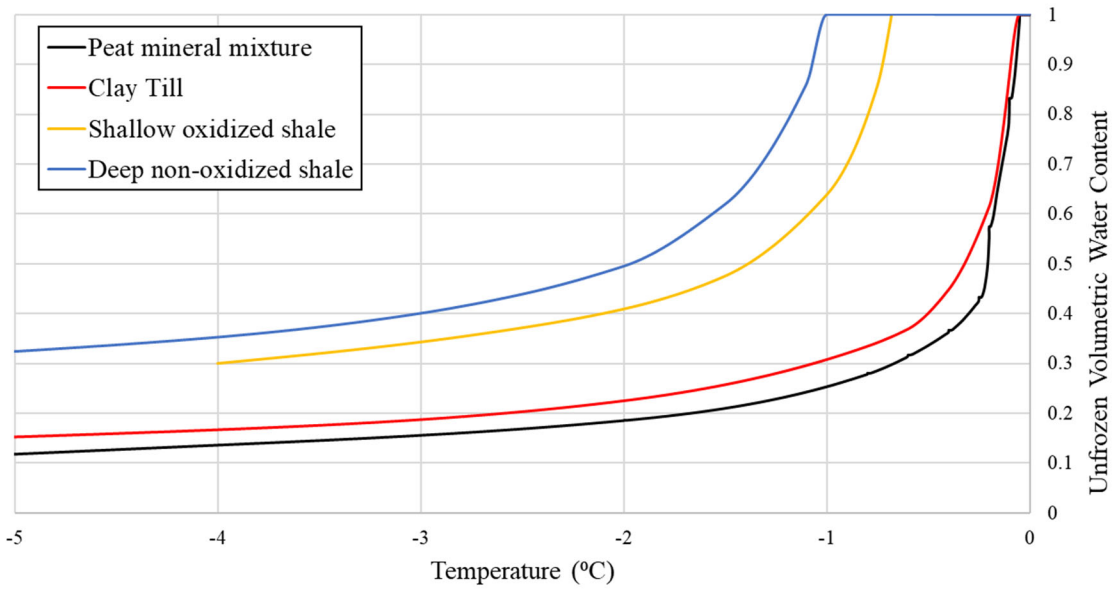

Figure 4-5. Soil-freezing characteristic curve for each material.

Bulk diffusion coefficients (D*) for each material are were derived from Millington et al. (1961) using the following equation and are summarized in Figure 4-6:

$$D^* = \frac{D_w \theta^{\frac{7}{3}}}{n^2} \tag{13}$$

where n is the porosity of the medium (m^3 m^{-3}) (values from Table 4-1), D_w is the free oxygen diffusion coefficients in water (m^2 s^{-1}) (modeling used D_w (SO_4^{2-}, 0C) = 5 x 10^{-10} m^2 s^{-1} from Li et al. (1974)) and θ is the soil water content (volume/volume). From Equation 15, it can be observed that D* decreases strongly with increasing saturation of the pore space, with a distinct breakpoint around 80–85% saturation (Aachib et al. 2004). It should also be noted that the bulk diffusion coefficients for each material were similar as the measured porosities for each material were comparable (Table 3-1). Longitudinal dispersivity (α_L) for the cover soils and shale were defined as 0.1 m and 0.01 m, respectively (Huang et al. 2015). Initial sulfate concentrations for the materials are described in Section 4.2.3.

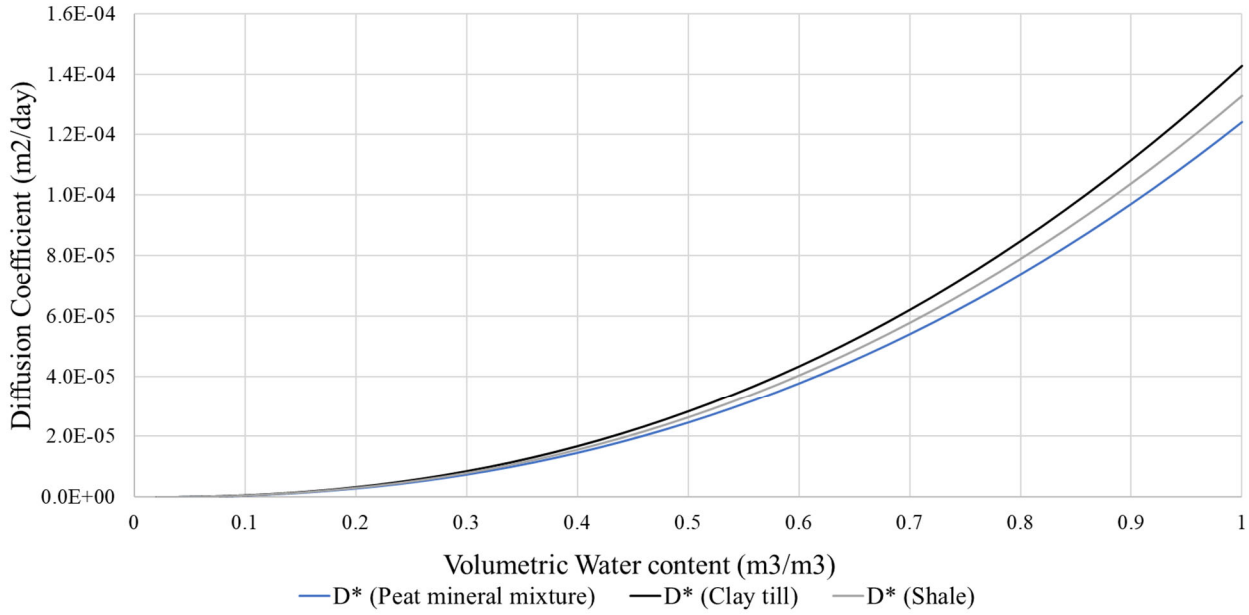

Figure 4-6. Bulk diffusion coefficient functions for each material.

4.2.3 Boundary Conditions

Based on the conceptual model of the site, the following initial conditions and boundary conditions were applied to the water flow, heat, and solute transport model. An initial pressure head distribution from the observed water content profile on November 1, 2000 was used. The upper boundary condition was a land-climate interaction boundary that included two components: net infiltration at the ground surface and transpiration within the soil profile. The net infiltration includes the following water fluxes: rainfall, snow melt, surface evaporation, runoff.

Transpiration was simulated using a root uptake model (Feddes et al. 2001) based on a specified normalized root density distribution in the profile, potential plant transpiration, and a water stress function (Huang et al. 2015). The fine root biomass distribution in the cover soils and upper shale at D3 was measured by van Rees et al. (2002) and van Rees (2014). Their results indicated that plant average maximum root depth increased from 60 cm in 2002 to 100 cm in 2012, whereas relative fine root density distribution presented changes in the profile with an obvious increase in the 15 to 40-cm soil layers. In the model simulations, the root depth was modelled as linear and the evolution of the root depth with time was considered by assuming a linear increase from

20 cm in 2000 until the maximum depth of 100 cm in 2008 which was carried forward to 2064 (end of model simulations).

The daily climatic data (i.e., the maximum and minimum temperatures, relative humidity, and net radiation) were collected from the automated meteorological station on the D3 plot as discussed in Section 3.2. The evapotranspiration was calculated using the Penman-Wilson equation (Wilson et al. 1994). The melt rate for the snowmelt flux was simulated using CRHM, as described in Section 4.2.4. Three different snowmelt infiltration scenarios were modelled and are further discussed in Sections 4.2.4 and 4.2.6.

To capture the drainage of any temporarily perched water along the shale surface, a lateral free drainage boundary condition was applied at the cover/shale interface to allow drainage if positive pressures develop at this location. A unit gradient boundary condition was applied to the base of shale (base of model domain) to allow deep drainage to occur through the shale if excess water is available at the base of the cover.

The initial temperature distribution for the thermal transport was from the measured temperature profile on November 1, 2000. A ground heat flux (using surface energy balance) was set as the upper boundary condition and a constant lower boundary condition of 1 °C was fixed at depth of seven meters (Wall 2005).

The baseline solute concentrations for each material were obtained from previous studies on the SBH site and are provided in Table 4-2. The baseline sulfate concentration in the till was estimated from the analysis of till samples obtained from a salvaged till stockpile (Kessler 2007) and the range of concentrations provided by Huang et al. (2015). The baseline sulfate concentrations for the shale are based on the observations presented in Nichol et al. (2006).

The upper boundary condition for the solute transport model was set as a zero-mass flux, and the lower boundary condition at the base of the modelled domain (i.e., at 7.02 m depth) was assigned as a fixed constant concentration of 0.00488 Mg/m^3.

Table 4-2. Initial sulfate concentration for the modelled materials.

Material	Initial Concentration	
	(mg/L)	(Mg/m^3)
Peat-mineral mixture	0.0	0.0
Glacial clay till	350.0	3.50×10^{-4}
Shallow shale	4880.0	4.88×10^{-3}
Deep shale	4880.0	4.88×10^{-3}

4.2.4 Snowmelt Fluxes

As described in Section 3.4 and 3.5, snowmelt was estimated using CRHM for the period between 2001-2015. Three snowmelt infiltration scenarios were considered as part of this modelling to improve the understanding of how varying assumptions of snowmelt effect the accumulation and distribution of salts within the cover.

The Granger et al. (1984) equation was used to determine the amount of snowmelt infiltration, independent of soil texture and vegetative cover:

$$\mathrm{INF} = 0.980\left(\frac{\mathrm{SWE}}{\theta_\mathrm{p}}\right)^{0.659} \tag{14}$$

where INF is the snowmelt infiltration, SWE is the snow-water equivalent and θ_p is the pre-melt soil moisture in the zone of infiltration. A pre-melt soil water content of 0.36 was used, which represents the average water content in the peat and till from 2001 to 2015.

The snowmelt infiltration scenarios considered as part of this modelling were:

- Baseline Condition (no enhanced infiltration rate applied to model): snowmelt infiltration flux applied to top of profile where the snowmelt infiltration and runoff were simulated using the water-heat transport model, no additional infiltration mechanism was added.

- 30 cm snowmelt injection (Granger et. al (1984) model, enhanced infiltration applied to top 30 cm): snowmelt infiltration volumes calculated using Granger et. al (1984) model and applied to the top 30 cm of the soil profile (i.e., the peat mineral mixture and top 10 cm of the till). The remaining snowmelt was directly converted as runoff.

- 150 cm snowmelt injection (Granger et. al (1984) model, enhanced infiltration applied to top 150 cm): Snowmelt infiltration volumes calculated using Granger et. al (1984) model and applied to the top 150 cm of the soil profile (i.e., to the base of the shallow oxidized shale). The remaining snowmelt was directly converted as runoff.

Note the same volume of infiltration was applied to the snowmelt injections scenarios (i.e., 30 cm snowmelt injection and 150 cm snowmelt injection scenarios) but were distributed differently within the soil column. The modelled scenarios are presented in detail in Section 4.2.6.

4.2.5 Sulfate Production Term

Past research at SBH has demonstrated that the weathering of shale overburden due to oxidation of sulphide minerals within the shale leads to sulfate production. To adequately capture the behavior of salt ingress of this system, it is necessary to include a production term within the solute transport model.

Huang et al. (2015) used a dual porosity water flow model and transport model to assess the controls on sulfate migration and the rate of sulfate generation within the pyritic shale. This study showed that the observed sulfate levels could only be simulated by including a production term related to the pyrite oxidation of the shale. The simulated oxidation rates used in Huang et al. (2015) models averaged from 1.89 and 0.3 g SO_4^{2-} $m^{-2}day^{-1}$ for various locations along the D3 cover.

Appels et al. (2017) analyzed the results of soil chemistry sampling, pore gases and numerical simulations to compare the sulfate production rates in the overburden dump. The SO_4^{2-} production rates calculated with these methods were observed to be significantly higher than the estimates obtained from optimized hydrological models for the sites by Huang (2015) as seen in Figure 4-7.

For this thesis, an average production rate based on the findings by Huang (2015) of 1 g $m^{-2}day^{-1}$ was implemented.

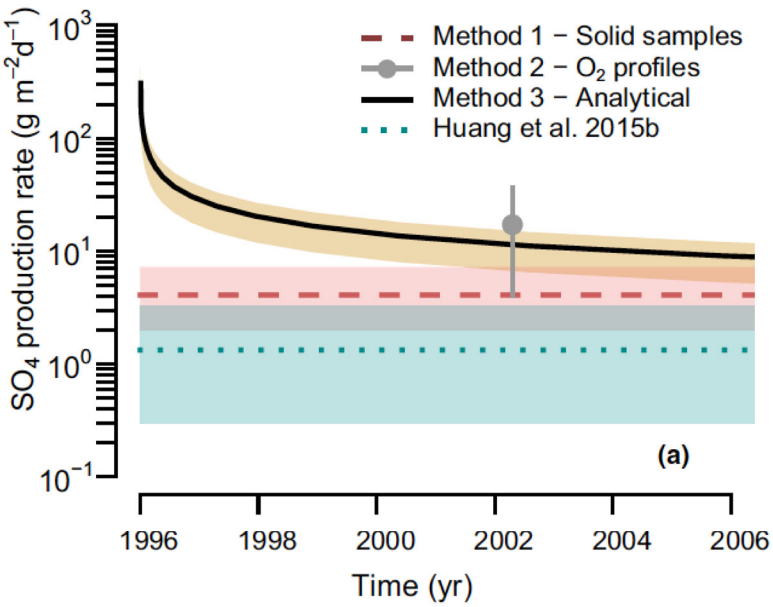

Figure 4-7. Sulfate production rates as a function of time, adapted from Appels 2017.

Two scenarios of sulfate production were considered for the model: a constant production rate of 1 g $m^{-2}day^{-1}$ and a decaying production function with time (i.e., production = 4.7896e $^{(-0.158d)}$), as shown in Figure 4-8. The constant rate is included as this is the simplest approach to take, And follows the approach of Huang et al., (2015b). In reality, we would expect exponential decay of sulfate generation due to consumption of source pyrite. The decaying production function was defined by creating the same total mass of sulfate over 30 years as the constant production rate with the rate dropping exponentially after 10 years. The definition of the decay function was based on the work completed Appels (2017), which indicated a half-life between six to seven years and an initial rate of approximately five times higher than that of the constant rate.

Model runs were simulated for 60 years (Section 4.2.6) into the future to capture the point in time where:

- constant rate sulfate production was greater than the decay production rate after ten years,
- cumulative production between the two functions were equal after 60 years and,

- to assess if quasi steady-state solute conditions were reached.

In the model, the sulfate production terms were applied to the 0.5 m layer of the oxidized shallow shale.

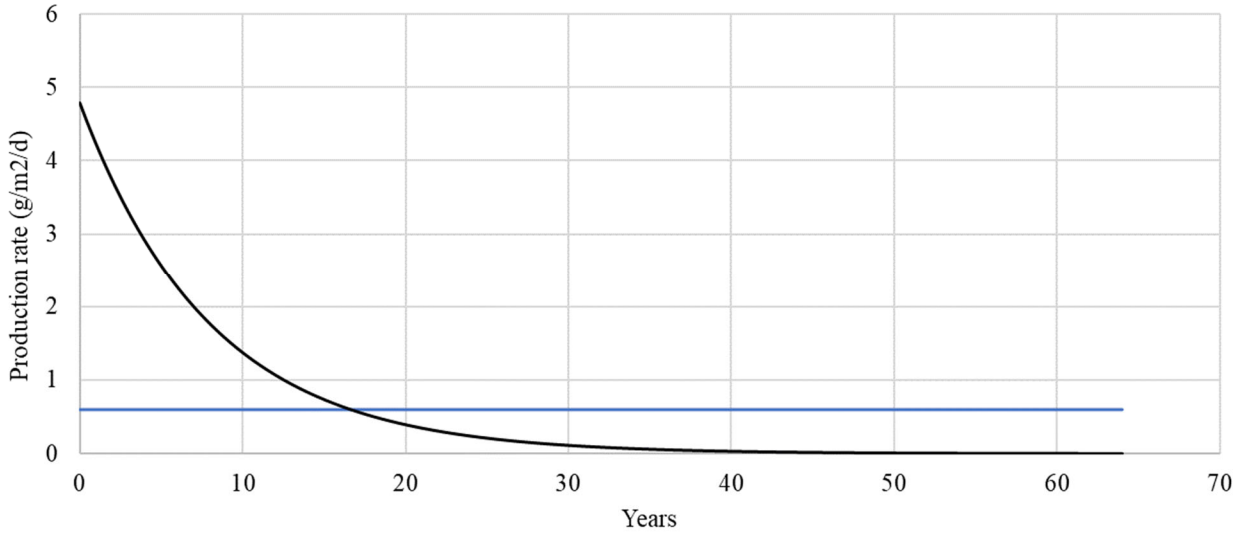

Figure 4-8: Rate of Mass Loading for Constant and Decaying Production Rates

4.2.6 Modelled Scenarios

As described in Section 4.2.1, flow through the one representative section of the D3 cover was modelled. For this study, multiple model scenarios were simulated to help address the following uncertainties: quantifying snowmelt infiltration and the amount of sulfate produced within the cover system by oxidation of pyrite within the shale.

A 60-year possible climate sequence was used based on historical weather data from Fort McMurray. For the snowmelt infiltration and sulfate production, a low, medium, and high estimate of infiltration and production were considered, as summarized in Table 4-3 (Sections 4.2.4 and 4.2.5). In summary, a total of nine modelled scenarios were simulated, which were run for 60-years into the future from 2001 (Table 4-4).

Table 4-3. Snowmelt Infiltration and Sulfate Production Scenarios.

Snowmelt Infiltration Scenarios	Baseline Conditions	Snowmelt infiltration and runoff were simulated using the water-heat transport model, no additional infiltration mechanism was added.
	30 cm - Granger et. al (1984) model	Snowmelt infiltration volumes calculated using Granger et. al (1984) model and injected into the top 30 cm of the soil profile. The remaining snowmelt was directly converted as runoff.
	150 cm - Granger et. al (1984) model	Snowmelt infiltration volumes calculated using Granger et. al (1984) model and injected into the top 150 cm of the soil profile. The remaining snowmelt was directly converted as runoff.
Sulfate Production Scenarios	No sulfate production	Initial sulfate distribution is free to redistribute with flowing water.
	Constant sulfate production rate	Constant rate of production based on Huang et. al (2015) considered for the 60-year period,
	Decaying production rate	Decaying production function such that the cumulative mass of sulfate equals that of the constant rate of production.

Table 4-4. Modelled Scenarios.

Model Scenario[1]	Snowmelt Infiltration Scenario	Sulfate Production Scenario
1	Baseline Conditions	No sulfate production
2		Constant sulfate production rate
3		Decaying production rate
4	30 cm - Granger et. al (1984) model	No sulfate production
5		Constant sulfate production rate
6		Decaying production rate
7	150 cm - Granger et. al (1984) model	No sulfate production
8		Constant sulfate production rate
9		Decaying production rate

Notes:

1. Each model scenario was simulated from 2001 to 2064.

4.3 Results and Discussion

4.3.1 Flow Model

The average water balance components for each snowmelt infiltration scenario are presented in Table 4-5 and shown in Figure 4-7. The annual water balance for all modelled scenarios and years may be found in Appendix B (Figure B-1).

The varying snowmelt infiltration scenarios impose different infiltration to runoff ratios on the system which has implications for the other water balance components. The baseline model shows minimal infiltration and a large amount of runoff, and as expected results in the lowest amount of transpiration, evaporation, and net percolation. When any amount of infiltration is imposed into the system, the net percolation increases compared to the baseline condition.

The baseline condition scenario overestimates runoff and underestimates infiltration resulting in the lowest infiltration. This was expected since conventional frozen soil infiltration/runoff algorithms tend to overestimate runoff and underestimate infiltration (Huang et al. 2015). The water balance components for the enhanced infiltration scenarios (using Granger et. al (1984)) are expected to be more representative.

The evaporation and transpiration are sensitive to the varying infiltration scenarios. The models predict increasing evapotranspiration with increasing snowmelt infiltration, consistent with general understanding. The Granger et. al (1984) 30 cm infiltration scenario resulted in the highest amount of evaporation and transpiration. Increased infiltration concentrated near the top of the profile results in more water available near surface that can be drawn up by evaporation processes which explains why less evaporation and transpiration is observed in the Granger et. al (1984) 150 cm since the same volume of water is distributed over deeper depths and less is available near surface for evaporation/transpiration processes.

Evaporation (as opposed to transpiration) is expected to have a significant role in salt accumulation by evapoconcetration and therefore, the different infiltration scenarios should have a significant impact on the solute transport simulations.

Table 4-5. Average water balance component for the three snowmelt infiltration scenarios.

Water Balance Component	Baseline Infiltration	Granger et al. (1984) 30 cm Infiltration	Granger et al. (1984) 150 cm Infiltration
Evaporation	65.7	86.1	70.9
Transpiration	256.3	264.9	272.0
Runoff	76.6	5.2	4.8
Net Percolation	9.6	10.5	16.3
Infiltration[1]	348.8	420.1	420.6
ΔStorage	17.3	59.3	62.3

Notes:

1. Infiltration is defined as precipitation and snowmelt. A portion of the snowmelt volume was injected into the Granger 30 cm and Granger 150 cm scenarios as described in Section 4.2.4.

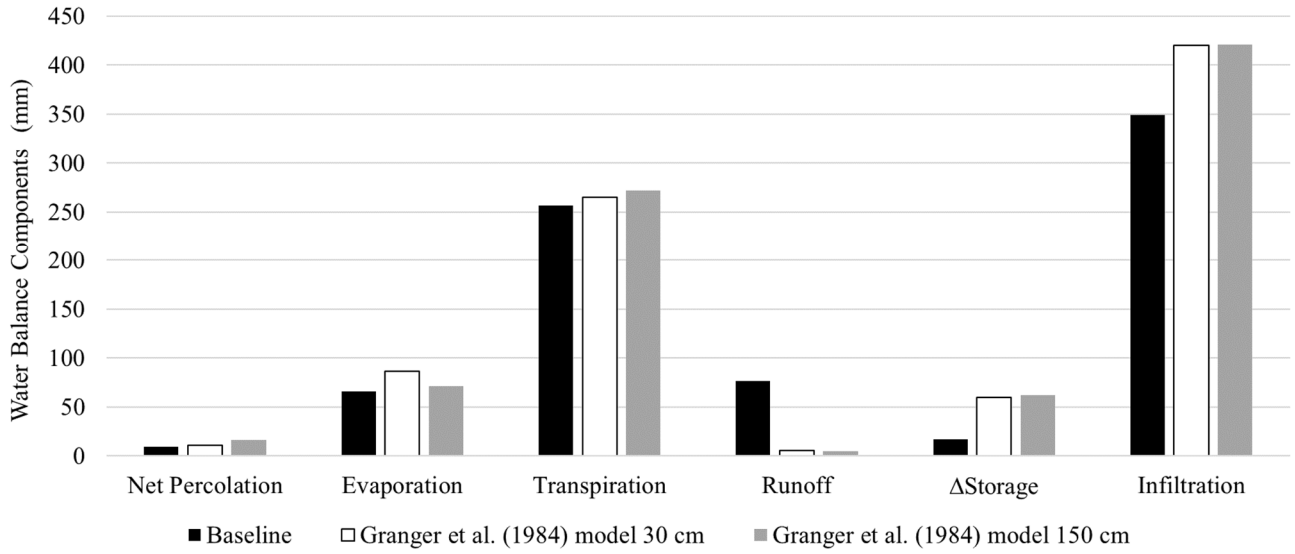

Figure 4-9. Simulated average water balance components for the modelled infiltration scenarios.

4.3.1.1 Interflow and Net Percolation

The average interflow measured at the toe of the D3 cover from 2001 to 2015 was 2.6 mm/year. The Granger et. al (1984) 150 cm model was the only model that predicted interflow, with an average of 0.25 mm/year. The models were not calibrated to this observation since it comprises a relatively small component of the water balance Section 4.1.

The simulated net percolation rates for each snowmelt infiltration model scenario are shown in Figure 4-10. No direct measurements of net percolation are available, however, the previous estimates of net percolation obtained by Hilderman (2011) based on profiles of the stable isotopes of water, were used as a basis of comparison. The isotope-based estimates of net percolation were for cumulative net percolation from 1999 to 2009 at eight locations on the D3 cover and plateau.

Hilderman (2011) noted that the average net percolation rate was a function of topographic position, varying from a maximum of 34.1 mm/year at plateau locations to minimum of 3.5 mm/year on the D3 slope, with a mean of 14.3 mm/year (Huang et al. 2015).

The models had a similar range of average annual net percolation from 2001-2009 with the highest values from the Granger et. al (1984) 30 cm and Granger et. al (1984) 150 cm infiltration scenarios (approximately 16–20 mm/year) and lower values from the baseline models (approximately 12–15 mm/year). The main reason for these differences is likely due to the increased snow melt infiltration that was applied for the Granger et. al (1984) 30 cm and Granger et. al (1984) 150 cm models.

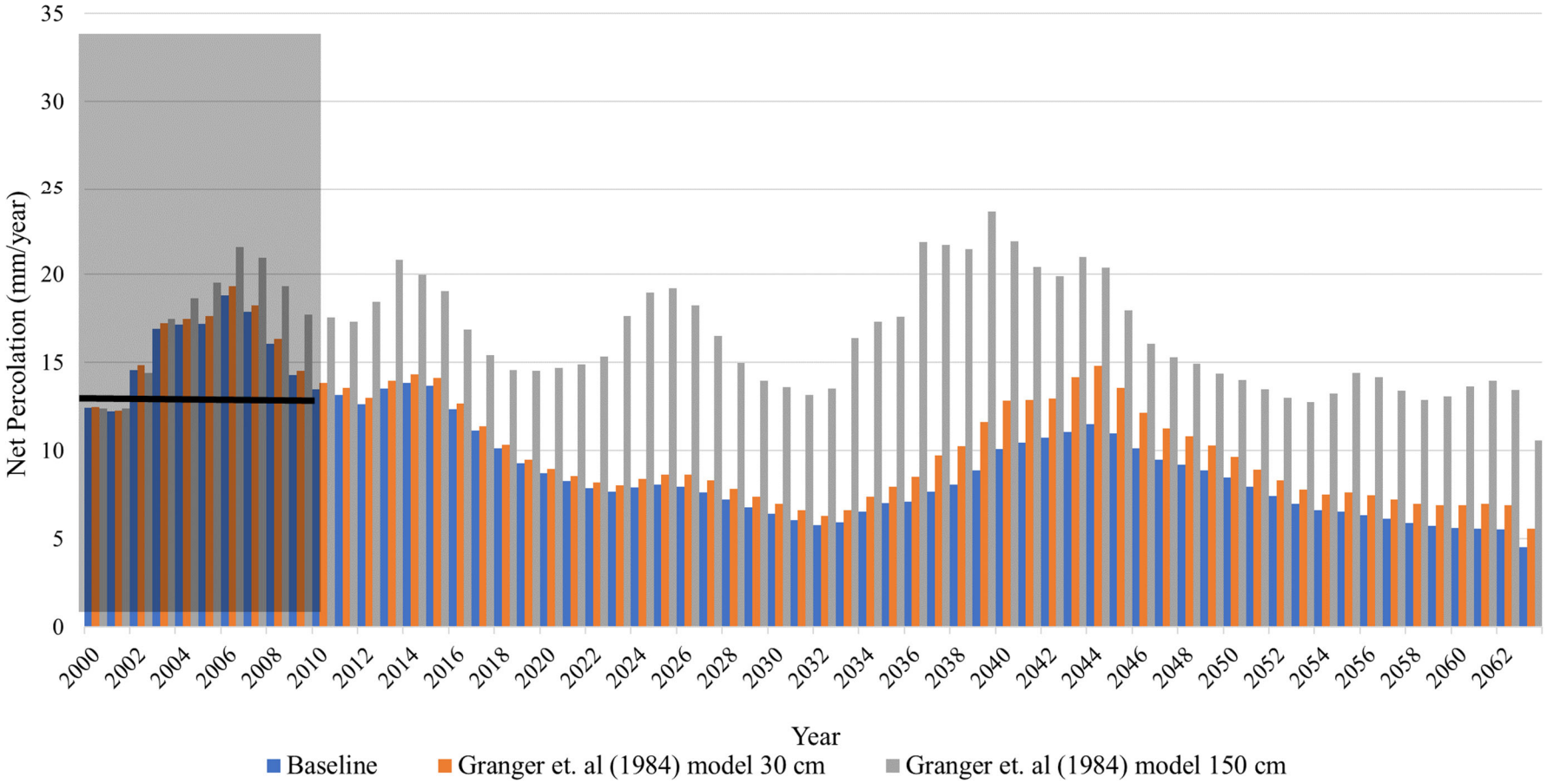

Figure 4-10. Simulated net percolation for the modelled snowmelt infiltration scenarios. The gray region shows the range and mean of the estimated average net percolation (1999–2009) using the monitored isotope profiles of water at SBH (Hilderman 2011).

4.3.2 Solute Transport Model

4.3.2.1 Solute Balance

Nine model scenarios were run using three different sulfate production scenarios: no sulfate production, constant rate of sulfate production, and a decay function sulfate production (as discussed in Section 4.2.5). The relative error of the nine scenarios over the simulated 60 years was satisfactory (i.e., relative error below 2%); the cumulative relative error of the model runs is presented in Figure B-2 (Appendix B).

Solute balance plots for each snowmelt infiltration scenario are provided in Appendix B (Figure B-3 through B-5). Mass loss from net percolation, domain dissolved mass (mass storage) and the total mass for each snowmelt infiltration scenarios are provided in Figure 4-11 through Figure 4-13. The domain dissolved mass is defined as the solute mass dissolved in the simulated domain. The total mass is equal to the mass loss with net percolation plus the domain dissolved mass; this metric was used to illustrate the accuracy of the mass balance for the three snowmelt infiltration scenarios.

Mass loss from net percolation was not sensitive to the varying sulfate production scenarios but did gradually increase from the baseline case to the Granger 30 cm and 150 cm infiltration scenarios. Similar to the flow model findings, mass loss from net percolation was sensitive to the varying snowmelt infiltration assumptions, with the greatest amount of mass loss from net percolation observed in the Granger et al. (1984) 150 cm infiltration scenario which corresponds to the highest simulated amount of net percolation (Section 4.3.1.1).

The domain dissolved mass for the whole simulated domain was similar for each sulfate production scenario, which is expected as the solute loss from net percolation was similar between each sulfate production scenario.

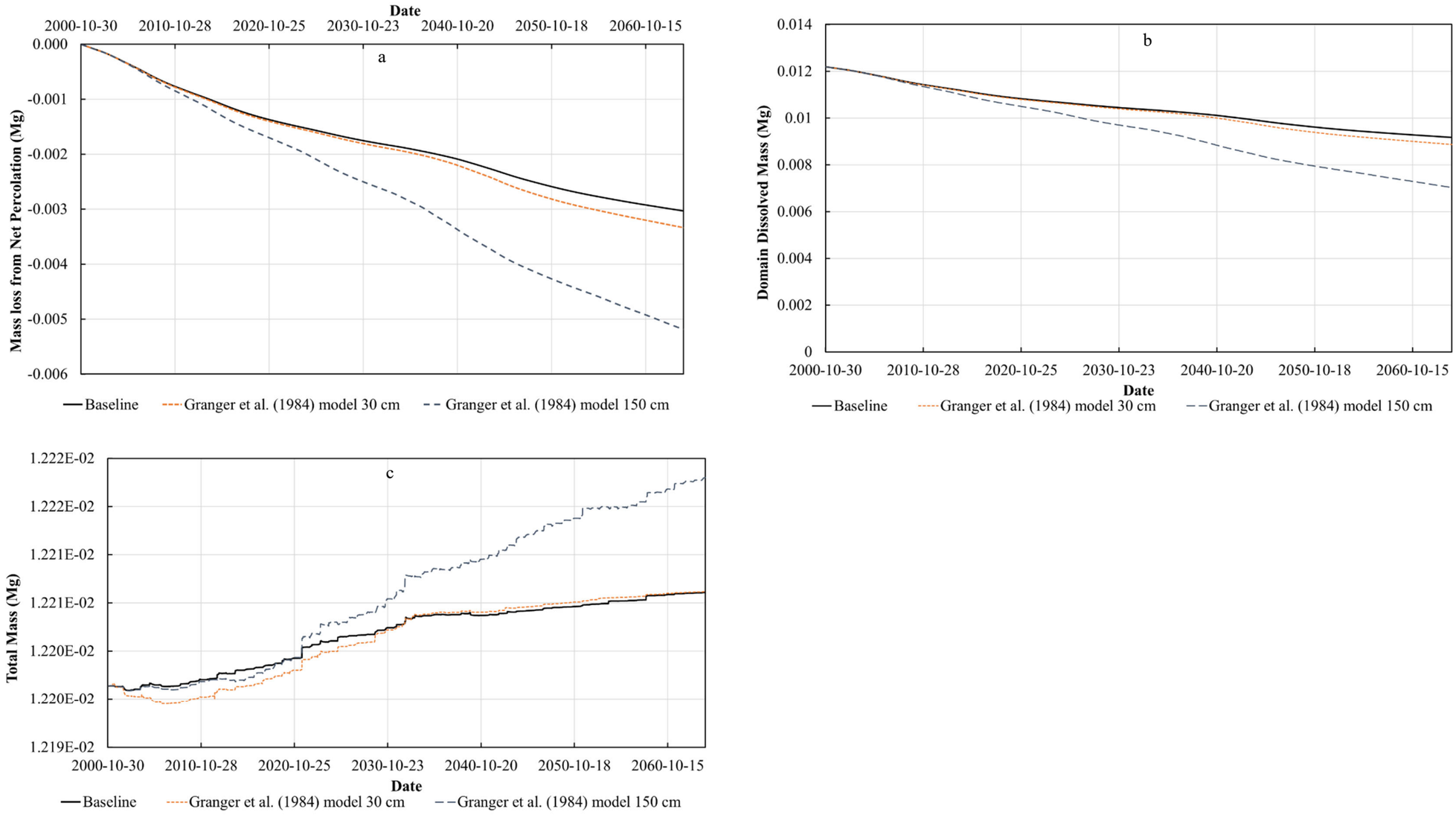

Figure 4-11. No sulfate production applied for the three snowmelt infiltrations scenarios (a) mass loss from net percolation, (b) domain dissolved mass and, (c) total mass.

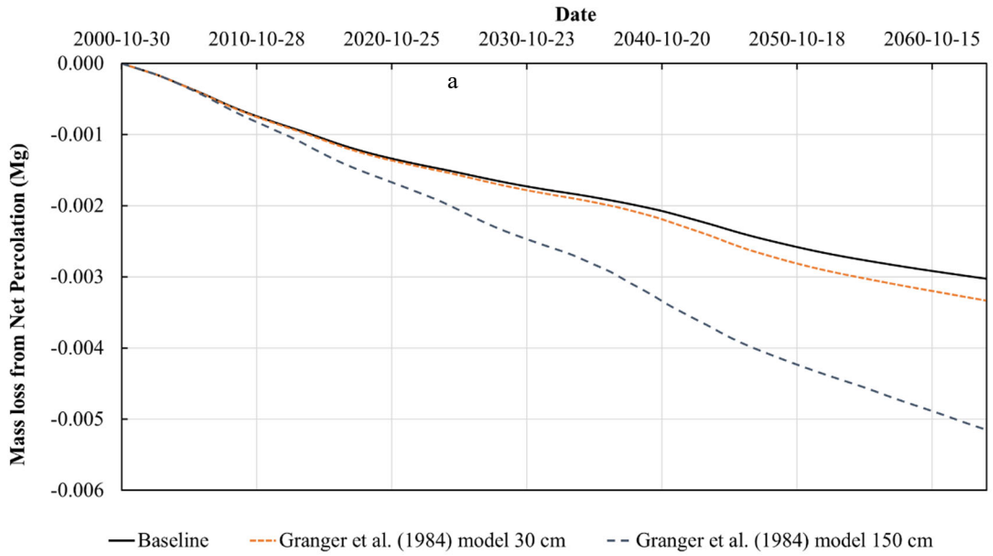

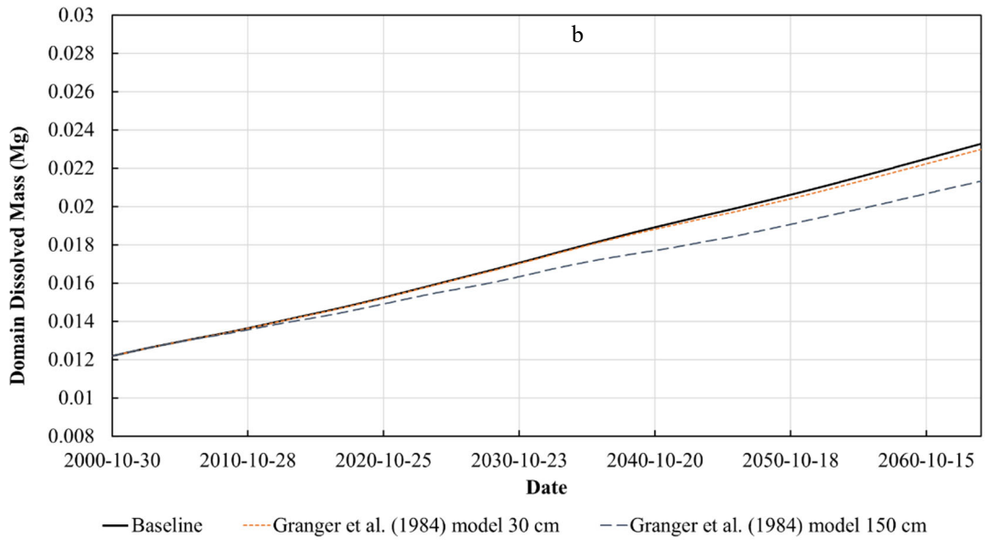

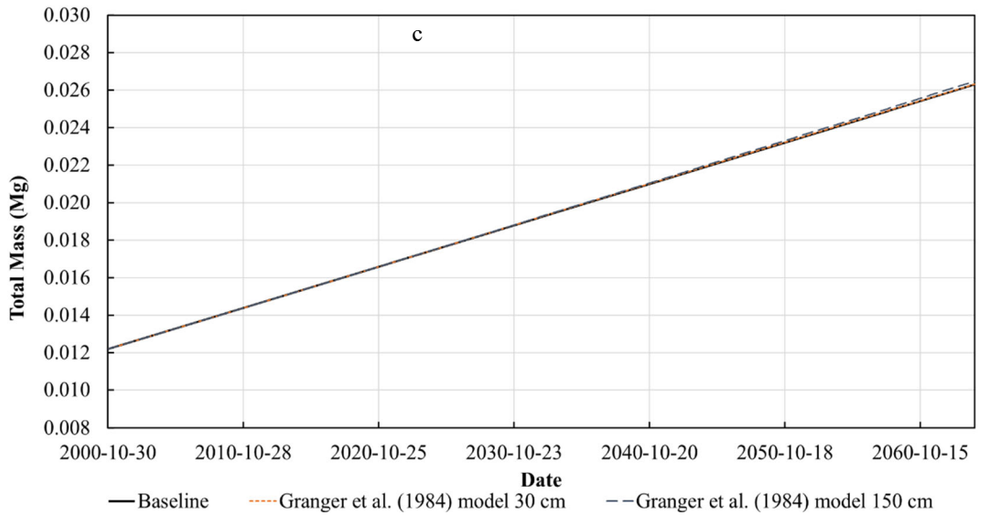

Figure 4-12. Constant sulfate production for the three snowmelt infiltrations scenarios (a) mass loss from net percolation, (b) domain dissolved mass and, (c) total mass.

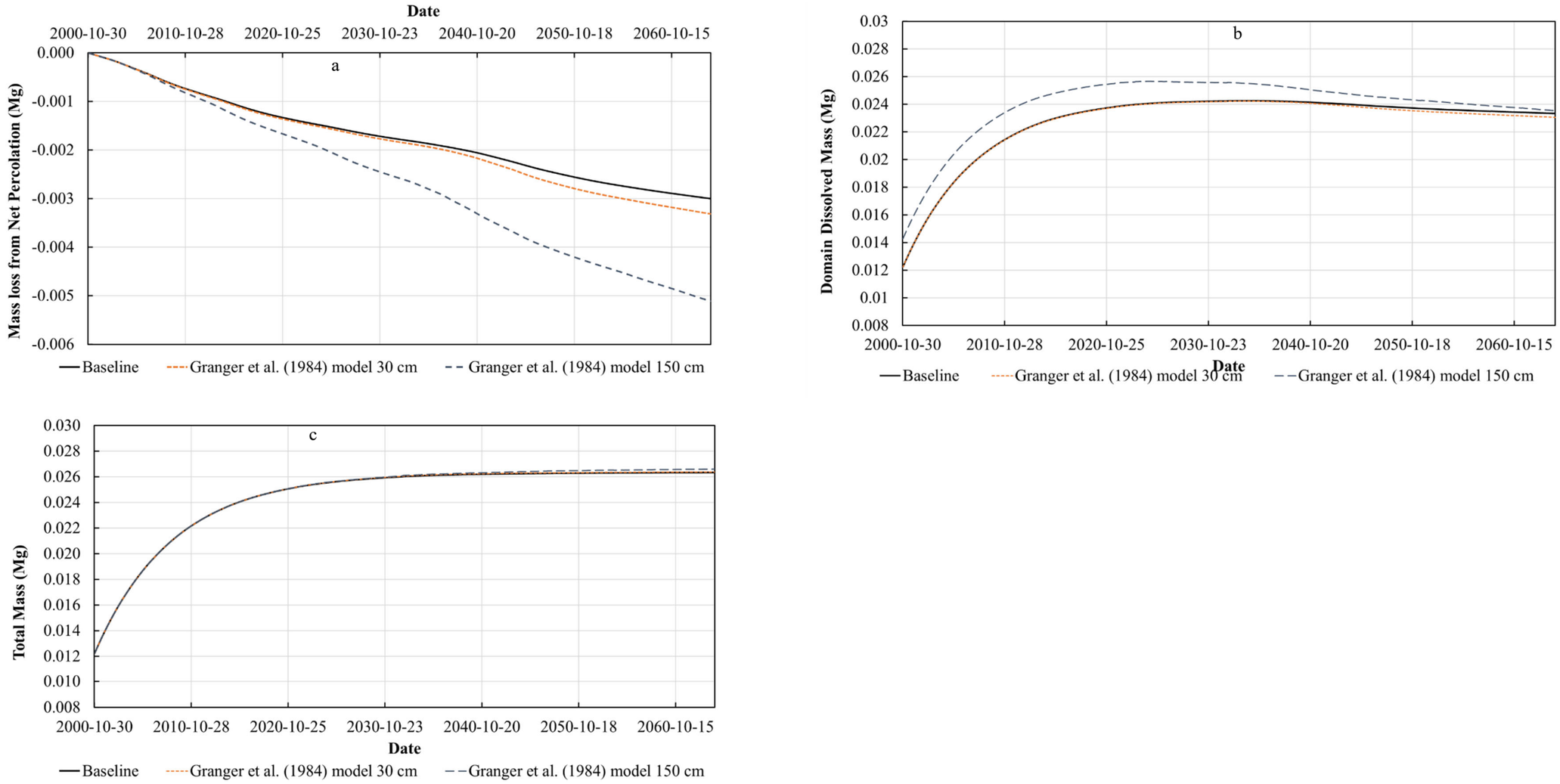

Figure 4-13. Decay sulfate production for the three snowmelt infiltrations scenarios (a) mass loss from net percolation, (b) domain dissolved mass and, (c) total mass.

4.3.3 Sulfate Accumulation over Time

The simulated sulfate profiles for model year 2007 is plotted against measured concentrations taken along the D3 cover (Kessler 2007), as shown in Figure 4-14. Without a sulfate production term, the simulated sulfate profiles fell below the observed profiles. The constant production rate scenario matched the observed sulfate profiles more accurately than the decay production scenario. The decay production scenario overestimated the amount of salt flushing from the upper 1.0 m suggesting the net percolation simulated for this model year was overestimated.

The simulated sulfate concentration over time for the three different snowmelt infiltration and sulfate production scenarios are presented in Figure 4-15 through Figure 4-17. The simulated sulfate profiles for model years 10, 20, 30, 45 and 64 (final model year) for the no sulfate production, constant sulfate production and decay sulfate production scenarios are presented in Figure 4-18 though Figure 4-20, respectively.

With no sulfate production, downward advection of salts by net percolation dominants the system resulting in a decrease in salinity within the cover and upper shale surface over time, as shown by Figure 4-15a, Figure 4-16a, Figure 4-17a and Figure 4-18. With the addition of a production term, the system is dominated by both advective and diffusive transport.

The salt production mechanism is not particularly sensitive. The sulfate profiles show a significant change between the no sulfate production and sulfate production scenarios, as expected. The solute profile between the constant sulfate and decay sulfate production show similar distributions (but with significantly different concentrations, as expected).

The infiltration scenario has a marked impact on the salt concentration. There is significant soil salinization as the amount of snowmelt infiltration increases. This is likely due to increased evaporation due to increased infiltration, which draws water and solute up into the near surface, leading to soil salinization. Increased infiltration also results in an increase in net percolation, which results in a reduction in the solute concentration within the shale. In the short term, this means more solute leaching to the deeper groundwater system. In the long term, this might lead to a reduction in the salinity of the reclamation cover, reversing the soil salinization.

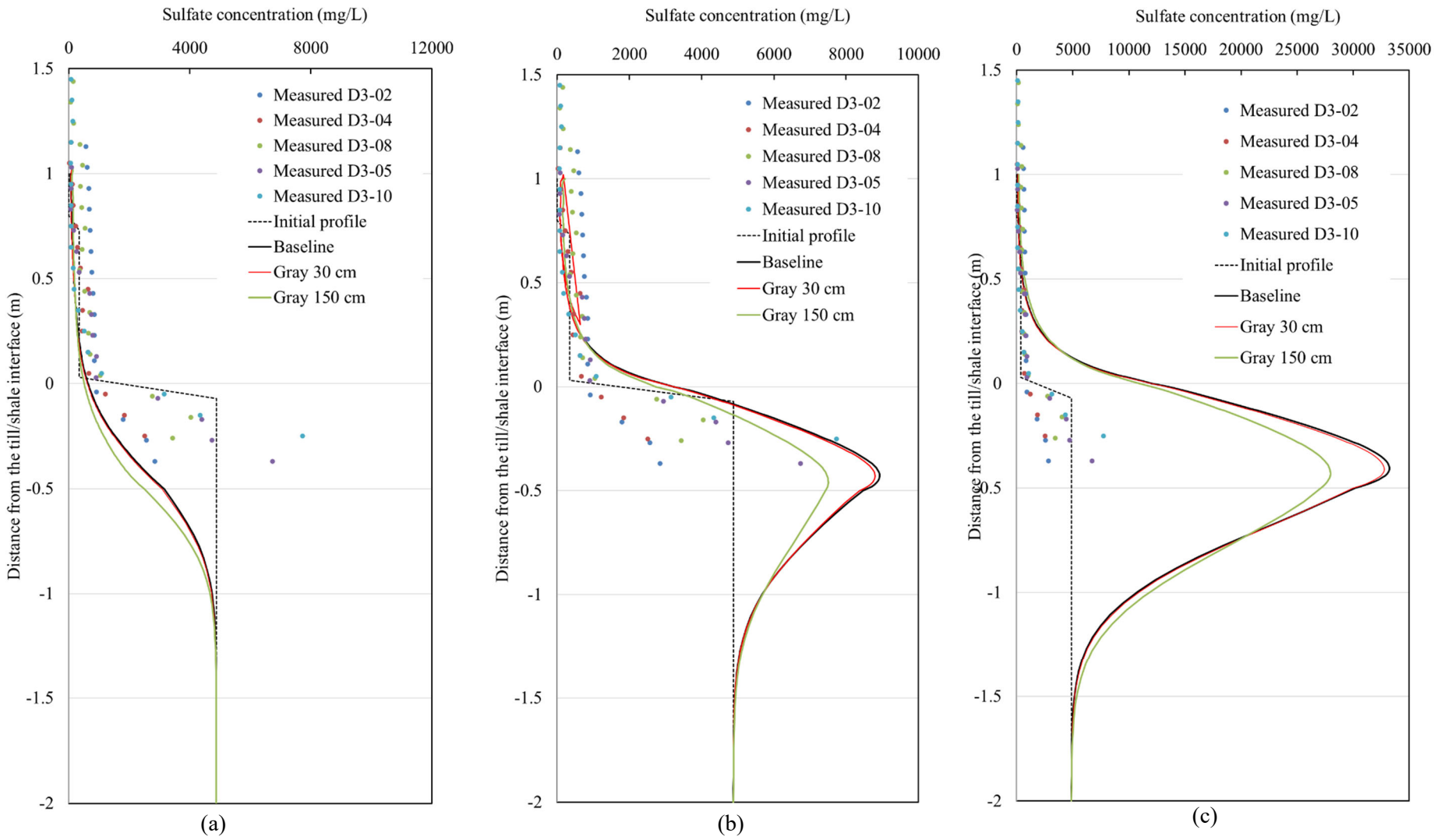

Figure 4-14. Simulated model year 2007 and measured sulfate profiles (Kessler 2007) (a) no production rate, (b) constant production rate, (c) decay production rate

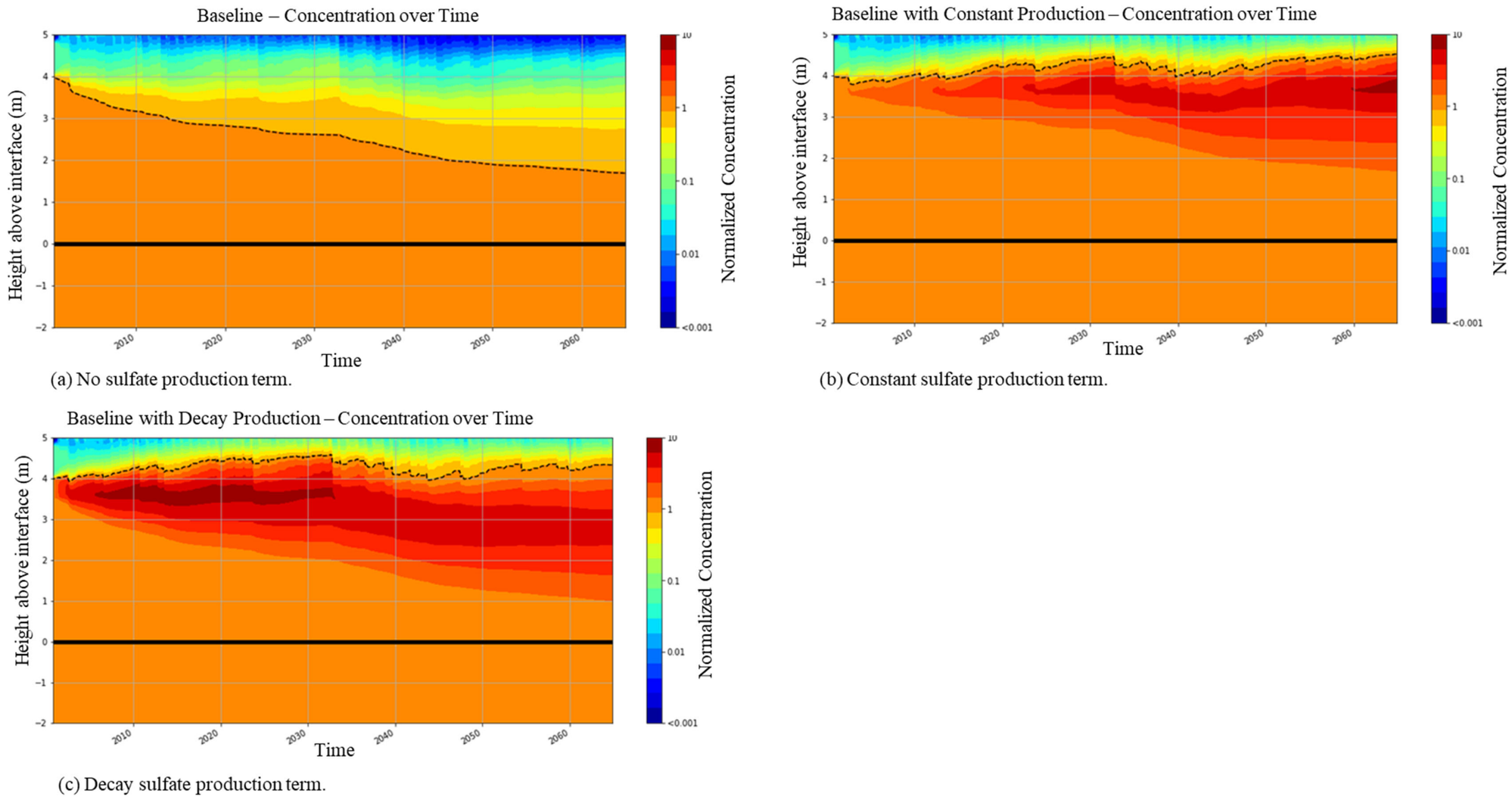

Figure 4-15. Simulated sulfate concentration for the baseline infiltration scenarios.

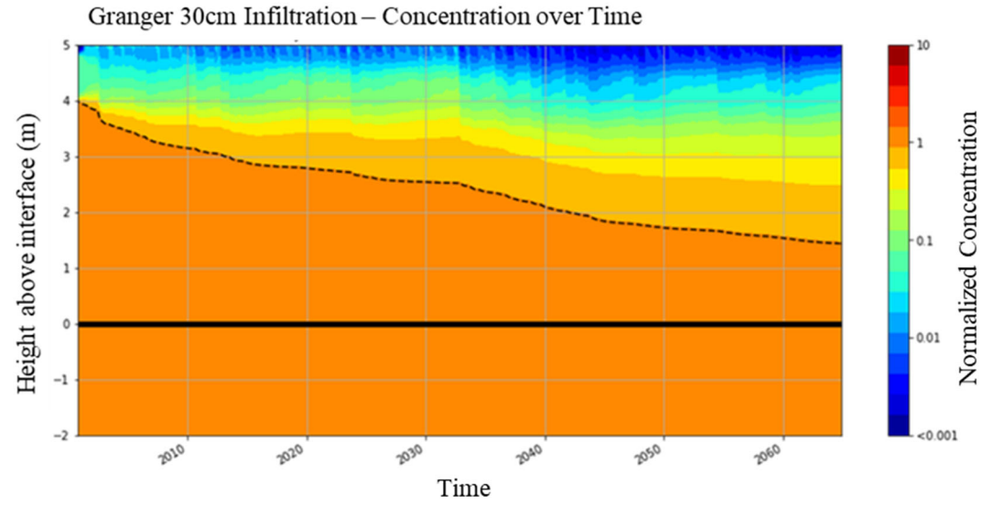

(a) No sulfate production term.

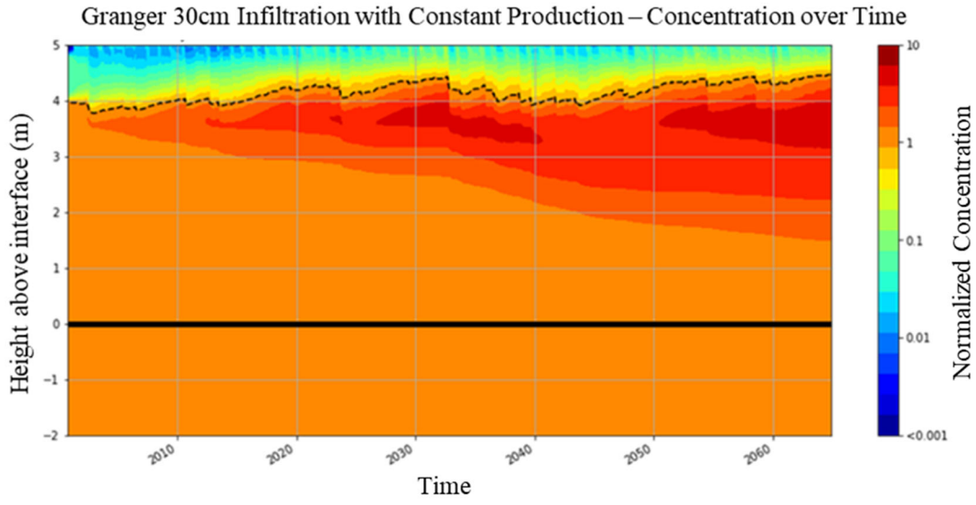

(b) Constant sulfate production term.

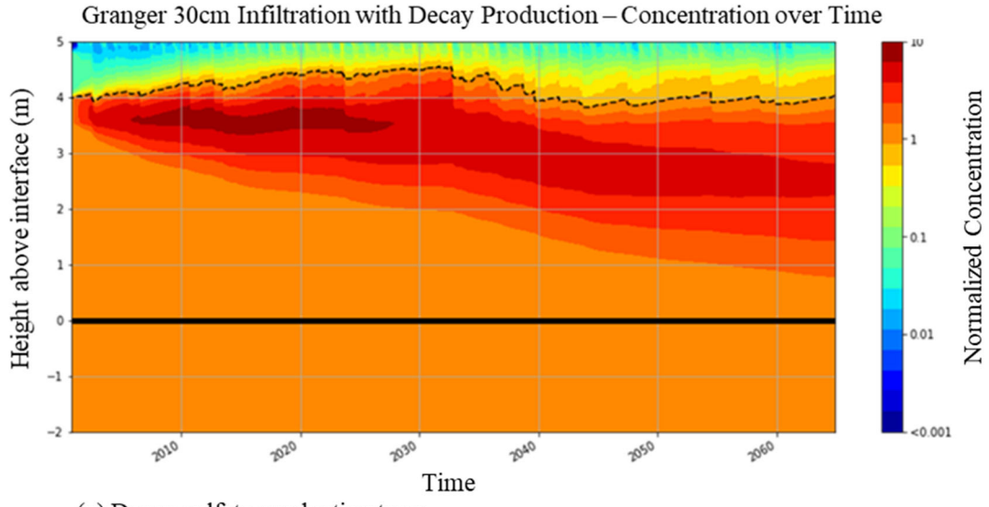

(c) Decay sulfate production term.

Figure 4-16. Simulated sulfate concentration for the Granger et al. (1984) 30 cm infiltration scenario.

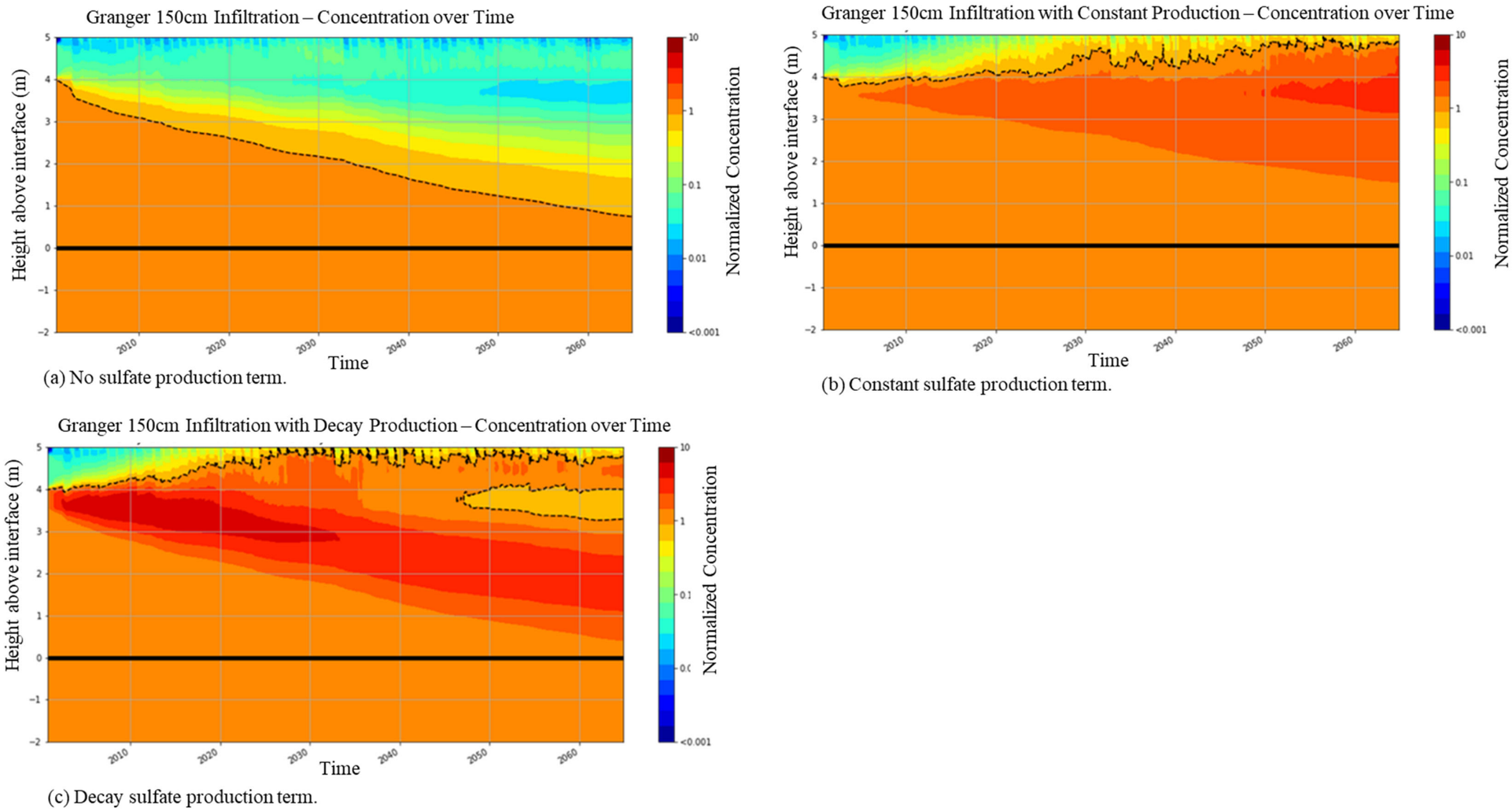

Figure 4-17. Simulated sulfate concentration for the Granger et al. (1984) 150 cm infiltration scenario.

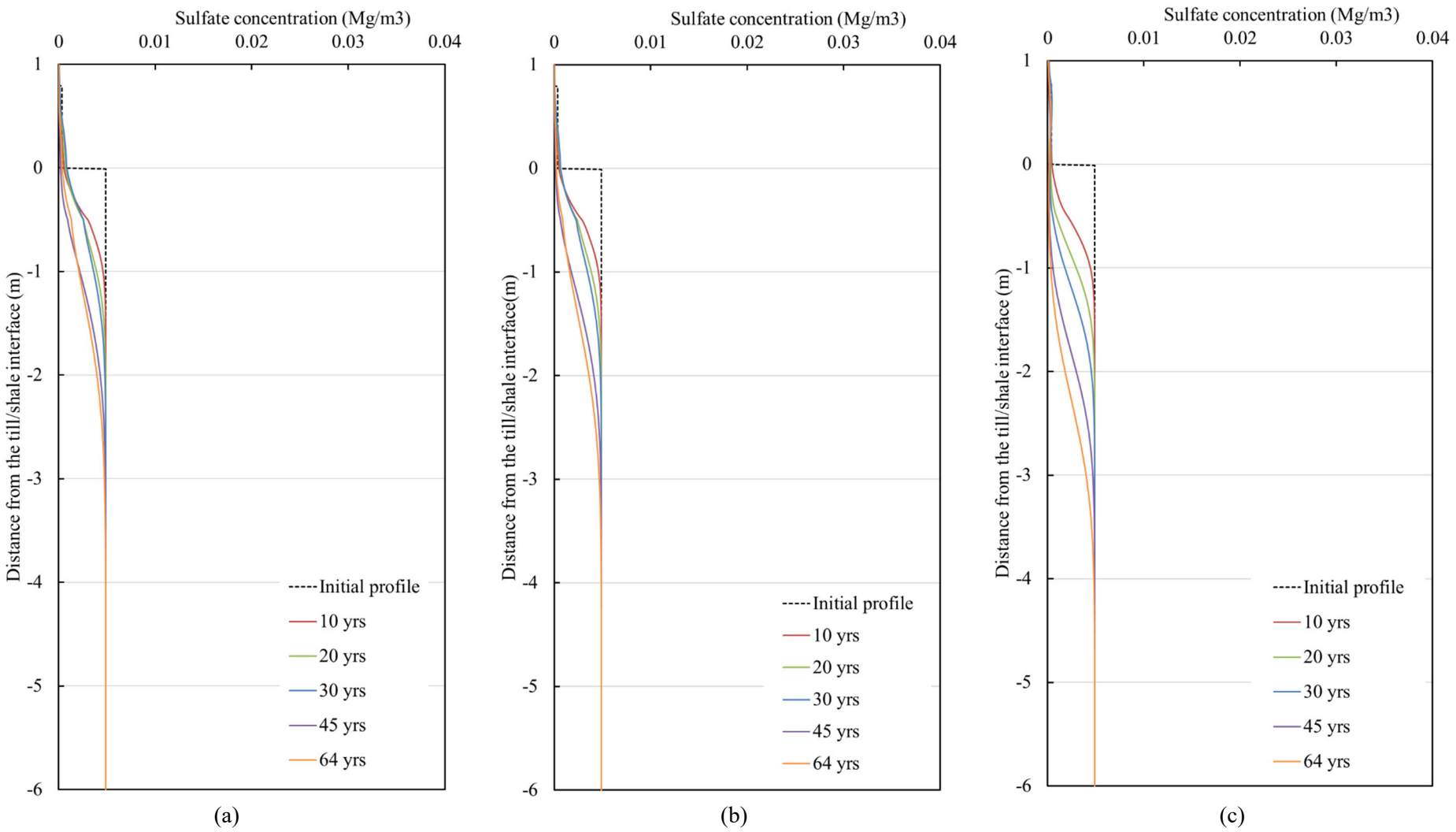

Figure 4-18. Simulated sulfate profiles for the no sulfate production scenarios (a) baseline, (b) Granger 30 cm infiltration, and (c) Granger 150 cm infiltration.

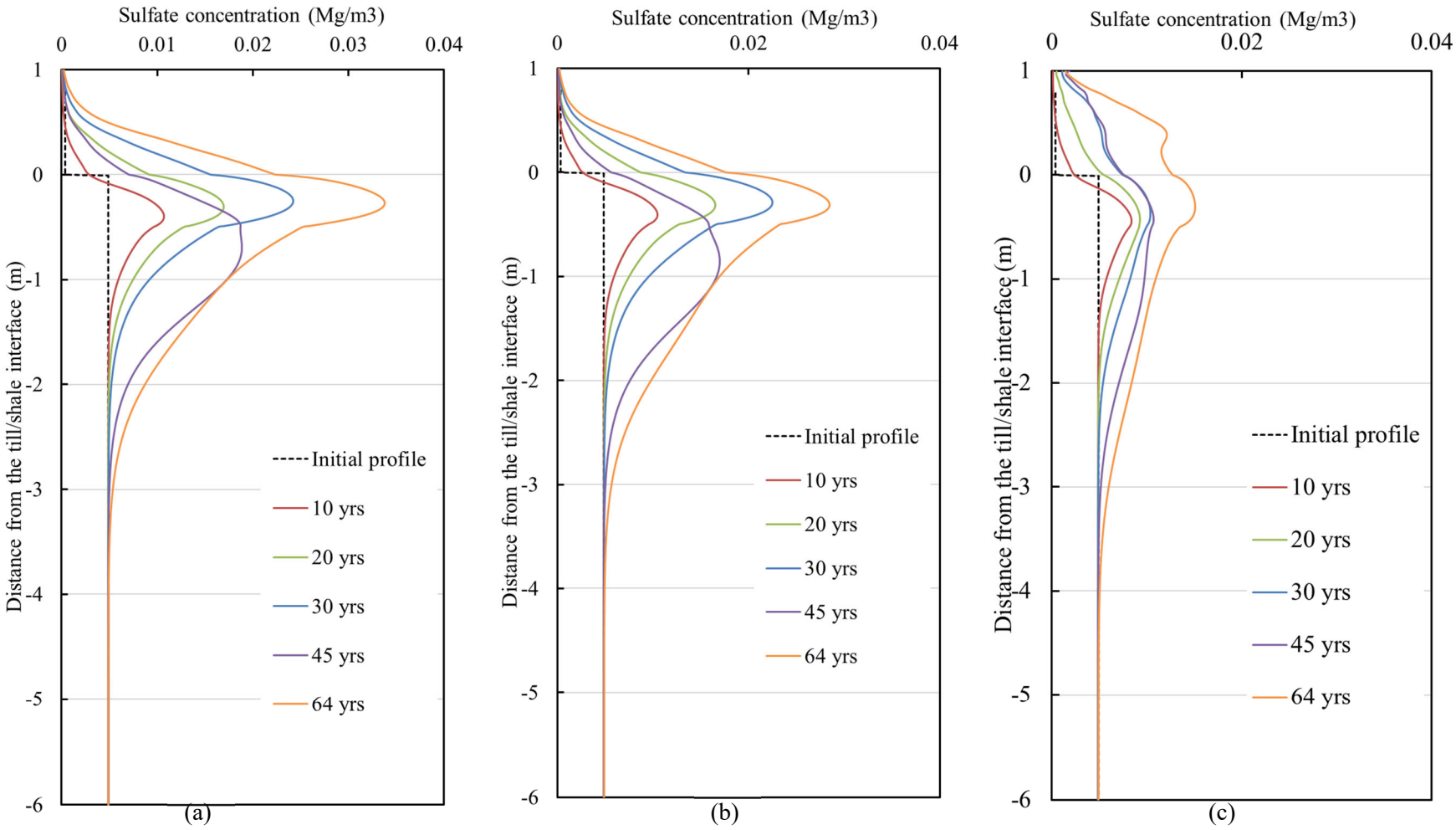

Figure 4-19. Simulated sulfate profiles for the constant sulfate production scenarios (a) baseline, (b) Granger 30 cm infiltration, and (c) Granger 150 cm infiltration.

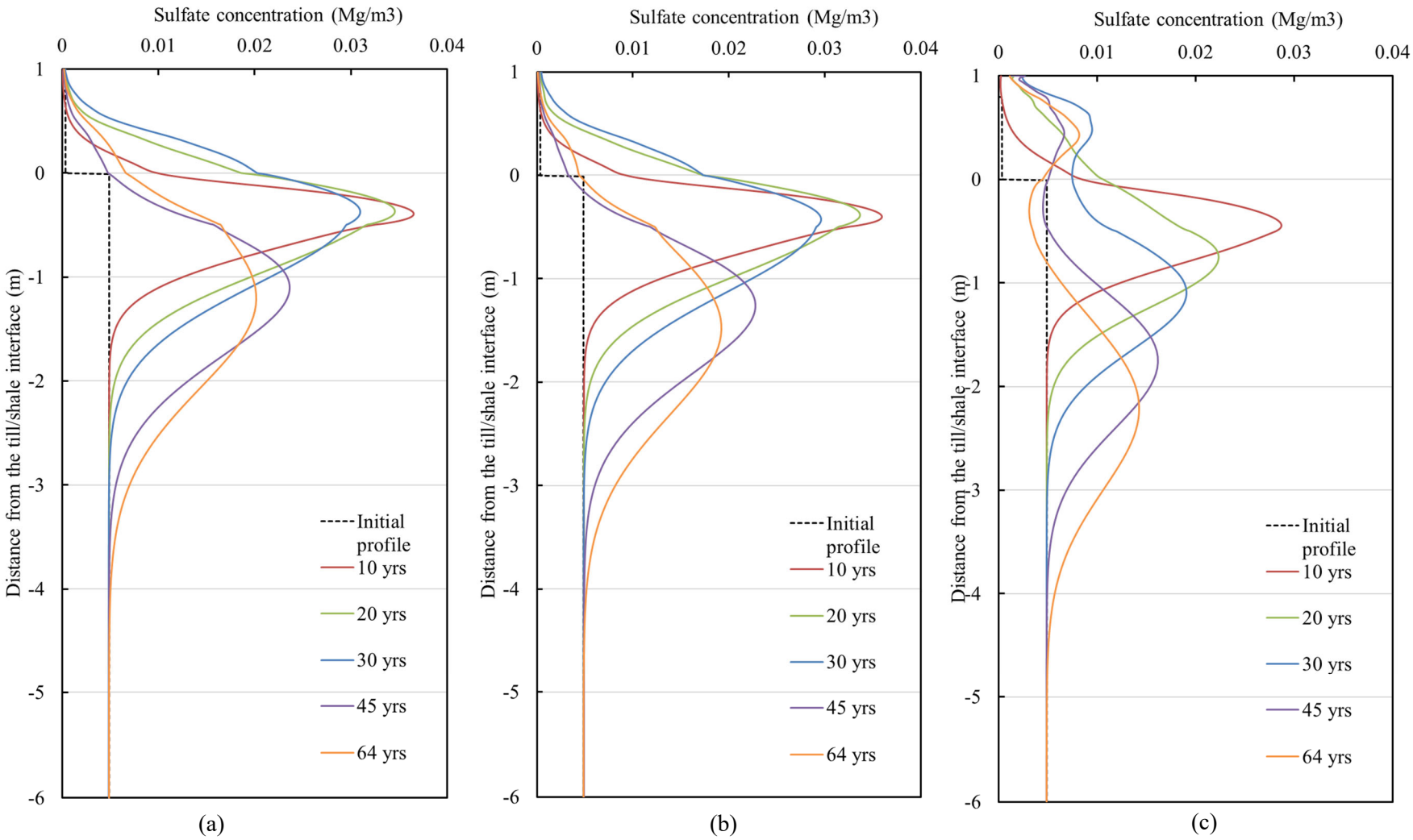

Figure 4-20. Simulated sulfate profiles for the decay sulfate production scenarios (a) baseline, (b) Granger 30 cm infiltration, and (c) Granger 150 cm infiltration.

4.3.4 Model Limitations and Uncertainties

The seepage and solute transport model presented herein summarizes the current (and anticipated) understanding of the system. As additional information or interpretations become available (e.g., field data) the model should be revaluated and updated as needed. The primary limitations of the model and recommendations for future work are listed below.

1. Past research at SBH has demonstrated that the weathering of shale overburden due to oxidation of sulphide minerals within the shale leads to sulfate production. The model presented herein, assumed two scenarios of sulfate production, a constant rate of production and decay rate of production. These functions were based on average values simulated by a dual porosity water flow and transport model (Huang et al. 2015). There is uncertainty with how the sulfate production term will evolve with time and further work should consider refining this flux by continual field monitoring and modelling.
2. The models were run into the future up to 2064, the modelling could be extended further into the future to see if quasi-steady state conditions can be reached.
3. Kelln (2007) indicated that infiltration occurs along preferential flow paths when the ground is frozen or when wet antecedent soil moisture conditions develop prior to precipitation events. This model does not incorporate preferential flow in this way but instead accounts for the volume that theoretically could be contributing to preferential flow by way of the Granger et al. (1984) model. The model is representing preferential flow in a simplified manner and may not capture the precise differences in preferential flow that may occur from year to year. Future modelling efforts are recommended to capture this process and refine the infiltration flux contributing to preferential flow.
4. The K_s functions for the cover materials and shale were varied with time from 2001 to 2005 based on field measurements. The K_s of the shallow oxidized shale increased approximately one order of magnitude over this time. The modelled assumed the same K_s function from 2005 to end of simulations. This is a simplified assumption as the physical characteristics of the shale are expected to evolve over time (e.g., Plasticity of shale varies with water content; Ks can decrease or increase depending on swelling and fracturing).

Future work should consider refining the material parameters of the shale as they are crucial for interpreting the amount of net percolation the system may experience.

5. The root distribution function for the model simulations assumed a linear increase from 20 cm in 2000 until the maximum depth of 100 cm in 2008 based on findings from measured data. However, the accumulation of sulfates (and other solutes) near surface would likely affect the evolution of the root mass with time (i.e., concentrated solutes near surface could result in a shallower root zone). Future modelling efforts should assess the salt accumulation sensitivity on the root distribution function.
6. A 60-year possible climate sequence was used based on historical weather data from Fort McMurray. The modelled scenarios did not consider other possible climate scenarios (i.e., wet year vs dry year) and how different climate cycles might affect soil salinization.

5 CONCLUSION

In this thesis, field data and a seepage and solute model were combined to obtain insights into how snowmelt infiltration processes and varying assumptions of solute production affect the accumulation and transportation of salts within a saline-sodic shale overburden reclamation cover.

Data analysis was conducted with the available dataset (including field observations and past research) at SBH to develop a conceptual model for the site and assess the water balance to develop insight for various hydrological processes. Interflow flow data was compared against melt period potential infiltration and surface water content in the fall and no unique relationship was observed, suggesting controls on infiltration are more complex than the simple model presented by Zhao and Gray (1999). However, different patterns of interflow generation are apparent with time. After vegetation established at SBH (post 2010), as evident by the LAI, interflow decreased significantly suggesting, vegetation maturity is likely correlated with interflow. Interflow was likely an important flux in the system in earlier years and may have resulted in early flushing of salts from the profile, however, in later years due to change in profile, interflow is interpreted to act as a marginal flux into the future. A conceptual one-dimensional model was developed to represent the subsurface flow and transport processes.

A one-dimensional heat, flow, and solute transport model was developed to simulate varying assumptions of snowmelt infiltration and sulfate production scenarios. The models were sensitive to varying snowmelt infiltration scenarios. When the amount of infiltration was increased, evaporation, transpiration and net percolation all increased. The baseline model overestimated runoff and underestimated infiltration. The Granger et. al (1984) 30 cm and 150 cm infiltration scenarios are more consistent with runoff observations and therefore more realistic of the system. The Granger et. al (1984) 30 cm infiltration scenario resulted in the highest amount of evaporation and transpiration due to increased infiltration concentrated near the top of the profile.

Nine model scenarios were used to simulate varying snowmelt and sulfate production scenarios. Mass loss from net percolation was not sensitive to the varying sulfate production scenarios. However, mass loss from net percolation was sensitive to the varying snowmelt infiltration assumptions, with the greatest amount of mass loss from net percolation observed in the Granger

et al. (1984) 150 cm infiltration scenario which corresponds to the highest simulated amount of net percolation.

The simulated sulfate profiles against measured values from the field indicate that the constant sulfate production matched the observed sulfate profiles most accurately. The decay production scenarios appeared to overestimate the amount of salt flushing.

The results of the models indicate that the snowmelt infiltration scenarios have a marked impact on solute concentration compared to the varying solute production scenarios and is therefore, likely a critical control on the distribution and export of solutes within the profile. As the amount of snowmelt infiltration increases, the model simulated increasing soil salinization, likely do in part to evapoconcentration. Increased infiltration also results in increased net percolation, as noted above, which results in more solute leaching to the deeper groundwater system, in the short term. In the long term, it is suspected enhance net percolation and increased infiltration might lead to a reduction in the salinity of the reclamation cover, reversing the soil salinization.

To understand the system more accurately and sensitives of varying assumptions and refinement of the numerical model, further steps should be taken to:

- Extend modelling further into the future to see if quasi-steady state conditions can be reached,
- Explore how the climate cycles affect soil salinization (wet year vs. dry year),
- Continue existing monitoring for water balance components (i.e., climate data, snow surveys),
- Obtain more field measurements (i.e., interflow, sulfate measurements across the profile, water quality).

The findings of this research have important implications in understanding the hydrological processes and solute accumulation and transport within reclamation covers. Enhanced net percolation within the covers could result in significant solute leaching that could affect receiving

water bodies. Additionally, the modelling indicated that enhanced infiltration into the cover system could result in soil salinization driving by evaporation in the long term.

REFERENCES

Aachib, M., Mbonimpa, M., and Aubertin, M. 2004. “Measurement and Prediction of the Oxygen Diffusion Coefficient in Unsaturated Media, with Applications to Soil Covers.” Water, Air, Soil Pollut, no. 15: 163–93.

Abrol, I.P., Yadav, J.S.P., and Massoud, F.I. 1988. “Salt-Affected Soils and Their Management.” Food & Agriculture Organization of the United Nations, no. 39: 5–25.

Allaire, S.E., Roulier, S., and Cessna, A.J. 2009. “Quantifying Preferential Flow in Soils: A Review of Different Techniques.” Journal of Hydrology 378 (1–2). Elsevier B.V.: 179–204. doi:10.1016/j.jhydrol.2009.08.013.

Alrtimi, A., Rouainia, M., and Manning, D.A. 2014. “An Improved Steady-State Apparatus for Measuring Thermal Conductivity of Soils.” International Journal of Heat and Mass Transfer 72: 630–36.

Appels, W.M., Wall, S.N., Barbour, S.L., Hendry, M.J., Nichol, C.F., and Chowdhury S.R. 2017. “Pyrite Weathering in Reclaimed Shale Overburden at an Oil Sands Mine near Fort McMurray, Canada.” Mine Water and the Environment 36 (4): 479–94. doi:10.1007/s10230-017-0454-4.

Azmatch, T.F., Sego, D.C., Arenson, L.U., and Biggar, K.W. 2012. “Using Soil Freezing Characteristic Curve to Estimate the Hydraulic Conductivity Function of Partially Frozen Soils.” Cold Regions Science and Technology 83–84. Elsevier B.V.: 103–9. doi:10.1016/j.coldregions.2012.07.002.

Boese, C.D. 2003. “The Design and Installation of a Field Instrumentation Program for the Evaluation of Soil-Atmosphere Water Fluxes in a Vegetated Cover over Saline/Sodic Shale Overburden.” M.Sc. Thesis, University of Saskatchewan, Saskatoon, SK.

Brandt, A.R. 2008. “Converting Oil Shale to Liquid Fuels: Energy Inputs and Greenhouse Gas Emissions of the Shell in Situ Conversion Process.” Environmental Science & Technology 42: 7489–95.

Bresler, E., McNea,l B.L., and Carter, D.L. 1982. Saline and Sodic Soils: Principles-Dynamics-

Modeling. New York: Springer-Verlag Berlin Heidelberg.

Dingman, S.L. 2015. Physical Hydrology. Third. Vol. 13. Long Grove, IL: Waveland Press, Inc. doi:10.1177/030913338901300106.

Feddes, R., Hoff H., Bruen, M., Dawson T., de Rosnay, P., Dirmeyer, P., Jackson R.B., Kabat, P., Kleidon, A., Lilly, A., Pitman, A.J. "Modeling Root Water Uptake in Hydrological and Climate Models." Bull. Am. Meterol. Soc. 82: 2797–2809.

Fetter, C.W. 1998. Contaminant Hydrogeology. 2nd ed. New Jersey: Prentice Hall.

Granger, R.J., Gray, D.M., and Dyck, G.E. 1984. "Snowmelt Infiltration to Frozen Prairie Soils." Canadian Journal of Earth Sciences 21 (6): 669–77. doi:10.1139/e84-073.

Gray, D.M., and Landine P.G. 1988. "An Energy-Budget Snowmelt Model for the Canadian Prairies." Canadian Journal of Earth Sciences 25 (8): 1292–1303. doi:10.1139/e88-124.

Gray, D.M., Pomeroy, J.W., and Landine, P.G. 1986. "Development and Performance Evaluation of Energy Balance Snowmelt Models."

Gray, D.M., Toth, B., Zhao, L., Pomeroy, J.W., and Granger R.J. 2001. "Estimating Areal Snowmelt Infiltration into Frozen Soils" 3111 (July 2000): 3095–3111. doi:10.1002/hyp.320.

Hayashi, M. 2013. "The Cold Vadose Zone : Hydrological and Ecological Significance of Frozen-Soil Processes." Vadose Zone Journal. doi:10.2136/vzj2013.03.0064.

Hilderman, J.N. 2011. "Net Percolation as a Function of Topographic Variation in a Reclamation Cover over a Saline-Sodic Overburden Dump," no. May.

Hillel, D. 2003. "Introduction to Environmental Soil Physics." Introduction to Environmental Soil Physics, 167–86.

Huang, M., Barbour, S.L., and Carey, S.K. 2015a. "The Impact of Reclamation Cover Depth on the Performance of Reclaimed Shale Overburden at an Oil Sands Mine in Northern Alberta, Canada." Hydrological Processes 29 (12): 2840–54. doi:10.1002/hyp.10229.

Huang, M., Hilderman, J., and Barbour, S.L. 2015b. "Transport of Stable Isotopes of Water and Sulfate within Reclaimed Oil Sands Saline–Sodic Mine Overburden." Journal of Hydrology 529, Part. Elsevier B.V.: 1550–61. doi:http://dx.doi.org/10.1016/j.jhydrol.2015.08.028.

Ireson, A.M., van Der Kamp, G., and Ferguson, G. 2013. “Hydrogeological Processes in Seasonally Frozen Northern Latitudes : Understanding , Gaps and Challenges,” 53–66. doi:10.1007/s10040-012-0916-5.

Kelln, C., Barbour, S.L., and Qualizza, C. 2007. “Preferential Flow in a Reclamation Cover: Hydrological and Geochemical Response.” Journal of Geotechnical and Geoenvironmental Engineering 133 (October): 1277–89. doi:10.1061/(ASCE)1090-0241(2007)133:10(1277).

Kelln, C., Barbour, S.L., and Qualizza, C. 2008. “Controls on the Spatial Distribution of Soil Moisture and Solute Transport in a Sloping Reclamation Cover.” Canadian Geotechnical Journal 45 (3): 351–66. doi:10.1139/T07-099.

Kelln, C., Barbour, S.L., and Qualizza, C. 2009. “Fracture-Dominated Subsurface Flow and Transport in a Sloping Reclamation Cover.” Vadose Zone Journal 8 (1): 96. doi:10.2136/vzj2008.0064.

Kessler, S. 2007. “Salinity Profiles in Reconstructed Soils Over Saline-Sodic Waste From the Oil Sands Industry.”

Kessler, S., Barbour, S.L., van Rees, K.C.J., and Dobchuk B.S. 2010a. “Salinization of Soil over Saline-Sodic Overburden from the Oil Sands in Alberta.” Canadian Journal of Soil Science 90 (4): 637–47. doi:10.4141/cjss10019.

Kessler, S., Barbour, S.L., van Rees, K.C.J., and Dobchuk B.S. 2010b. “Salinization of Soil over Saline-Sodic Overburden from the Oil Sands in Alberta.” Canadian Journal of Soil Science 90 (4): 637–47. doi:10.4141/cjss10019.

Kirkby, M. 1988. “Hillslope Runoff Processes and Models.” Journal of Hydrology 100 (1–3): 315–39. doi:10.1016/0022-1694(88)90190-4.

Li, Y.H., and Gregory, S. 1974. “Diffusion of Ions in Sea Water and Deep-Sea Sediments.” Geochimica et Cosmochimica Acta 38: 703–14.

McMillan, R., Quideau, S.A., MacKenzie, M.D., and Biryukova, O. 2007. “Nitrogen Mineralization and Microbial Activity in Oil Sands Reclaimed Boreal Forest Soils.” Journal of Environmental Quality 36 (5): 1470.

Meiers, G., Barbour, L., and Qualizza, C. 2006. “The Use of In Situ Measurement of Hydraulic Conductivity to Provide an Understanding of Cover System Performance Over Time.” Proceedings of the 7th International Conference on Acid Rock Drainage, 1259–72. file:%5C%5Csas1-s-filesrv1%5CData%5CAdmin%5Cgeoscience%5CReferences%5CICARD%5C2006.

Meiers, G.P., Barbour, S.L., Qualizza, C. V, and Dobchuk, B.S. 2011. “Evolution of the Hydraulic Conductivity of Reclamation Covers over Sodic/Saline Mining Overburden.” Journal of Geotechnical and Geoenvironmental Engineering 137 (10): 968–76. doi:10.1061/(ASCE)GT.1943-5606.0000523.

Merrill, S.D., Doering, E.J., Power, J.F., and Sandoval, F.M. 1983. “Sodium Movement in Soil-Minespoil Profiles: Diffusion and Convection.” Soil Science.

Millington, R.., and Quirk, J.P. 1961. “Permeability of Porous Solids.” Faraday Society Transactions 57: 1200–1206.

Nachshon, U., Ireson, A., van der Kamp, G., and Wheater, H. 2013. “Sulfate Salt Dynamics in the Glaciated Plains of North America.” Journal of Hydrology 499. Elsevier B.V.: 188–99. doi:10.1016/j.jhydrol.2013.07.001.

Nichol, C.F., Qualizza, C., Kessler, S., Wall, S., Barbour, S.L, and Hendry, M.J. 2006. “30 Dump Instrumented Watersheds Geochemical Analysis: A Report Prepared for Syncrude Canada Ltd.”

O’Kane Consultants. 2012. “Syncrude Canada Ltd. Temperature Correction for Matric Suction at D1A Monitoring Station.”

Pasquale, V., Gola, G., Chiozzi, P., and Verdoya, M. 2011. “Thermophysical Properties of Po Basin Rocks.” Geophysical Journal International 186: 69–81.

Patterson, D., and Smith, M. 1985. “Unfrozen Water Content in Saline Soils: Results Using Time-Domain Reflectometry.” Canadian Geotechnical Journal 22: 95–101.

Pomeroy, J.W., Gray, D.M., Brown, T., Hedstrom, N.R., Quinton, W.L., Granger, R.J., and Carey, S.K. 2007. “The Cold Regions Hydrological Process Representation and Model: A Platform

for Basing Model Structure on Physical Evidence." Hydrological Processes 21 (19): 2650–67. doi:Doi 10.1002/Hyp.6787.

Redding, T., and Devito, K. 2008. "Lateral Flow Thresholds for Aspen Forested Hillslopes on the Western Boreal Plain, Alberta, Canada." Hydrological Processes 2274 (November 2008): 2267–74. doi:10.1002/hyp.

Ren, J., Vanapalli, S.K., and Han, Z. 2017. "Soil Freezing Process and Different Expressions for the Soil-Freezing Characteristic Curve." Sciences in Cold and Arid Regions 9: 221–28.

Shackelford, C.D., and Daniel, D.E. 1991. "Diffusion in Saturated Soil II: Results for Compacted Clay." J Geotech Eng 117 (3): 485–506.

Shurniak, R.E. 2003. "Predictive Modeling of Moisture Movement within Soil Cover Systems for Saline / Sodic Overburden Piles." University of Saskatchewan.

Spaans, E.J.A., and Baker, J.M. 1996. "The Soil Freezing Characteristic: Its Measurement and Similarity to the Soil Moisture Characteristic." Soil Sci Soc Am J, no. 60: 13–19.

Stott, D.F., and Aitken, J.D. 1991. "Interior Platform, Western Basins and Eastern Cordillera; Geological Exploration of the Interior Plains." In In Sedimentary Cover of the Craton in Canada. Ottawa, ON: Geological Survey of Canaa.

van Genuchten, M.T. 1980. "A Closed-Form Equation for Predicting the Hydraulic Conductivity of Unsaturated Soils." Soil Science Society of America Journal 44 (5): 892–98. doi:10.2136/sssaj1980.03615995004400050002x.

van Rees, K. 2014. "Comparison of Rooting Distributions for Vegetation Growing on Reclaimed Saline-Sodic Overburden and Natural Undisturbed Landscapes."

van Rees, K., and D. Jackson. 2002. "Syncrude Canada Ltd. Root Distribution Data in Reclamation Covers over Sodic/Saline Mining Overburden."

Van Stempvoort, D.R., Hendry, M.J., Schoenau, J.J., and Krouse, H.R. 1994. "Sources and Dynamics of Sulfur in Weathered till, Western Glaciated Plains of North America." Chemical Geology 111 (1–4): 35–56. doi:10.1016/0009-2541(94)90081-7.

Wall, S.N. 2005. "Characterizing the Geochemical Reactions in an Overburden Waste Pile:

Syncrude Mine Site, Fort McMurray, Alberta, Canada." University of Saskatchewan.

Watanabe, K., and Flury, M. 2008. "Capillary Bundle Model of Hydraulic Conductivity for Frozen Soil." Water Resources Research 44 (12): 1–9. doi:10.1029/2008WR007012.

Wiebe, B.H., Eilers, R.G., Eilers, W.D., and Brierley, J.A. 2007. "Application of a Risk Indicator for Assessing Trends in Dryland Salinization Risk on the Canadian Prairies." Canadian Journal of Soil Science 87 (2): 213–24. doi:10.4141/S06-068.

Williams, P.J., and Smith, M.W. 1989. Frozen Earth: Fundamentals of Geocryology. Cambridge, UK: Cambridge Univ. Press.

Wilson, G.W., Fredlund, D.G., and Barbour, S.L. 1994. "Coupled Soil-Atmosphere Modelling for Soil Evaporation." Canadian Geotechnical Journal1 31: 151–61.

Zhang, T., Barry, R.G., Knowles, K., Ling, F., and Armstrong, R.L. 2003. "Distribution of Seasonally and Perennially Frozen Ground in the Northern Hemisphere." In Proceedings of the 8th International Conference on Permafrost, 1289–94. Zurich, Switzerland.

Zhao, L.T., and Gray, D.M. 1999. "Estimating Snowmelt Infiltration into Frozen Soils." Hydrological Processes 13 (12–13): 1827–42. doi:10.1002/(sici)1099-1085(199909)13:12/13<1827::aid-hyp896>3.0.co;2-d.

Zhao, Y., and Si, B. 2018. "Thermal Properties of Sandy and Peat Soils under Unfrozen and Frozen Conditions." Soil and Tillage Research 189: 64–72.

APPENDIX A

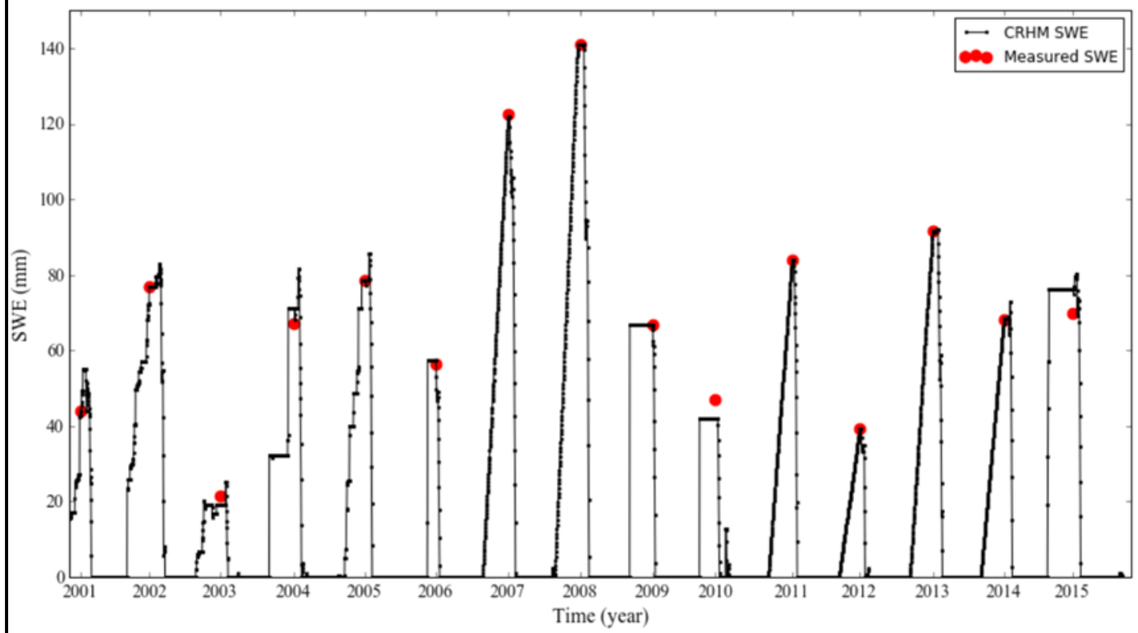

(a) Measured SWE vs. SWE calculated by CRHM for 2001 – 2015.

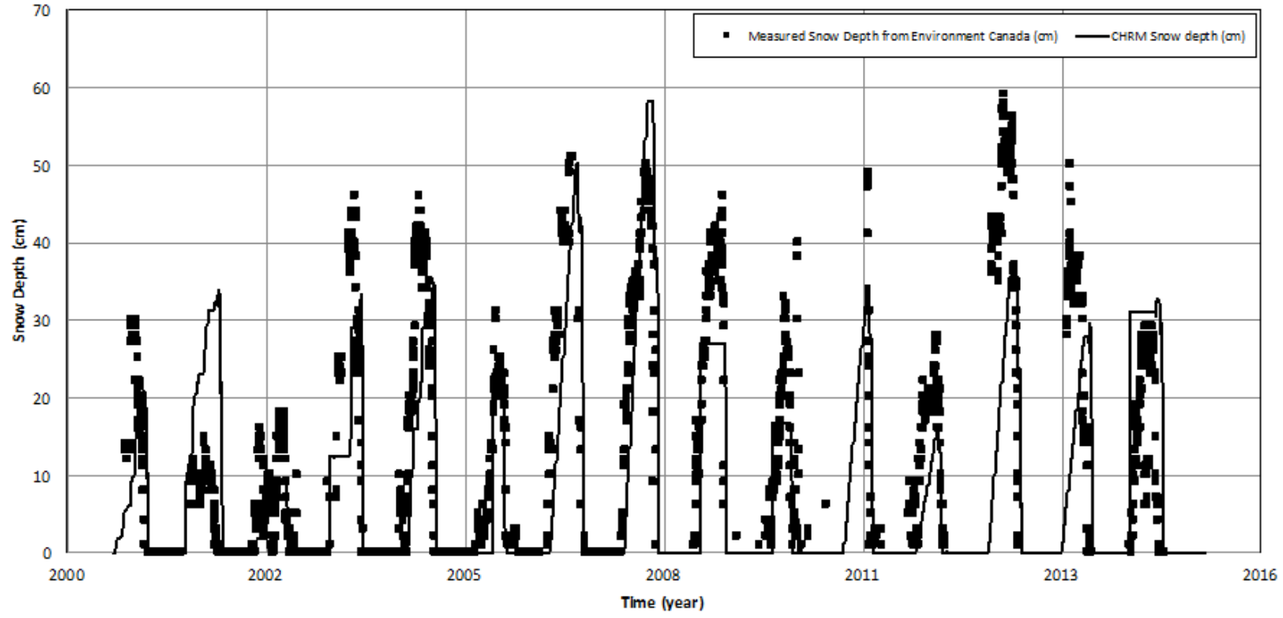

(b) Snow depth calculated by CHRM and measured snow depth from the Fort McMurray Airport, AB (Environment Canada) from 2001-2015.

FIGURE TITLE

Figure A-1. Snow water equivalent (SWE) comparison.

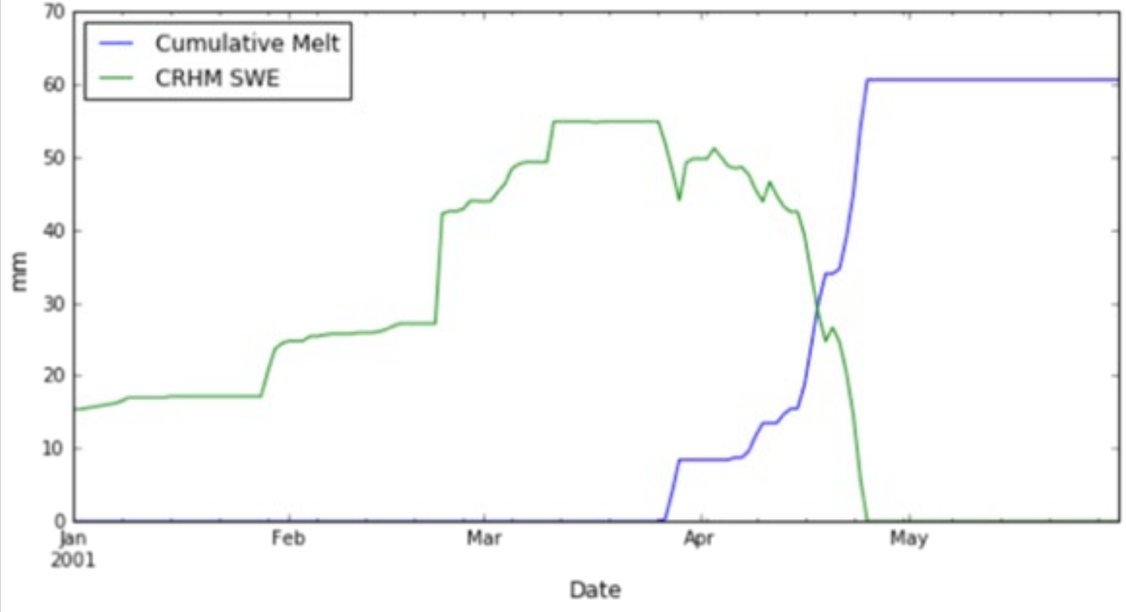

(a) Cumulative snowmelt and SWE calculated for 2001.

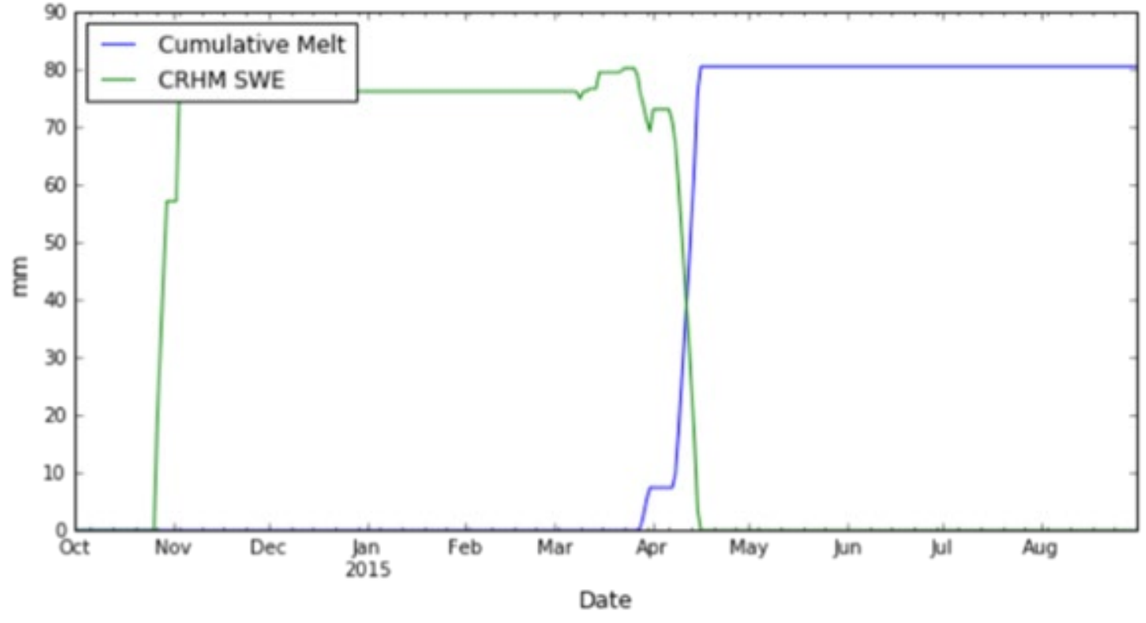

(b) Cumulative snowmelt and SWE calculated for 2015.

FIGURE TITLE

Figure A-2. Cumulative snowmelt and SWE as calculated by CHRM.

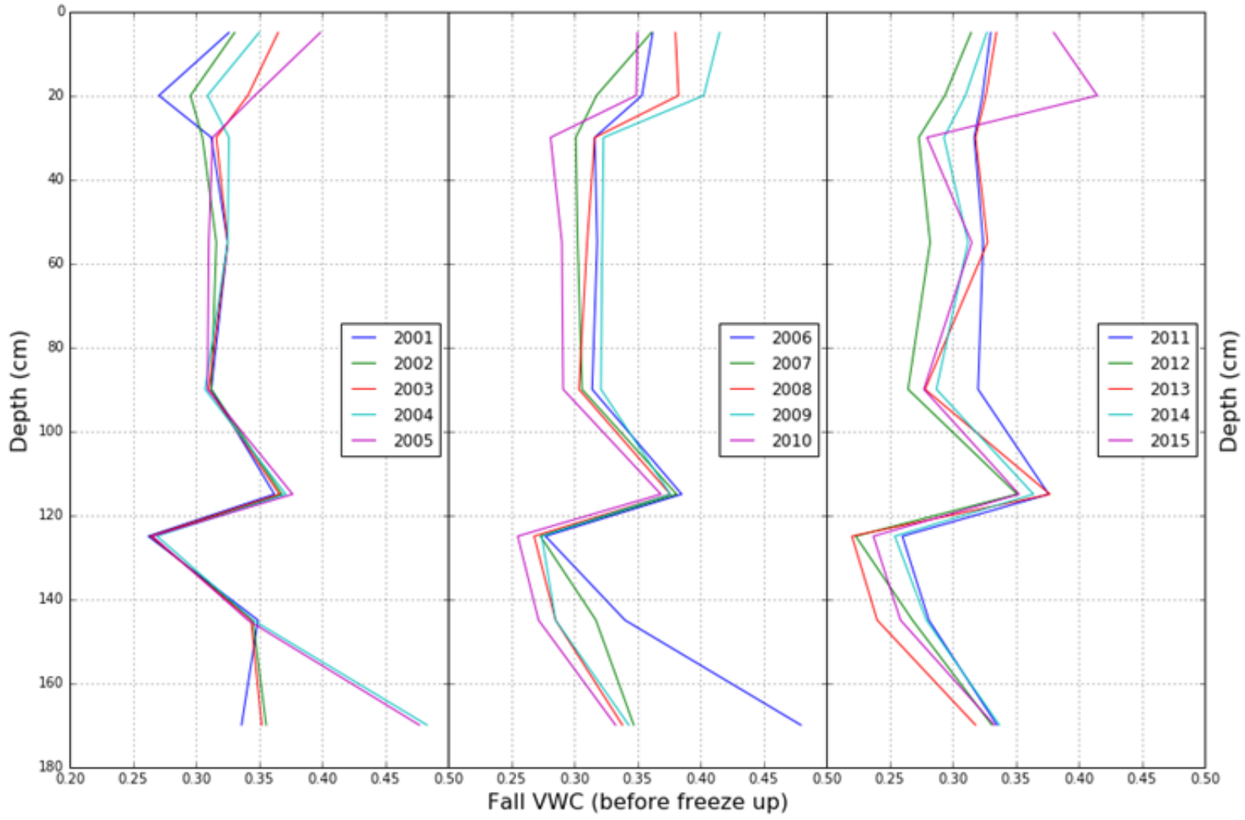

(a) VWC profiles before soil freeze-up.

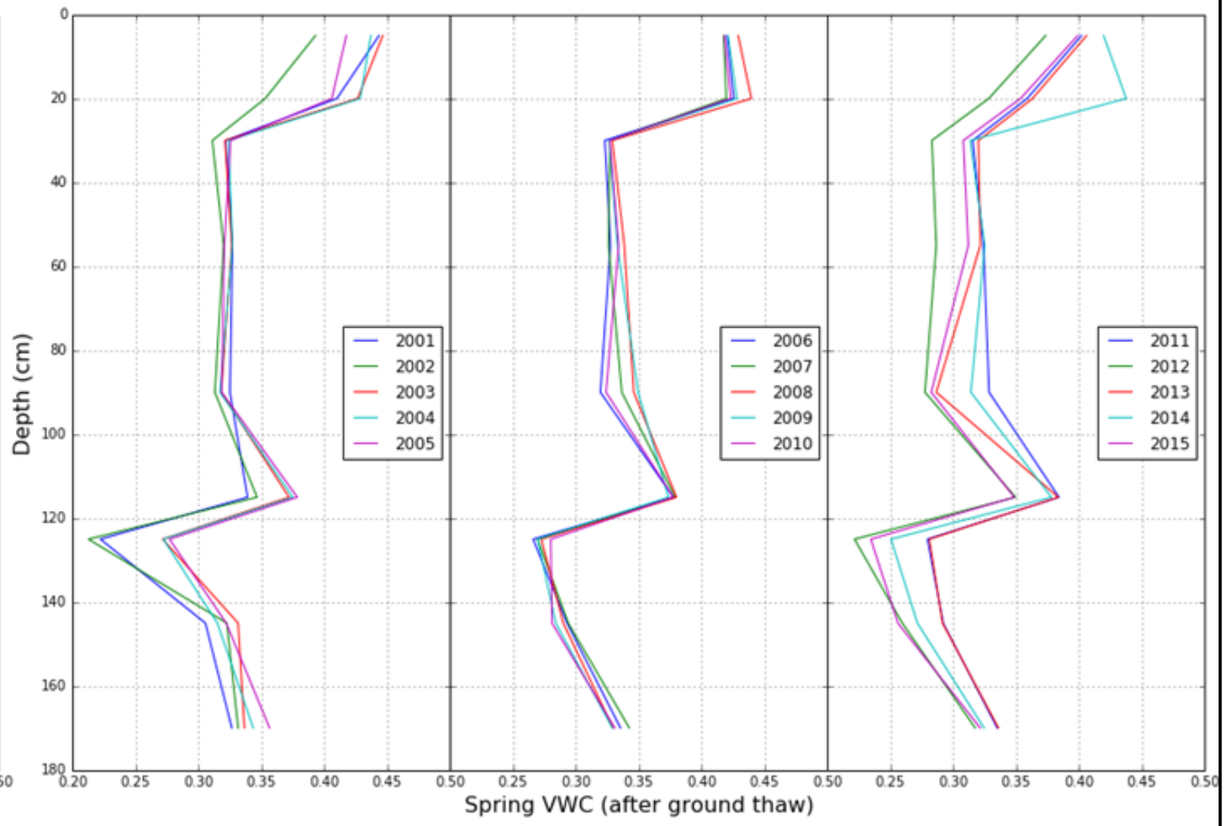

(b) VWC profiles before soil thaw.

FIGURE TITLE

Figure A-3. Volumetric water content (VWC) profiles for D3 cover.

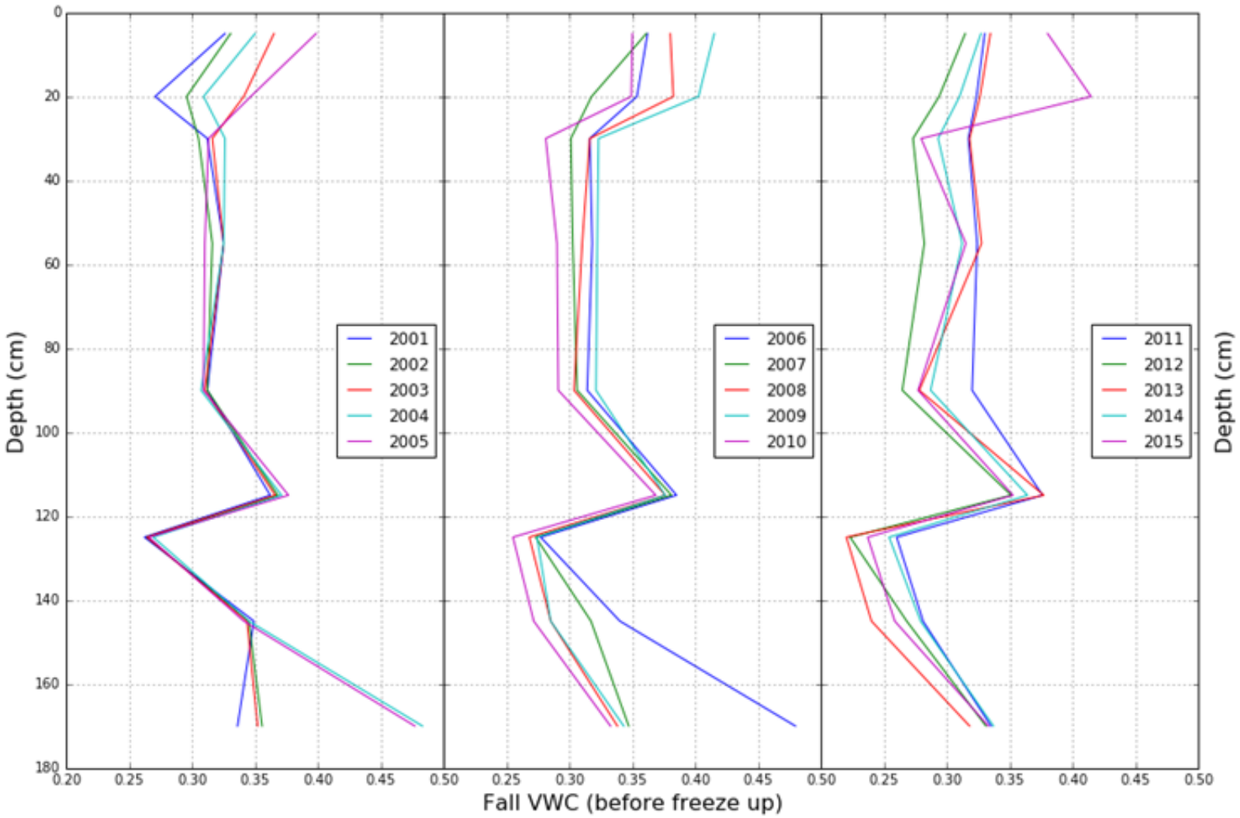

(a) VWC profiles before soil freeze-up.

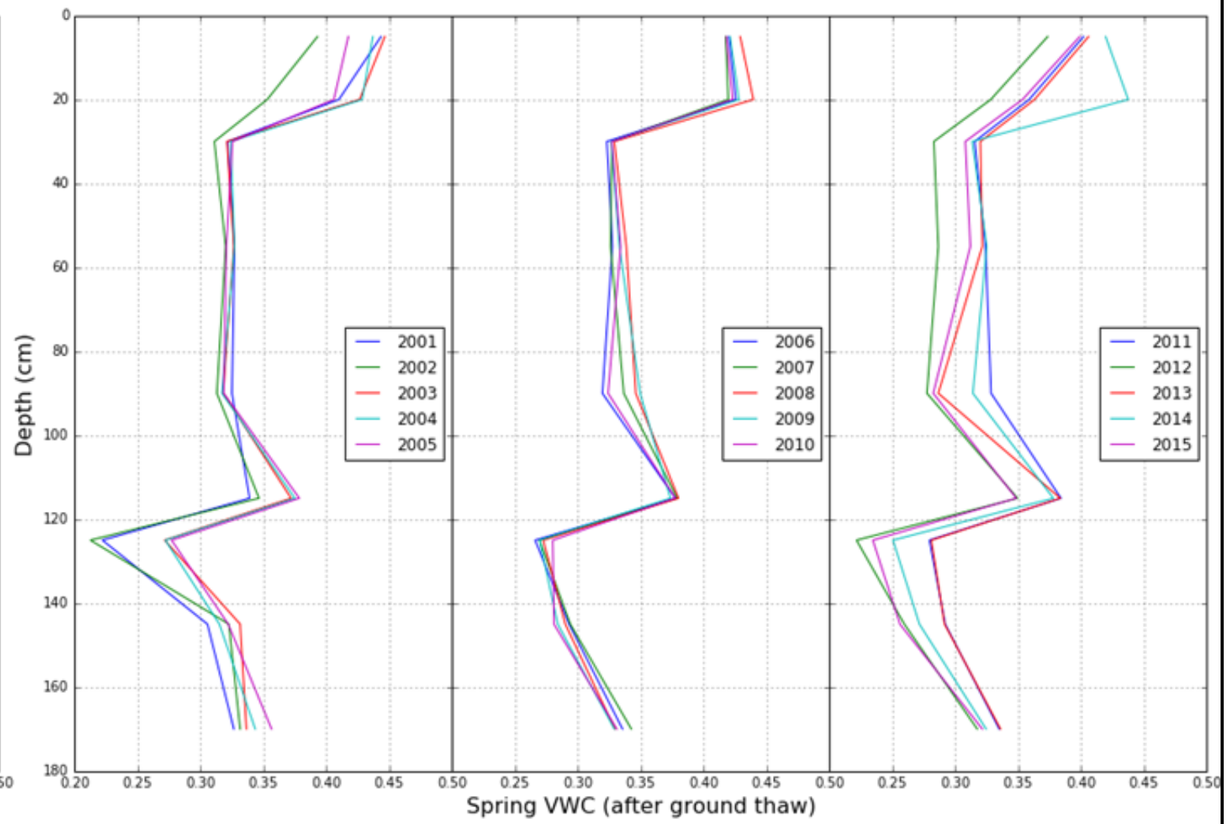

(b) VWC profiles before soil thaw.

FIGURE TITLE

Figure A-4. Volumetric water content (VWC) profiles for D2 cover.

APPENDIX B

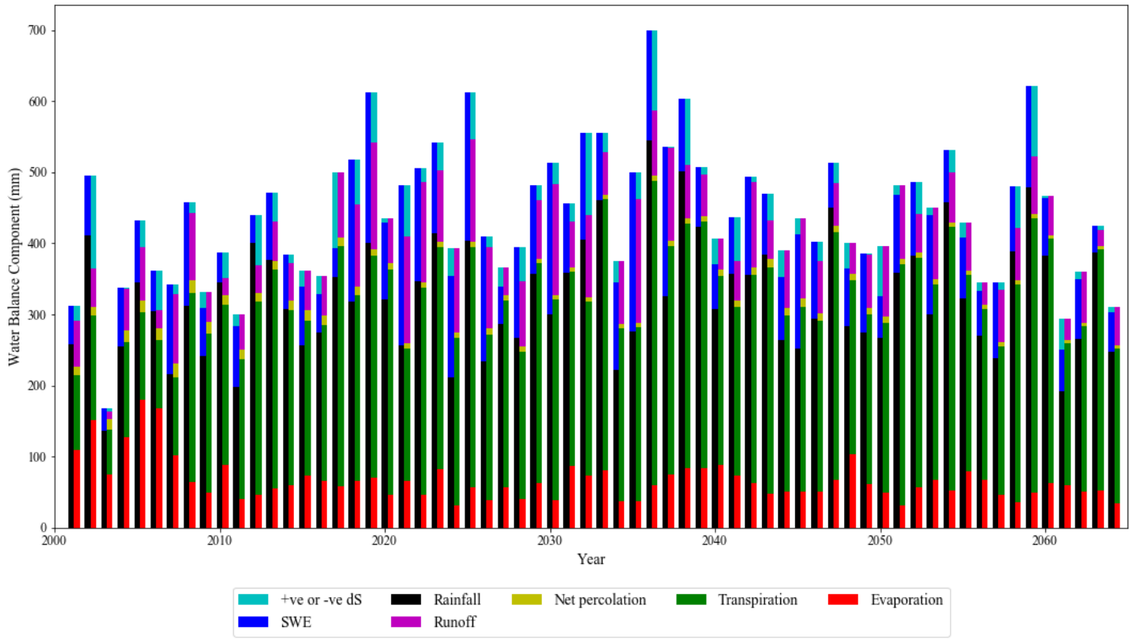

(a) Baseline infiltration.

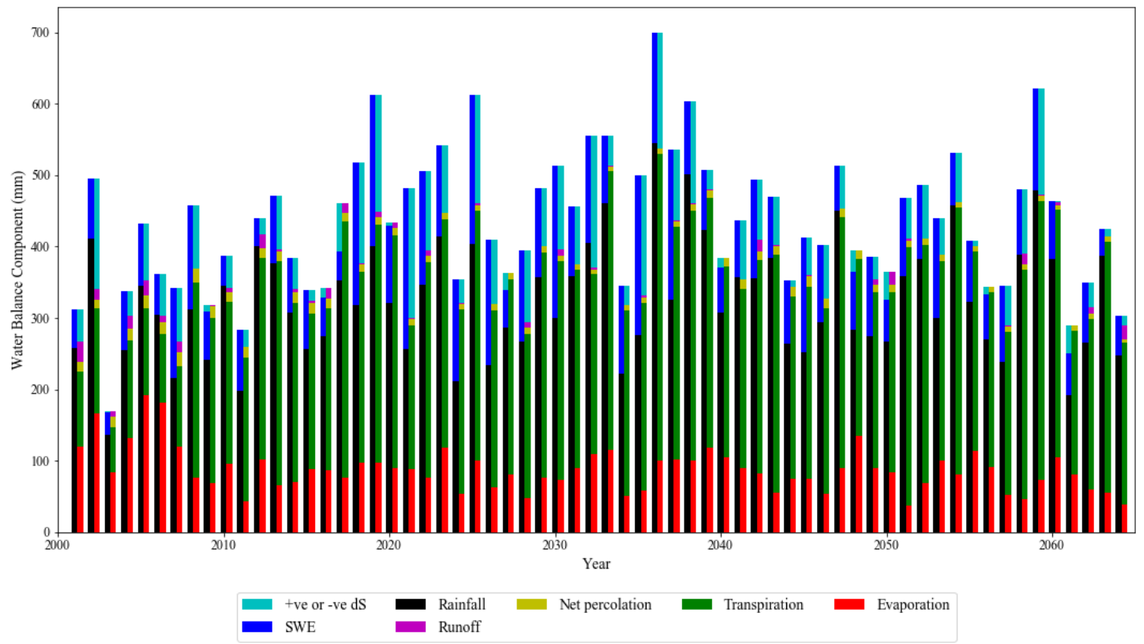

(b) Gray infiltration into the top 30 cm of the cover profile.

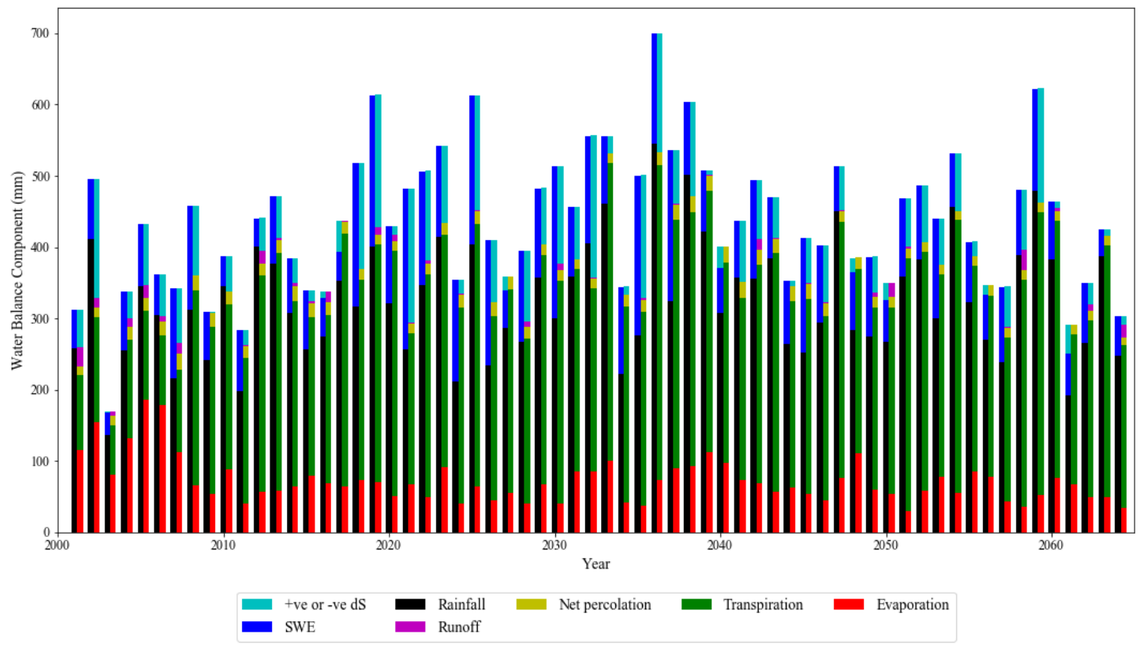

(c) Gray infiltration into the top 150 cm of the cover profile.

FIGURE TITLE

Figure B-1. Annual Water Balance for Modelled Scenarios

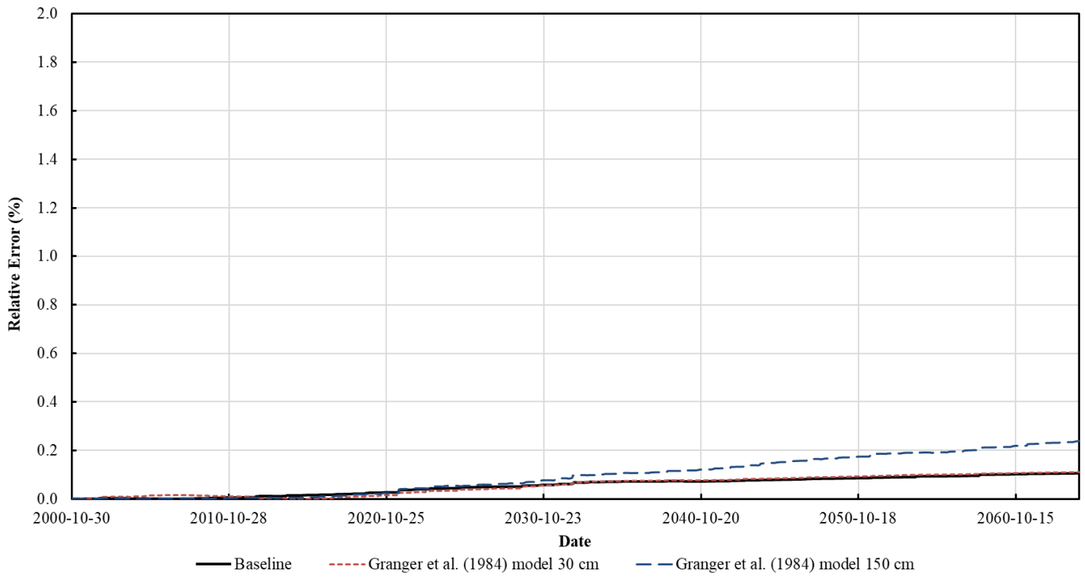

(a) Baseline infiltration.

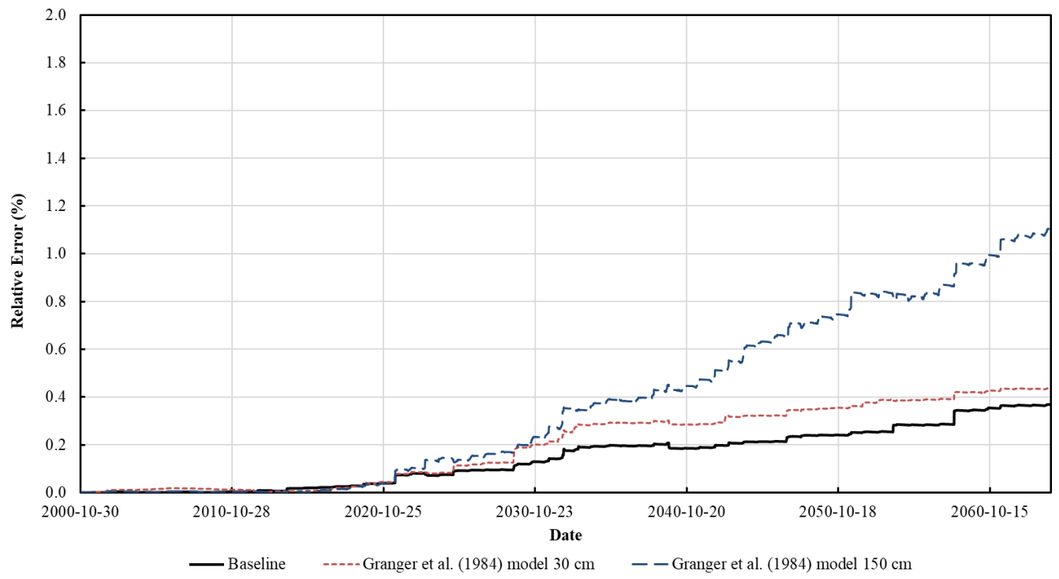

(b) Gray et al. (1984) infiltration into the top 30 cm of the cover profile.

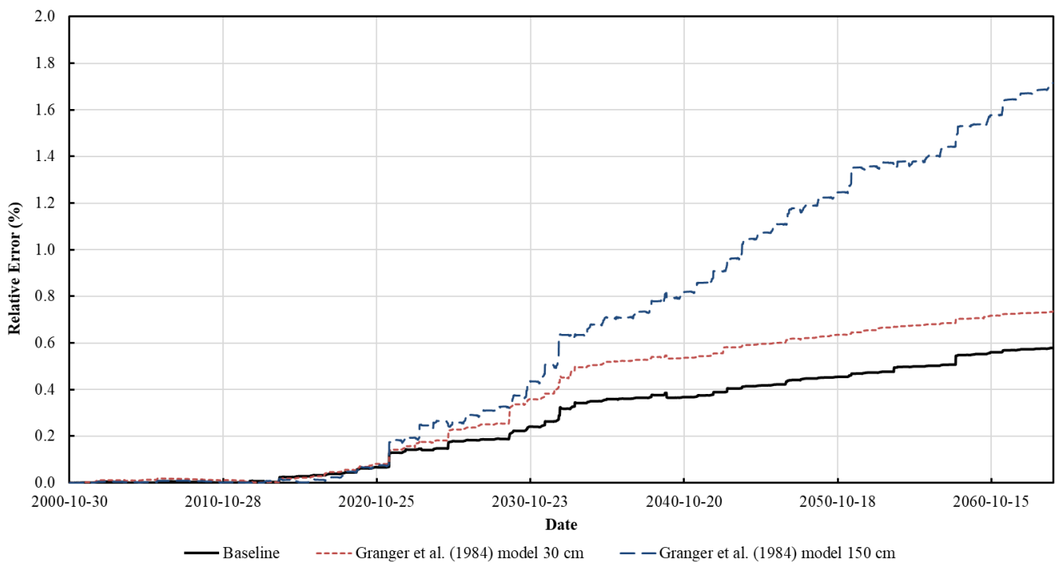

(c) Gray et al. (1984) infiltration into the top 150 cm of the cover profile.

FIGURE TITLE

Figure B-2. Solute transport model error for each snowmelt infiltration scenario

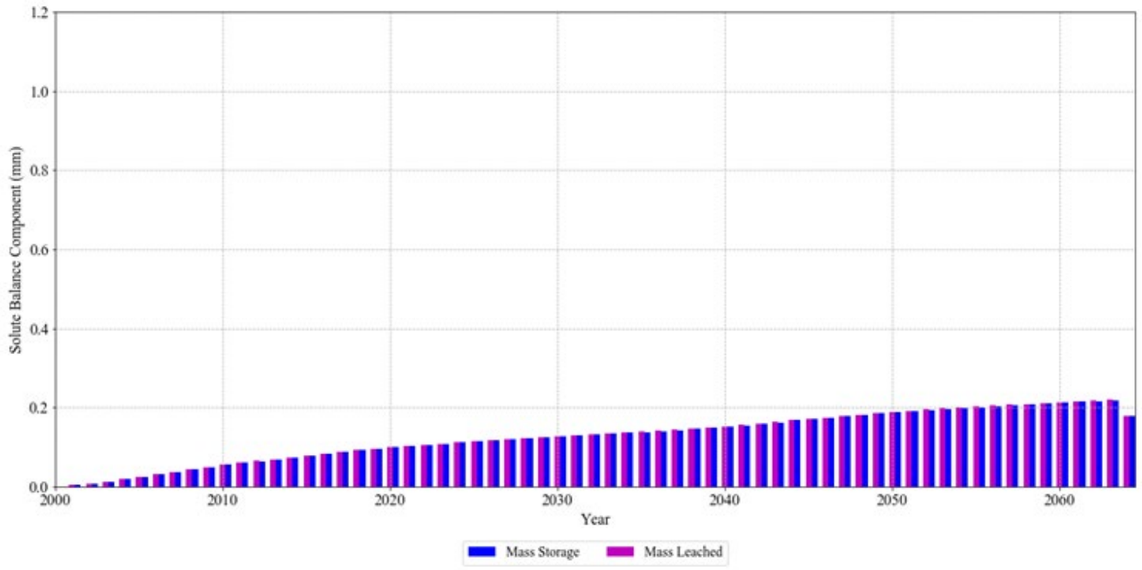

(a) No sulphate production term.

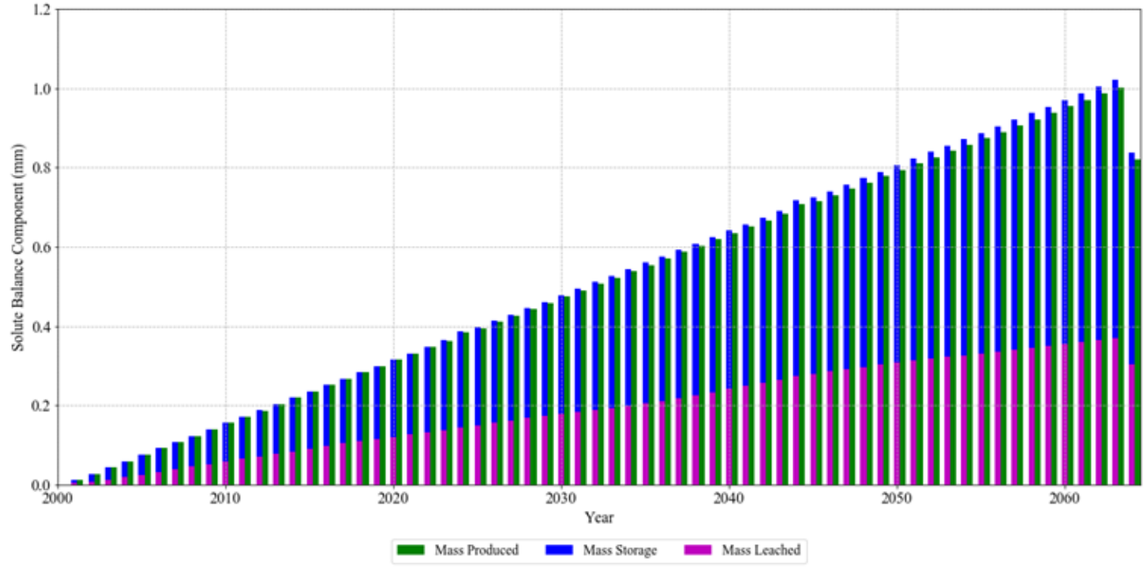

(b) Constant sulphate production term.

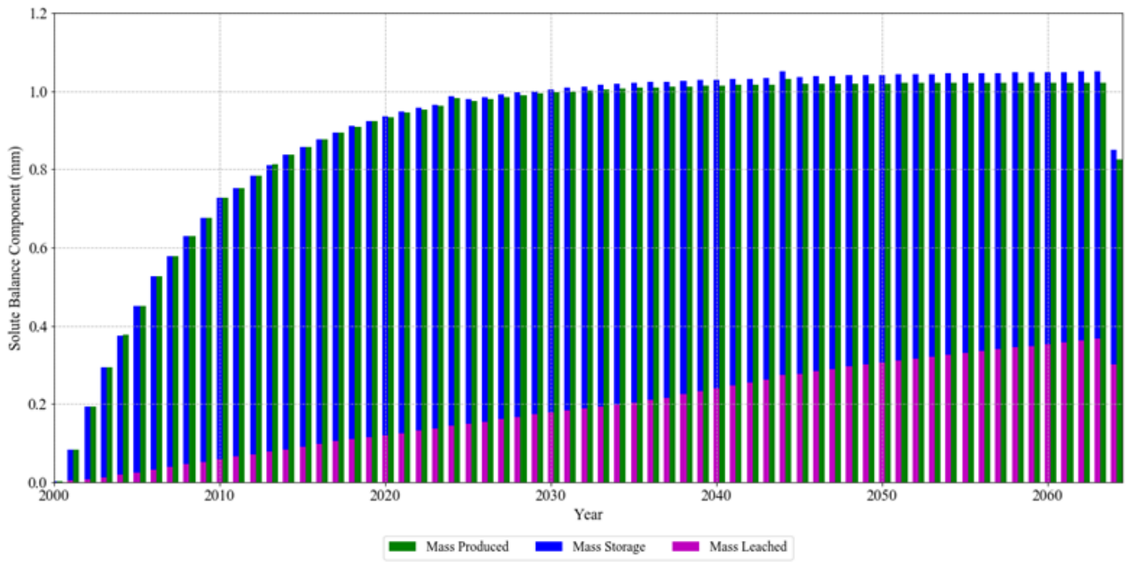

(c) Decay sulphate production term.

FIGURE TITLE

Figure B-3. Solute balance plots for baseline infiltration scenario.

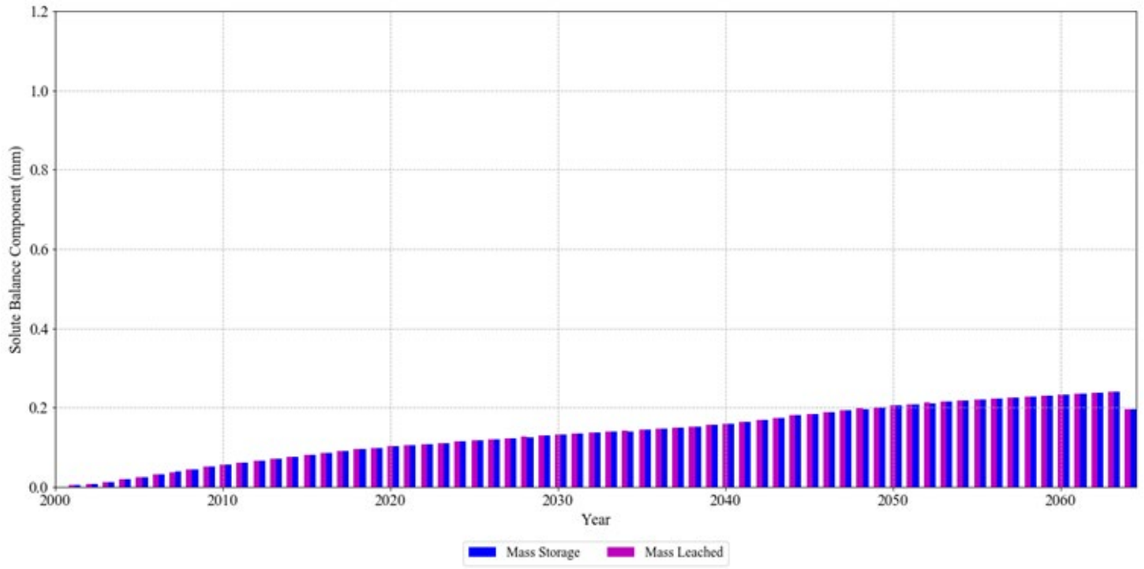

(a) No sulphate production term.

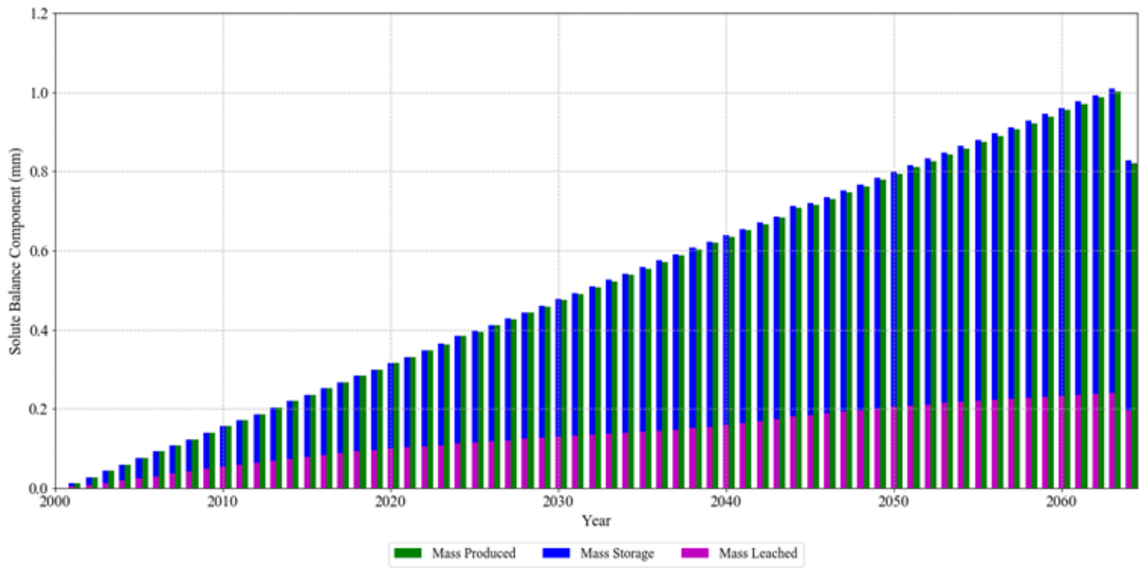

(b) Constant sulphate production term.

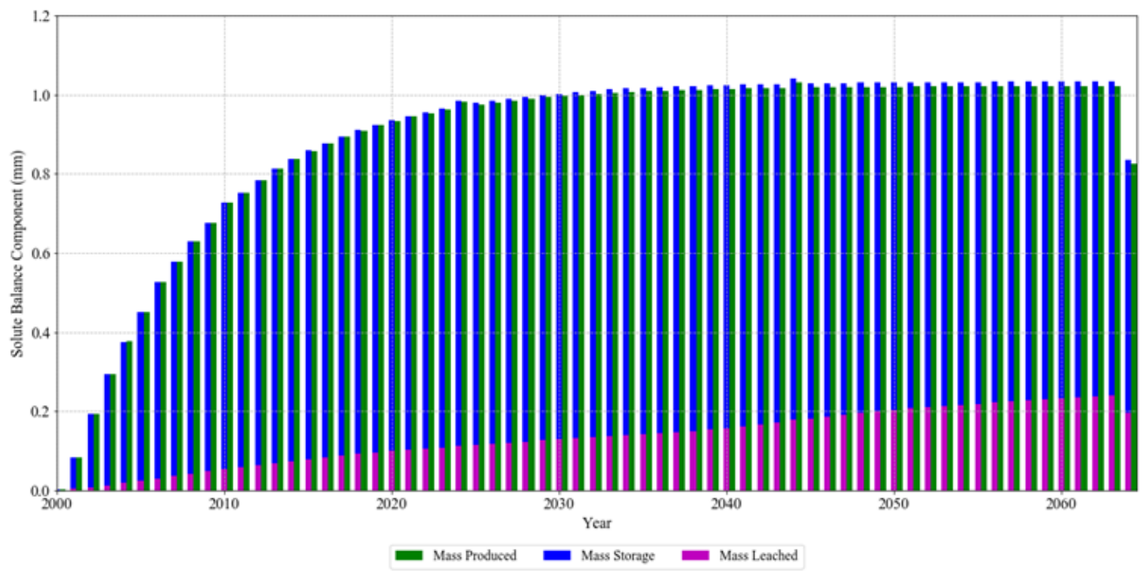

(c) Decay sulphate production term.

FIGURE TITLE

Figure B-4. Solute balance plots for Gray et al, (1984) 30 cm infiltration scenario.

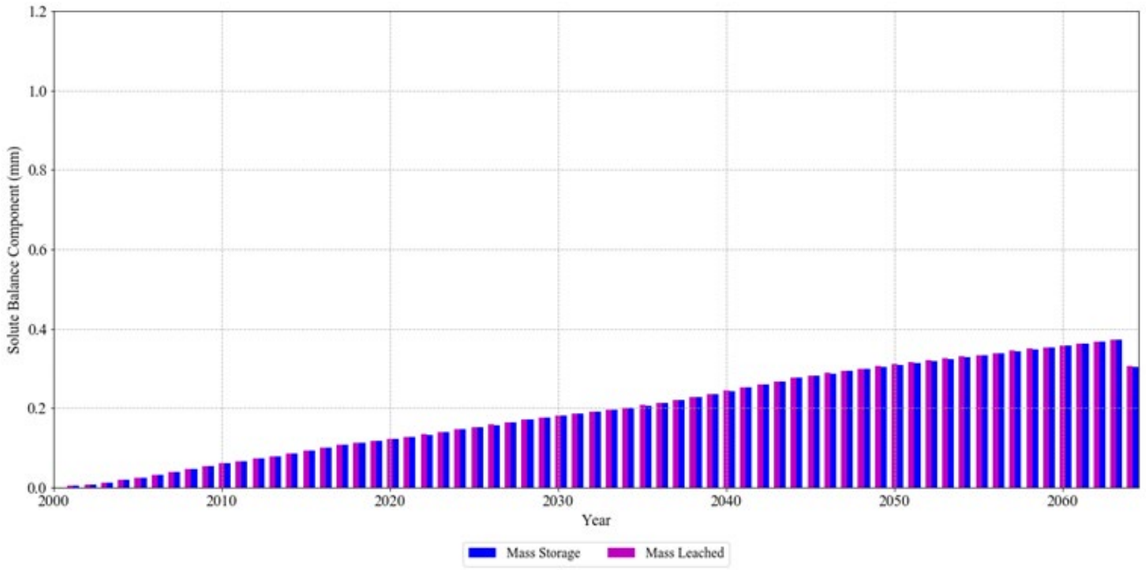

(a) No sulphate production term.

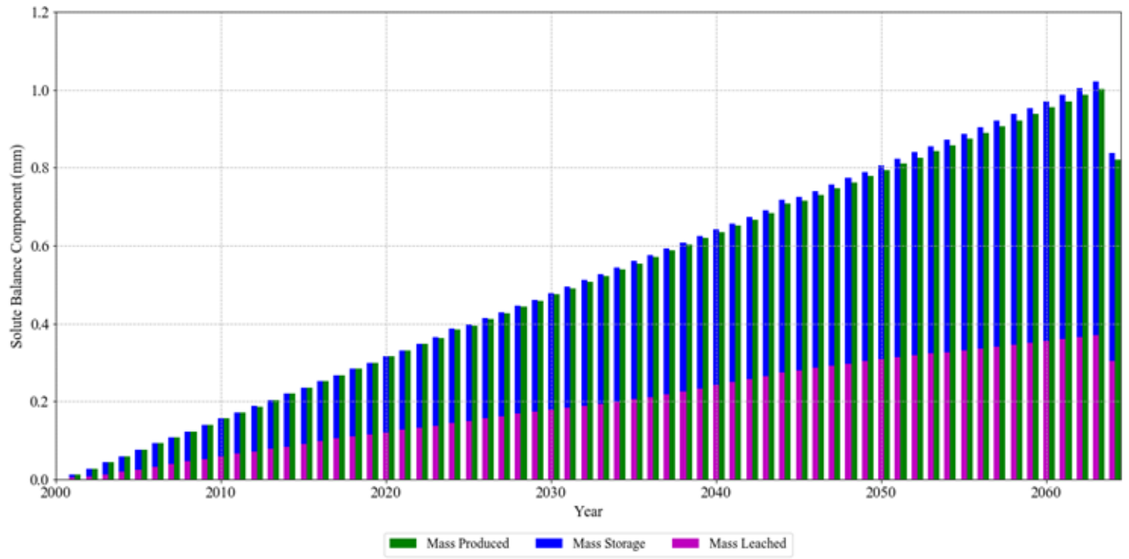

(b) Constant sulphate production term.

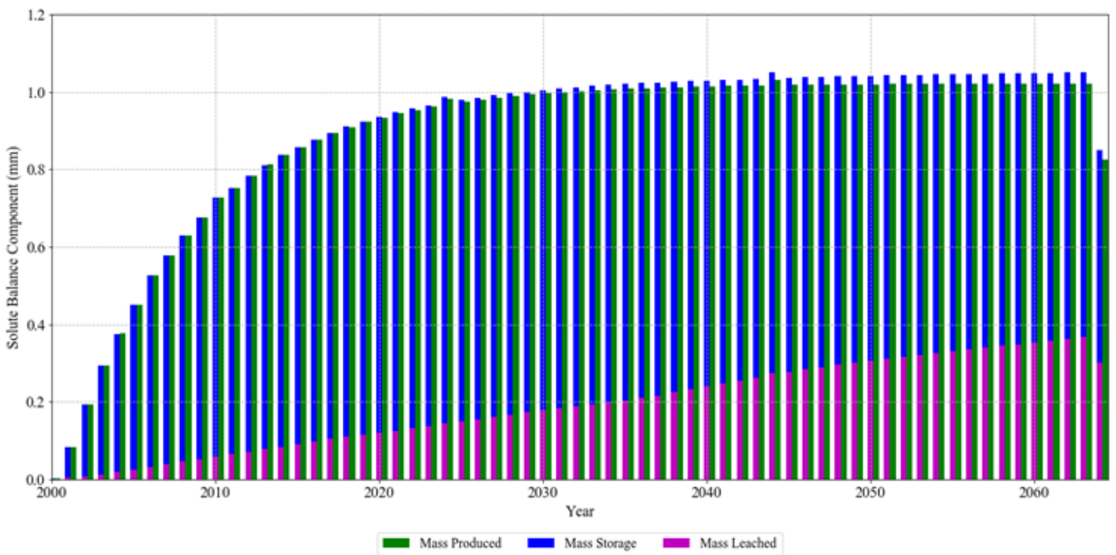

(c) Decay sulphate production term.

FIGURE TITLE

Figure B-5. Solute balance plots for Gray et al, (1984) 150 cm infiltration scenario.